Title
Antiadhesive and Antibacterial Coatings for Biofouling Control

Permalink
https://escholarship.org/uc/item/7sf8b3c3

Author
Marambio Jones, Catalina Stephanie

Publication Date
2014

Peer reviewed|Thesis/dissertation

UNIVERSITY OF CALIFORNIA

Los Angeles

Antiadhesive and Antibacterial Coatings for Biofouling Control

A dissertation submitted in partial satisfaction of the

requirements for the degree Doctor of Philosophy

in Civil Engineering

by

Catalina S. Marambio Jones

2014

ABSTRACT OF THE DISSERTATION

Antiadhesive and Antibacterial Coatings for Biofouling Control

by

Catalina S. Marambio Jones

Doctor of Philosophy in Civil Engineering

University of California, Los Angeles, 2014

Professor Eric M. V. Hoek, Chair

Biofouling in membrane technologies accounts for up to 50% of operational costs; its main effects include flux decline, increased required pressure, expensive pretreatment requirements, cleaning-related production interruptions and accelerated membrane replacing. Despite the efforts, current biofouling control strategies, such as feed water disinfection and chemical cleaning have not entirely solved the problem. Therefore, new approaches are being developed. Since biofouling is a biofilm based phenomena, which starts from an initial reversible bacterial adhesion, followed by irreversible attachment, cell reproduction and finally biofilm formation; it is hypothesized that preventing the initial bacterial adhesion would stop biofouling. This research exploits this idea by creating cross-linked polyvinyl alcohol (PVA) coating films

with low bacterial adhesion propensity, which are subsequently embedded with antibacterial cation-exchanged zeolites (LTA), forming antibacterial nanocomposites able to inactivate bacteria from replication.

A combinatorial array of PVA films and nanocomposites were prepared with varying degree of polymerization, hydrolysis and cross-linking, as well as, different cross-linking agents, zeolite loadings and antibacterial ion utilized. Then, model bacteria reversible-irreversible adhesion and inactivation rates were analyzed, utilizing a high throughput based assay, in several aquatic matrices.

Determined free energy of adhesion and cohesion showed that most PVA films were hydrophilic and had low propensity to bacterial adhesion. Less cross-linked PVA films prepared from less hydrolyzed PVA produced more adhesion resistant films. PVA molecular weight or cross-linking agent did not affect significantly the outcomes. Overall, the bacterial attachments decreased with increasing free energies, but correlations were low because of large adhesions variability. This leaded to concluded that physical heterogeneity of the films, like nanoscale features formation, were significant in the biofouling propensity.

The effect of embedded zeolites on bacterial adhesion varied with the type of antibacterial ion and zeolite loads. Nanocomposites with Ag-LTA (10%) or Zn-LTA and the combined AgCuZn-LTA had lower irreversible adhesion than corresponding PVA films. While, Cu-LTA worsened the antiadhesive properties, because of a higher surface roughness and a higher rate of inactivation; that left more dead cells, which are more prone to adhesion, on the nanocomposite surface. Overall, irreversible adhesions correlated more strongly with surface roughness than free energy of adhesion.

The dissertation of Catalina S. Marambio Jones is approved.

Michael K. Stenstrom

Jennifer Ayla Jay

Richard B. Kaner

Robert D. Damoiseaux

Eric M. V. Hoek, Committee Chair

University of California, Los Angeles

2014

I would like to dedicate this dissertation to Rodrigo, my loved husband. His support and

encouragement were essential in this journey.

TABLE OF CONTENTS

CHAPTER II: EVALUATION OF BACTERIAL ADHESION ON POLYVINYL ALCOHOL COATING FILMS

CHAPTER III: ANTIBACTERIAL PROPERTIES OF SILVER NANOPARTICLES AND SILVER-EXCHANGED ZEOLITE NANOCRYSTALS AND ITS POTENTIAL USE IN ANTIBACTERIAL COATING FILMS

CHAPTER IV: EVALUATION OF BACTERIAL ADHESION AND INACTIVATION ON POLYVINYL ALCOHOL -ZEOLITES NANOCOMPOSITES

LIST OF FIGURES

LIST OF TABLES

ACKNOWLEDGEMENTS

I want to thank my son, Mateo, for illuminating ours lives with his smile, for sitting next to me for hours and pretend that he was also working while I was writing this document; but mainly for giving me perspective when facing the good and bad moments in life. Finally, I like to thank Rodrigo, my husband, for his unconditional support, love and encouragement at each moment of my PhD years. You were fundamental in the development of this work.

VITA

2003	B. A., Civil Engineering Pontificia Universidad Católica de Chile Santiago, Chile
2006	M.S. Civil and Environmental Engineering Pontificia Universidad Católica de Chile Santiago, Chile
2006-2007	Trainee Engineer Aguas Andinas, SA Santiago, Chile
2009-2013	Teaching Assistant Department of Civil & Environmental Engineering University of California, Los Angeles Los Angeles, California
2009-2013	Research Assistant Department of Civil & Environmental Engineering University of California, Los Angeles Los Angeles, California

PUBLICATIONS

McVerry, B.; Wong, M.; Marsh, K.; Temple, J.; Marambio-Jones, Catalina; Hoek, Eric; Kaner, R. Scalable Anti-fouling Reverse Osmosis Membranes Utilizing Perfluorophenyl Azide Photochemistry *J Am Chem Soc* **2014**, *(submitted in review)*

Jones, C. S. M.; Peng, F. B.; Hoek, E. M. V.; Damoiseaux, R., Antiadhesive and antibacterial coatings for biofouling control. *Abstr Pap Am Chem S* **2012**, *244*.

Li, M. H.; Noriega-Trevino, M. E.; Nino-Martinez, N.; Marambio-Jones, C.; Wang, J. W.; Damoiseaux, R.; Ruiz, F.; Hoek, E. M. V., Synergistic Bactericidal Activity of Ag-TiO2 Nanoparticles in Both Light and Dark Conditions. *Environ Sci Technol* **2011,** *45* (20), 8989-8995.

Marambio-Jones, C.; Hoek, E. M. V., A review of the antibacterial effects of silver nanomaterials and potential implications for human health and the environment. *J Nanopart Res* **2010,** *12* (5), 1531-1551.

Li, M. H.; Noriega-Trevino, M. E.; Nino-Martinez, N.; Marambio-Jones, C.; Wang, J.; Damoiseaux, R.; Ruiz, F.; Hoek, E. M. V., Synergistic bactericidal activity of Ag-TiO2 hybrid nanoparticles in dark condition. *Abstr Pap Am Chem S* **2011,** *241*.

Jin, X.; Li, M. H.; Wang, J. W.; Marambio-Jones, C.; Peng, F. B.; Huang, X. F.; Damoiseaux, R.; Hoek, E. M. V., High-Throughput Screening of Silver Nanoparticle Stability and Bacterial Inactivation in Aquatic Media: Influence of Specific Ions. *Environ Sci Technol* **2010,** *44* (19), 7321-7328

Reyes, V. C.; Marambio-Jones, C.; Li, M. H.; Hoek, E. M. V.; Mahendra, S., Impacts of water chemistry on nanoparticle stability and bioavailability for freshwater bacteria and algae. *Abstr Pap Am Chem S* **2010,** *240*.

Pasten, P. A.; Alsina, M. A.; Segura, R.; Marambio, C. S., Removal of aqueous As(V) using amorphous biogenic and abiotic manganese oxides under different pH and ionic strengths: Equilibrium and kinetic studies. *Abstr Pap Am Chem S* **2006,** *231*.

CHAPTER I

INTRODUCTION-BACKGROUND HYPOTHESIS AND SCOPE OF WORK

1.1   Problem statement and significance

Inadequate access to clean water and improved sanitation is perhaps the main problem faced by today's society. According to WHO/UNICEF in their Joint Monitoring Programme for Water supply 768 million people worldwide lacks access to clean fresh water. Moreover, rising water demand to meet the food and energy requirements of a ever growing world population; coupled with the decrease in water quality due to anthropogenic pollution of water bodies and the decrease in fresh water availability produced by global warming effects, such as glaciers receding, snow melt and draughts[1] promises to deteriorate the situation even further.

This problem, incentivizes the use of alternatives water sources for the production of drinking water, water sources that before were considered not suitable for human consumption, whether for socio-political or technical-economical concerns are now considered viable and more economically competitive; for example the use of brackish, sea and wastewater . Membrane technologies, such as reverse osmosis have a key role in the water purification of nontraditional water sources[2].

Water production using membrane technologies have the advantage over conventional technologies in that the produced water quality does not depend on the influent water quality. For example, compared to conventional filtration, membrane technologies do not suffer from breakthrough, therefore the water effluent is always safe. In spite of the technological effectivity, membrane technologies have a main drawbacks in their operation, fouling. This phenomena leads to water flux decline and increasing pressure requirements and thus increasing the water production costs.

Fouling is defined as a process resulting in loss of performance of a membrane due to the deposition of suspended or dissolved substances on its external surfaces, at its pore openings, or within its pores [3]. Fouling is classified depending on the type of foulant involved [4] as crystalline fouling, the deposition of inorganic material precipitating on a surface (scaling); organic fouling, the deposition of organic substances; particulate and colloidal fouling, i. e. the deposition of clay, silt, debris, silica and microbial fouling or "biofouling" , i.e., the adhesion and accumulation of microorganisms forming biofilms.

While scaling and colloidal fouling can be controlled, for example trough the use of scaling-inhibitor or pretreatment, such as ultrafiltration, organic and microbial fouling remain elusive[4b]. Biofouling is inherently more complicated than other membrane fouling phenomena because microorganisms can grow, multiply, and relocate, thus even if high microbial removal rates are achieved, enough cells are left that can growth nourishing on biodegradable substances in the feed water. For this reason biofouling is considered the "Achilles heel" of the membrane technologies[5]. It has been reported that biofouling accounts for 25-50% of their operational cost. This cost originates from higher energy requirements, incorporation of pretreatment to slow biofouling, the production stopping during cleaning cycles and the periodic membrane replacements[6].

1.2 Biofouling mechanisms of formation on membrane surfaces

Biofouling phenomena, is a series of steps which begins with a clean surface/membrane exposed to water containing microorganism, inorganic colloids, organic and ionic constituents[7]. The key steps of biofilm formation are as follow[8]:

1. Membrane modification by adsorption of natural organic matter (NOM). The layer of organic matter can mask the original physicochemical properties of membrane surface and make it more suitable for cell adhesions.

2. Reversible bacterial adhesion ("primary adhesion"): Microbial cells are hydrodynamically trasported towards the membrane-solution interface. Primary adhesion or initial deposition is the result of net colloidal and hydrodynamic interfacial forces between the microbial cells and the membrane surfaces.

3. Irreversible bacterial adhesion: Adhered microbial cells anchor themselves more permanently to membrane surface through the production and excretion of extra-cellular polymeric substances (EPS), which are largely comprised of polysaccharides, but can vary widely depending on microbial species and nutrient conditions.

4. Biofilm formation: Firmly attached bacteria cells grow and reproduce using organics and other nutrients in the feed water along with excess EPS and other cellular matter. Given enough time, complex and organized microbial communities may develop giving rise to hardy biofilms with much higher resistance to biocides than planktonic microbes.

1.3 Conventional biofouling control strategies

The conventional approach to prevent biofouling in water treatment and distribution systems is to filter the water and to apply chemical disinfection using

oxidizing biocides Typical biocides for biofouling control include the use of hypochlorite, ozone, bromide, chlorine dioxide and ultraviolet light. However, this biocides have not been able to fully solve the biofouling problem

Chlorine and hypochlorite are effective for bacterial control but typical polymeric membranes utilized in membrane technologies, such as polyamide are chlorine intolerant, thus if dechlorination is not applied effectively the membrane will degrade, and the selectivity of the membrane will drastically decrease. Additionally, the use of chlorine leads to the formation of assimilable organic compound (AOC) that microorganisms can consume to growth and replicate[9].

Ozone is very effective in deactivating microorganism, unfortunately needs to be produce on site and can form carcinogenic and mutagenic products. Additionally, in the same way as chlorine leads to the formation AOC, that enhance bacterial growth[10].

Ultraviolet light is very effective at inactivating bacteria and virii, it is a physical process that general hydroxyl radicals that inhibit the bacteria growth and at the same time reduce AOC by breaking down the macromolecules without the requirement of chemicals[11]. But its effectivity is limited by the light intensity the distribution of the microorganisms, it cannot be utilized in membrane modules and it has an elevated cost[12].

The main problems with the current practices is not the effectivity of the cleaning agent to inactivate microorganism but the fact that the organism biomass remains as carbon source promoting later microbial growth and that the chemicals deteriorate the properties of the membranes. Other branches of biofouling control research are trying to overcome these challenges and are currently under investigation.

One is biological control, that intents to control the biological mechanisms leading to bacterial attachment and biofilm formation as inhibition of quorum sensing system, which nitric oxide-induced biofilm dispersal, enzymatic disruption of extracellular polysaccharides, proteins, and DNA, inhibition of microbial attachment by energy decoupling, use of cell wall hydrolases, and disruption of biofilm by bacteriophage[13]. This type of control is attractive since it does not involve the use of chemicals, thus should have low toxicity and low development of bacterial resistant. However, these methods are still under research and not used in the practice.

Other branch of biofouling control research lays on the modification of the surface of the membrane technologies, which typically intent to produce surfaces that do not promote bacterial adhesion, or antibacterial membranes that incorporate some form of antibacterial quality.

1.4 New approaches for biofouling control tailoring antifoulant and antibacterial properties

Research on surface modification for biofouling control in the past years has targeted antifouling (antiadhesive) and antibacterial properties. Antifouling characteristics have been approached by hydrophilic modifications using graft polymerization[14]; the incorporation of polyvinyl alcohol (PVA) during the formation of membranes by interfacial polymerization[15] or as surface coatings[16]; the use of polyelectrolyte coatings that produce more negatively charge membranes[17], and the incorporation of hydrophilic nanoparticles[18]. In general, previous research[19], has shown that relatively hydrophobic and rougher membrane surfaces had a higher microbial

deposition rate, and thus, membrane modification generally seeks to form *smoother* and *more hydrophilic* surfaces.

PVA surface modification are very promising because PVA is non toxic and is very hydrophilic and chemically stable. Therefore, in this section further evidence of PVA use in such modification is discussed in section 1.4.1.

The second form of surface modification currently under study is the formation of surfaces with antibacterial properties. Very attractive for this purpose is the use of antibacterial nanomaterials. Nanomaterials are defined as materials that have at least one of its dimension in the nanoscale (1-100nm). The properties of these materials change as their size approaches the nanoscale as the percentage of atoms at the surface of a material becomes significant larger than in the corresponding bulk material. Due to its nanoscale antibacterial nanoparticles are believe to exhibit increase reactivity and thus they become more effective antibacterial. In the literature, some surface modification targeting antibacterial activity have been performed by the use of nanoparticle such as titanium oxides nanoparticles[20], silver nanoparticles[21] and zeolite nanoparticles[22]. Since the antibacterial mechanisms of nanoparticles and bulk material are different a literature review was performed to understand the mechanism of action behind antibacterial nanoparticles. This review is presented in the following section using silver nanoparticles as case of study.

1.5 Silver and silver nanoparticles: evidence of their role as a biocide and mechanisms of action

Throughout history, silver has been widely used in different fields such as biomedical applications, water purification, and food storage. Historical examples include the storage of water, wine, milk and vinegar in silver containers to prevent spoilage. Also, during an important part of last century it was used to control eye infections in newborns and for the treatment of skin burns. The development of nanotechnology has increased silver antimicrobial applications, and to date, silver nanomaterials have found their way to many commercially available products such as households water filters, detergents, dietary supplements, cutting boards, socks, shoes, cell phones, and children toys, among others.

Silver nanomaterials in these products are typically as metallic silver nanoparticles, silver-impregnated zeolites powders, silver-dendrimer complexes and composites, silver-chloride nanoparticles, and polymer-silver nanocomposites. Silver nanoparticles have shown to be effective biocides against different bacteria, fungi and viral species. Tables 1.1 and 1.2 summarize key aspects of the antibacterial and antimicrobial effects of silver nanoparticles found in the literature.

Table 1.1   Summary of nano-silver antibacterial properties [23].

Nano-silver	Strain	Key Aspects	Reference
Silver nanoparticles/ nanosized silver powders	*E. coli, S. aureus*	Minimal inhibition concentration against *E. coli* was lower than 6.6nM and higher than 33 nM for S. Aureus	24
	E. coli	Complete inhibition of CFU ability at 60 μg/mL	25
	E. coli, S. aureus	CFU reduced by 4 to 5 log units	26
	Standard strains and strains isolated from clinical material	Minimal inhibition concentration from 1.69 to 13.5 μg/mL	27
	E. coli, S. aureus	Growth inhibition achieved at 5 μg/mL	24
	L. mesenteroides	Growth inhibition achieved at 2.5 μg/mL	
Silver nanoparticles deposited in activated carbon fibers	*B. subtilis*	76 % CFU reduction by applying silver nanoparticles aerosol	28
Silver Zeolite	*E. coli*	CFU reduced by 8 log units in 5 min.	29
Zeolite containing Silver and Zinc	*E.coli*	Minimal bactericidal concentration of 78μg/mL (as Ag^+) for bacteria grown in Luria-Bertani broth	30
	E. coli, S. aureus, P. aeruginosa	Minimal bactericidal concentration of 39ug/mL (as Ag^+) for bacteria grown in Tryptic Soy broth	
Silver dendrimer complexes and nanocomposites	*S. aureus, P. aeruginosa, E.coli*	Antimicrobial activity was comparable or better than that of silver nitrate solutions. The activity and solubility did not decrease even in the presence of sulfate or chloride ions.	31
Silver nanoparticles stabilized in Hyper branched polymers	*E. coli, S. aureus, B. subtilis, K. mobilis*	Microbial activity increases as silver content in polymer decreases due to a decrease in silver nanoparticle size	32

Table 1.2   Summary of nano-silver toxicity to other microorganisms [23]

Strain	Nano-silver	Key Aspects	Reference
Fungi:			
A. niger	Myramistin® stabilized silver nanoparticles	MIC were found to be 5 mg/L	24
	Silver nanoparticles stabilized in hyper branched polymers	Formation of inhibition zones around nano-silver inoculated spots in agar plates	32
	AgCl embedded in a silica matrix on cotton fabric	The effective antifungal doses were found significantly higher than bacterial doses	33
S. cerevisiae	Myramistin® stabilized silver nanoparticles	MIC were found to be 5 mg/L	24
T. mentagrophytes	Silver nanoparticles	IC_{80} between 1-4 mg/L	34
C. albanicas	Silver nanoparticles	Silver nanoparticles inhibited micelial formation, which is responsible for pathogenicity	34
	Silver nanoparticles	Antifungal activity may be caused by cell membrane structure disruption and inhibition of normal budding process.	35
	Silver nanoparticles coated on plastic catheters	Catheter coated with silver nanoparticles inhibited growth and biofilm formation	36
Yeast (isolated from bovine mastitis)	Silver nanoparticles	MIC estimated between 6.6 nM and 13.2 nM	37
P. citrinum	Silver nanoparticles stabilized in hyper branched polymers	Formation of inhibition zones around nano-silver inoculated spots in agar plates	32
Viruses:			
hepatitis B virus	Silver nanoparticles	Inhibition of virus replication	
HIV-1	Silver nanoparticles	1-10 nm silver nanoparticles attached to virus restraining virus from attaching to host cells	38
Syncitial virus	Silver nanoparticles	44% inhibition of Syncitial virus infection	39
Algae:			
C. reinhardtii	Silver nanoparticles	EC_{50} for the photosynthetic yield was found in 0.35 mg/L of total silver content after 1 hr of exposure	40

Although vast research exists on the antimicrobial properties of silver nanoparticles, the

mechanisms of silver nanomaterial antibacterial properties have not been completely

elucidated. In the following section, a summary of the literature regarding this point is provided.

1.5.1 *Mechanisms of silver nanoparticle antibacterial properties*

The most typical mechanisms of silver nanoparticle antibacterial properties proposed to date are (1) uptake of free silver ions followed by disruption of ATP production and DNA replication, (2) silver nanoparticle and silver ion generation of ROS, and (3) silver nanoparticle directly damaging cell membranes. The various observed and hypothesized interactions between silver nanomaterials and bacteria cells are conceptually illustrated in Figure 1.1 .
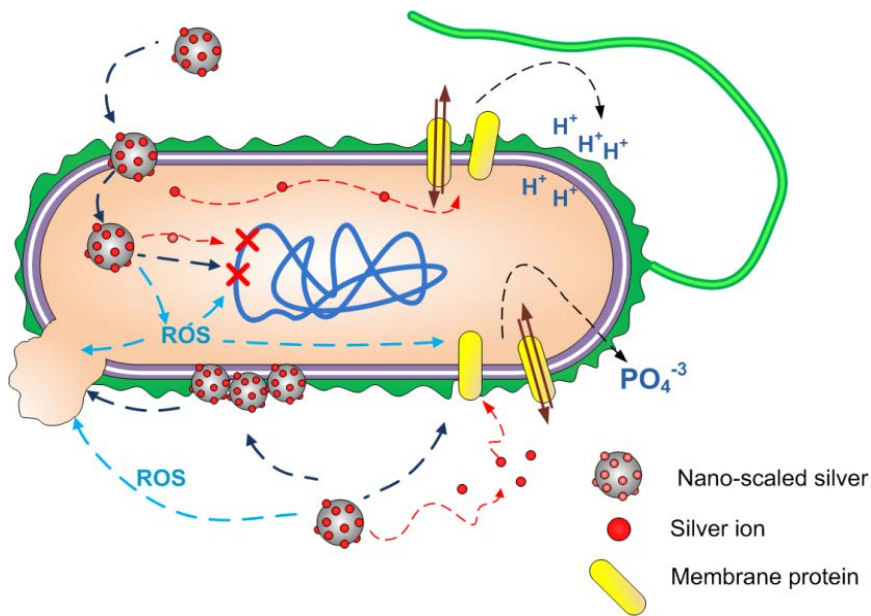
Figure 1.1   Conceptual illustration of the antibacterial mechanisms of silver nanoparticles [23]

11

Free silver ion uptake: Silver nanoparticles may dissolve, generating silver ions, which is believed to be the product of an oxidative dissolution. In previous research, it was proposed that the oxidative dissolution would occur in the mitochondria of eukaryotic cells as a result of silver nanoparticle reaction with H_2O_2 as shown in reaction 1.1[41]; on the contrary, it is hypothesized that a similar mechanism could occur in the bacterial cell membrane where the proton motive force takes place. Other form of oxidative dissolution is proposed to occur in presence of oxygen, see reaction 1.2, Choi et al. attributed this reaction to the change in color of silver nanoparticles suspension observed after a week[42].

$$2Ag + H_2O_2 + 2H^+ \rightarrow 2Ag^+ + 2H_2O \quad E^0 = 0.17V \qquad 1.1$$
$$4Ag + O_2 + 2H_2O \leftrightarrow 4Ag^+ + 4OH^- \qquad 1.2$$
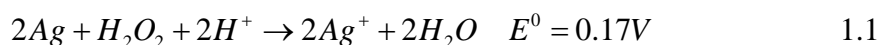
The eluted ions from silver nanoparticles are believed to cause part of their antibacterial properties. At sub-micromolar concentrations, Ag^+ interacts with enzymes of the respiratory chain reaction such as NADH dehydrogenase resulting in the uncoupling of respiration from ATP synthesis. Silver ions also bind with transport proteins leading to proton leakage, inducing the collapse of the proton motive force[43]. Silver inhibits the uptake of phosphate and causes the efflux of intracellular phosphate[44]. The interaction with respiratory and transport proteins is due to the high affinity of Ag^+ with thiol groups present in the cysteine residues of those proteins [43b, 44-45]. Additionally, it has been reported that Ag^+ increases DNA mutation frequencies during polymerase chain reactions [46].

It has been observed that bacterial cells exposed to milli-molar Ag^+ doses suffer morphological changes such as cytoplasm shrinkage and detachment of cell wall membrane, DNA condensation and localization in an electron-light region in the center of the cell, and cell membrane degradation allowing leakage of intracellular contents[47]. Physiological changes occur together with the morphological changes; bacterial cells enter an active, but non-culturable state in which physiological levels can be measured but bacteria are not able to growth and replicate.

Generation of oxygen species: Reactive oxygen species (ROS) are natural byproducts of the metabolism of respiring organisms . While small levels can be controlled by the antioxidant defenses of the cells such as altering the glutathione/glutathione disulfide (GSH/GSSG) ratio, excess ROS production may produce oxidative stress[48]. The additional generation of free radicals can attack membrane lipids and lead to a breakdown of membrane and mitochondrial function or cause DNA damage[49]. Metals can act as catalysts and generate ROS in the presence of dissolved oxygen[50]. In this context, silver nanoparticles may catalyze reactions with oxygen leading to excess free radical production.

Studies done in eukaryotic cells suggest that silver nanoparticles inhibit the antioxidant defense by interacting directly with GSH, binding GSH reductase or other GSH maintenance enzymes[51]. This could decrease the GSH/GSSG ratio, and subsequently, increase ROS in the cell. Silver ions eluted from nano-scaled silver or chemisorbed on its

13

surface may also be responsible for the generation of ROS by serving as electron acceptor. In bacterial cells, silver ions would likely induce the generation of ROS by impairing the respiratory chain enzymes through direct interactions with thiol groups in these enzymes or the superoxide radical scavenging enzymes such as superoxide dismutases[52]. ROS generation from silver nanoparticles and silver ions may also be induced photocatalytically; however, no correlations have been reported between antibacterial action and photocatalytic ROS concentration[53].

Evidence of toxicity related to ROS generated from silver nanoparticles and silver ions released from or chemisorbed on their surface, has been shown previously. Kim et al. determined the existence of free radicals from silver nanoparticles by means of spin resonance measurements and silver nanoparticles and silver nitrate toxicity against *S. aureus* and *E. coli* was eliminated in the presence of an antioxidant[54]. Bactericidal activity of silver ions loaded in nanoporous materials such as zeolites has also been related to the generation of ROS. Using ROS scavengers, it was determined that superoxide anions, hydrogen peroxide, hydroxyl radicals, and singlet oxygen contributed to the antibacterial activity against *E. coli*[29].

Cell membrane damage: Silver nanoparticles interact with the bacterial membrane and are able to penetrate inside the cell. Transmission electron microscopy data show that silver nanoparticles adhere to and penetrate into *E. coli* cells and are also able to induce the formation of pits in the cell membrane[29, 42, 55]. Silver nanoparticles have been

14

observed within *E. coli* cells albeit at sizes much smaller than the original particles; moreover, silver nanoparticles with oxidized surfaces induce the formation of ''huge holes'' in *E. coli* surfaces after the interaction, and large portions of the cellular content seemed to be ''eaten away'' [26]. Accumulation on the cell membrane and uptake within the cell has also been reported for other bacteria such as *V. cholera*, *P. aeruginosa*, and *S. typhus* [56].

The detailed mechanism by which silver nanoparticles interact with cytoplasmic membranes and are able to penetrate inside cells has not been fully determined. One hypothesis is that the interaction between nanoparticles and bacterial cells are due to electrostatic attraction between negatively charged cell membranes and positively charged nanoparticles [25]. However, this mechanism does not likely explain the adhesion and uptake of negatively charged silver nanoparticles. It has also been proposed that the preferential sites of interaction for silver nanoparticles and membrane cells might be sulfur containing proteins—in a similar way as silver interacts with thiol groups of respiratory chain proteins and transport proteins, interfering with their proper function[56].

Another proposed mechanism of *E. coli* membrane damage by silver nanoparticles relates to metal depletion, i.e. the formation of irregular-shaped pits in the outer membrane and change in membrane permeability by the progressive release of LPS molecules and membrane proteins[55, 57]. This may be fairly general for gram-negative bacteria. It has been reported that extrusion pump systems such as Mex-AB-OprM system of *P.*

aeruginosa could also play an important role in controlling the accumulation of silver nanoparticles in living cells[58].

1.5.2   Silver resistance

Bacterial strains resistant to specific toxicants are naturally selected in environments where these agents are present[59]. In this way, the widespread use of silver, whether in nano or bulk form, could lead to selection of bacterial communities exhibiting silver resistance. Since most commercial uses of silver and silver nanoparticles relate to fighting infection, widespread silver resistance is a growing concern.

Although resistance is mainly encoded by plasmids, bacterial chromosomes have also been reported to encode Ag^+ resistance genes (sil) in strains such as *E. coli* K-12 and O157:H7[60]. The plasmid pMG101 has been studied in detail[60a, 61]; this plasmid has nine genes, whose products have been identified to be proteins responsible for heavy metal resistance. Here, the resistance is achieved by two efflux systems SilCBA and SilP acting in combination with two periplasmic binding proteins SilE and SilF. These two efflux pumps work jointly with proteins SilE and SilF, which bind to Ag^+. SilF is thought to act as a ''chaperone'' by taking one Ag^+ ion from its release site in SilP to its uptake site in SilCBA while SilE binds 5 Ag^+ ions to 10 histidines preventing silver ions entrance to the cytoplasm[54b].

Limited evidence has been reported of the resistance shown by silver-resistant strains to silver nanoparticles. In one study, it was reported that albumin-stabilized oxidized silver nanoparticles were unable to inhibit growth of 116 AgNO3R and J53 (pMG101) silver-resistant strains even when applied at a concentration of up to 80 nM[54a]. Therefore, it seems that silver resistance may also be of concern for the efficacy of silver nanoparticles as an antibacterial agent. Bacterial resistance and sensitivity to silver is affected by environmental conditions such as the presence of halides in the media mainly due to the variation of silver bioavailability experienced at different concentrations of Cl^- and other halides.

1.5.3   *Factors affecting the antibacterial properties of silver nanomaterials*

Several factors have been reported to influence silver nanoparticle toxicity like particle size, shape, crystallinity, surface chemistry, capping agents, as well as, environmental factors such as pH, ionic strength, and the presence of ligands, divalent cations, and macromolecules[26-27, 51, 53-54, 56, 62]. Many publications have shown size dependent toxicities of silver nanoparticles [51, 53, 56, 63]. As particle size decreases, the specific surface area increases leaving a higher number of atoms exposed on the surface available for redox, photochemical, and biochemical reactions in addition to physicochemical interactions with cells.

As discussed previously, one of the key mechanisms for silver nanomaterials to exert biocidal activity is through the release of silver ions. The rate of ion release, in general, is proportional to particle surface area, nanoparticles can release ions more rapidly than

larger particles and macroscopic materials. In effect, chemisorbed silver ions would be the cause of the antibacterial activity observed by Lok et al., who reported that only partially oxidized silver nanoparticles exhibit antibacterial activities, while zero valent silver nanoparticles do not[54a].

Stability of silver nanoparticles also influences toxicity since the formation of aggregates tends to decrease biocidal activity[64]. Different surfactants and polymers (e.g., sodium dodecyl sulfate, polyoxyethylene-sorbitan monooleate, polyvinylpyrrolidone, Na^+-carrying poly(glutamic acid), hydroxyl functionalized ionic liquids and hydroxyl functionalized cationic surfactants) have been used to stabilize silver nanoparticle dispersions and enhance biocidal activity[27, 65]. However, some ligand-capped silver nanoparticles—although highly stable and monodisperse in suspension—were less bioactive because the capping agent hindered release of silver ions[26].

Environmental conditions such as pH, ionic strength, presence of complexing agents, and natural organic matter, also affect the toxicity of silver nanoparticles. High salt concentrations and pH values close to the isoelectric point promote nanoparticle aggregation by screening electrical double layer repulsion[66]. However, water chemistry also governs silver dissolution and/or re-precipitation through various possible redox and precipitation reactions[54a]. Dissolved Ag^+ ions are sparingly soluble in the presence of various ligands such as chloride (pK = 9.75), sulfate (pK = 4.9), sulfide (pK = 49), hydroxide (pK = 7.8) and dissolved organic carbon (pK=7.5)[42, 67]. The released Ag^+ can

also form Ag^0 -containing clusters through light or chemical reduction[56]. Therefore, nanomaterials in aqueous suspensions must be considered in a continuous state of flux where the apparent speciation is controlled by the aquatic media pH, redox potential, ionic composition, and exposure to light.

Previously, cysteine ligands and chloride were used to scavenge or precipitate eluted silver ions from silver nanoparticles; thus, diminishing their toxicity [40]. Sulfide ligands have also been used to reduce the inhibition of silver nanoparticles to nitrifying bacteria[68]. More recently, it was reported that halide ions act as precipitating agents and profoundly affect the ''bioavailability'' of Ag^+ in unexpected ways[61]. For example, at low chloride concentrations, soluble Ag^+ binds to cell membranes impacting respiration and producing other toxics effects[69]. As chloride concentration increases, silver becomes less bioavailable because the solubility of AgCl is very low. However, further increase in halide concentration results in the formation of water-soluble anionic complexes in the form of $AgCl_2^-$ and $AgCl_3{}^{2-}$. These anionic complexes are more bioavailable and increase silver toxicity to both silver-sensitive and silver-resistant bacteria. Other halides such as Br^- and I^- have similar effects, but the concentrations at which ionic complexes form depends on their respective solubility limits.

1.6 Polyvinyl alcohol (PVA) use for antibacterial coatings

Polyvinyl alcohols are synthetic polymers widely use in industrial and commercial application. PVA has high chemical stability, high hydrophilicity and high water permeability, which makes it a good candidate for coating applications that pursue fouling resistant characteristics. Surface modification of membranes is an example of these applications; in this case, PVA is interesting because it can be tailored to produce fouling resistance and possible chorine tolerant membranes within tolerable flux declines. In addition, PVA is considered non-toxic because its lethal doses (LD50s) are high in the range 20g/Kg and it is poorly absorbed in the GI tract if ingested[70], making it suitable for drinking water fields.

Several studies have reported the use of PVA to produce more hydrophilic and smother membranes For instance, Zhang et al in 2008 observed that a PVA-coated polypropylene non-woven fabric cross-linked by a solution containing acetic acid, methanol, sulfuric acid and glutaraldehyde suffer lower flux decline and BSA fouling after the hydrophilic modification[71]. The authors reported that the increased hydrophilicity of the PVA-coated fabric was caused by the incorporation of C-O and C-O-C moieties that resulted in a decrease in the contact angles from $86 \pm 1°$ of the unmodified fabric, to $43 \pm 3°$ after PVA modification.

Polyethersulfone ultrafiltration membranes modified by adsorption-crosslinking of PVA experienced improved antifouling properties and higher hydrophilicities[16b]. Specifically, after the phase inversion process, the membranes were subsequently immersed in PVA followed by borax solutions. Higher cycles of PVA/borax immersions increased the adsorbed PVA concentration from 0 to 2 wt%, and decreased the contact

angles from 64.1° to 42.8°. The modification incorporated C-C and C-O moieties to the membrane surface, which were detected by XPS and would be partly responsible for the higher hydrophilicity.

PVA modification have been reported to decrease the roughness of ultrafiltration membranes. A coating of PVA on poly(vinylidene fluoride) ultrafiltration membranes, cross-linked by glutaralhdehyde in the vapor phase resulted in roughness membrane decrease of 50% (change from 16 to 8 nm). Additionally, the modification produced a more hydrophilic membrane, where water contact angle were reduction from 81°to 68°. The modified membrane produced a significantly lower flux decline after the filtration of both BSA protein and real river water containing humic substances and biopolymers [16a]. In a different research, the incorporation of PVA during interfacial polymerization of trimesoyl chloride and piperazine reduced the roughness of the polyamide nanofiltration membrane from 110.7 nm to 41.6 nm for a PVA/piperazine mass fraction of 16%. As PVA/PIP mass fraction increased, the membrane became smother, flux decline was lowe and better recoveries were recorded[15].

In another study PVA was utilized to form nanofiltration membranes. By dip-coating of ultrafiltration membrane in PVA and cross-linking it with succinic acid at different cross-linking degrees, the authors made defect-free thinfilm nanocomposite membranes that had high chemical stability[16c]. Film with these characteristics are desired because, they should experience low fouling and could have a good chlorine tolerance. The authors report that PVA films had high hydrophilicity with contact angles in the 25-32° range and presenting -C=O-O-C- groups after the cross-linking reaction. Films with higher cross-linking degree showed higher water permeabilities, what was attributed to

21

lower crystallinities of films crosslinked at a higher extent. The authors also reported that films formed with higher PVA molecular weights had higher crystallinities and subsequently showed lower permeabilities. In a different study by the same authors, PVA coating films formed using succinic acid as the cross-linking agent were use to evaluate bacterial adhesion. Higher cross-linking degrees produced more hydrophobic films and showed a higher bacterial attachment[72].

1.7   Membranes modified with nanomaterials to improve antifouling properties

In the last years, some research has been done regarding nanoparticles incorporation in membranes for fouling control. In general, the nanomaterials have been use to change the membrane properties and to produce more hydrophilic surfaces[73]. For example, thin film polyamide nanocomposite membranes incorporating NaA zeolite nanoparticles have shown not only to nearly double water permeability compared to hand-casted pure polyamide membranes, but to also produce more hydrophilic, negatively charged and smother membrane surfaces that eventually would be more fouling resistant. The authors concluded that water would preferentially flow through the super hydrophilic nanoparticles and the solute rejection would be maintained at similar levels[18].

Figure 1.2 shows the conceptual model of thin films nanocomposites (left) and TEM images indicating the location of the nanoparticles in the thin film. It can be clearly observed that the films incorporating zeolites are smoother, and this observation was also supported by the authors by roughness measurements done in AFM.
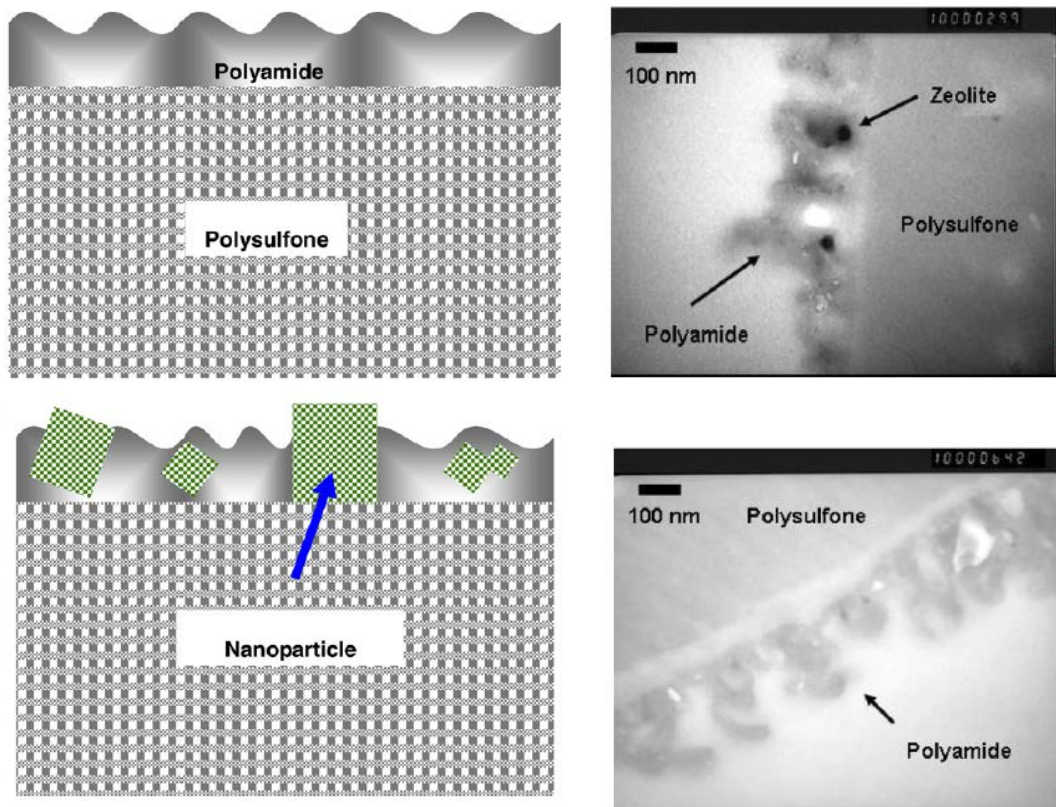
Figure 1.2   Conceptual illustration of thin film composite (top-left) and thin film nanocomposite (bottom-left) and corresponding TEM images. (Figures were taken from Jeong[18])

In subsequent works by the same group, other parameters such as zeolite crystal size and different cation loadings have been analyzed for these thin film nanocomposite membranes. When incorporating different crystal sizes it was observed that smaller crystal sizes (100nm) resulted in higher water permeabilities while thin films incorporating zeolite particles of 200 and 300 nm produced rougher surfaces but with lower contact angles and more negatively charged surfaces [74]. Zeolites exchanged with silver ions AgA instead of the typical sodium exchanged zeolite NaA used in the thin film nanocomposites were also investigated. AgA thin films had higher water

permeabilities at comparable NaCl and PEG rejections than the thin film nanocomposites incorporating NaA and thin film composites without nanoparticles. Moreover, the AgA nanocomposite presented biocidal effects against *P. putida*, although the bactericidal effect of AgA nanoparticles was significantly masked within the film[22].

Other nanomaterials have also been considered for biofouling, typically nanomaterials displaying some antimicrobial activity such as silver and TiO_2 nanoparticles. Silver nanoparticles show several antibacterial mechanisms, however, for their use in membranes the release of silver ions is the most exploited one. In this context, silver nanoparticles and silver ions have been use for cellulose acetate, polyimide, polyamide, polysulfone and poly(2-ethyl-2-oxazoline) membranes[75].

In the case of TiO_2, its antimicrobial properties are based on its photocatalytic action. When irradiated with UV greater than its band gap, energy-rich electron hole pairs are formed due to the transfer of one electron from the valence band gap to the conduction band. The reaction with water or oxygen can then lead to the formation of reactive oxygen species that can cause oxidative damage and posterior microbial inactivation[76]. TiO_2 antimicrobial action have been exploited in polyamide nanofiltration membranes[20a, 20b] and terylene microfiltration membranes[20c], among others.

Polyamide membranes incorporating silver nanoparticles during interfacial polymerization of MPD (1,3-phenylene diamine) and BTC (1,3,5-benzene tricarbonyl chloride) at a 10 wt% relative to the polymer showed almost no growth of *Pseudomonas* after 24 hr of incubation time. This considerable antibacterial activity is believed to be

able to enhance the lifetime of the membranes given that less chemical cleaning and feed chlorination would be required[21a].

In a study by Zodrow *et al*. silver nanoparticles were incorporated in polysulfone membranes during the wet phase inversion process. The authors observed that in terms of morphology, permeability and surface charge, the membranes containing silver nanoparticles were similar to the unmodified membranes. However, the membranes containing silver were 10% more hydrophilic, which could grant the membrane some fouling resistance. Furthermore, the membrane showed antibacterial properties, specifically reducing by 2 log *E. coli* growth after filtration and decreasing by 94% the bacterial attachment tested in membrane coupons immersed in an *E. coli* suspension.

Moreover, biofouling tests using P*seudomonas mendocina,* a prolific biofilm formation organism, showed almost no bacterial growth on the membrane and virus removal improvement was also observed. It was reported that silver ions released from the embedded nanoparticles were the responsible antibacterial agents and that only the silver nanoparticles close to the membrane surface, (about 10% of the loading) would participate on the antibacterial properties. A drawback from this application is that the antibacterial action was quickly lost because of the silver nanoparticles depletion from the membrane surface[21b].

Silver nanoparticles have also been coated on a RO membrane and RO spacer following a chemical reduction method. Both the modified membrane with unmodified spacer and the modified spacer with unmodified membrane showed slower permeate flux decline and lower decrease of TDS rejection than the case with unmodified membrane

and spacer. In terms of antimicrobial effect, the spacer coated with nanoparticles had longer lasting antibacterial effect than the membrane coated case. It was discussed that over time the membrane loses antibacterial activity because the residual biofilm formation will gradually block the release of silver ions. Conversely, the spacer would continue to release Ag^+ allowing a longer antibacterial effect[77].

TiO_2 nanoparticles incorporated in PVA thin films have been used to increase the hydrophilicity of nanofiltration membranes and to provide potential antibacterial characteristics. Because both PVA and TiO_2 have a large number of hydroxyl groups, it was expected that their incorporation would inherently improve the hydrophilicity of the membranes. It was observed that PVA hydrolysis degree was more important in the resulting hydrophilicity over PVA molecular weight or presence of TiO_2. Super hydrophilic membranes with increased salt rejection and good permeability were obtained using 88% hydrolysis degree PVA cross-linked with malic acid. Incorporation of TiO_2 did not further affect the hydrophilicity but increased the membrane roughness and decreased the pore size of the lower hydrolysis degree PVA membrane. However, TiO_2 did increase the hydrophilicity of the membrane prepared with the higher (98%) hydrolysis degree PVA[78].

1.8 Summary

Biofouling phenomenon starts from an initial bacterial adhesion, followed by bacteria replication and secretion of exopolysacharides forming a biofilm on a surface. If left unattended biofouling phenomena occur, which translates into higher requirements of energy, maintenance of the system and periodic replacement of membranes. The cost associated with biofouling issues in water treatment by membranes is between 25 to 50%

of the total operational cost[6]. Given that conventional biofouling control methods are not completely effective, new approaches need to be developed.

Preventing the initial bacteria adhesion before biofilm formation can occur is the key to control biofouling. For this, membrane surface modification including antifouling and antibacterial characteristics need to be developed.

1.9 Research hypothesis and objectives

My preliminary results and bibliographic review shows that silver, zinc and copper nanoparticles and nano size silver-exchanged zeolite have significant antibacterial qualities, being able to inactivate bacterial growth a low dosing rates. My bibliographic review also shows that PVA can be used to improve membrane hydrophilicity and roughness and that nanoparticles can be effectively embedded in it to provide the film with antibacterial or other desired properties.

My hypothesis is that, PVA films incorporating silver, copper and zinc exchanged zeolites nanoparticles, could be tailored to perform antiadhesive and antibacterial roles, which in combination would compose a fouling-resistant film. For a given PVA film chemistry, the zeolite loading represents the key parameter for this fouling-resistant film; increasing zeolite loading should increase the film hydrophilicity and the delivery of antibacterial agents but at the same time it should increase the film roughness promoting additional fouling.

In order to test the hypothesis the following objectives have been drawn. The first objective is to evaluate bacterial adhesion on PVA coating films considering the impacts

of bacterial cell type, PVA molecular weight, cross-linking agent, degree of cross-linking and to determine what PVA chemistry is more appropriated to produce an antiadhesive film. The second objective is to evaluate the antibacterial activity of the antibacterial nanonoparticles considering changes in solution chemistry and bacteria type. The third objective is to evaluate adhesion and inactivation behavior in PVA-nanoparticle nanocomposites.

To meet with this objectives this work is divided in four chapters. Chapter 1 is a review of biofouling phenomena and surface modification for biofouling control. In chapter two an evaluation of bacterial adhesion experiment in PVA films will be performed. In chapter three a comparison of the properties of the silver exchanged in zeolite and antibacterial nanoparticles is presented. Finally, chapter four evaluates both bacterial adhesion and inactivation on PVA-nanoparticle nanocomposites.

References

1. Shannon, M. A.; Bohn, P. W.; Elimelech, M.; Georgiadis, J. G.; Marinas, B. J.; Mayes, A. M., Science and technology for water purification in the coming decades. *Nature* **2008,** *452* (7185), 301-310.

2. Baker, R. W., *Membrane technology and applications*. 2nd ed.; J. Wiley: Chichester, New York, 2004.

3. Koros, W. J.; Ma, Y. H.; Shimidzu, T., Terminology for membranes and membrane processes. *Pure Appl Chem* **1996,** *68* (7), 1479-1489.

4. (a) Matin, A.; Khan, Z.; Zaidi, S. M. J.; Boyce, M. C., Biofouling in reverse osmosis membranes for seawater desalination: Phenomena and prevention. *Desalination* **2011,** *281*, 1-16; (b) Vrouwenvelder, J. S.; van Paassen, J. A. M.; Wessels, L. P.; van Dam, A. F.; Bakker, S. M., The Membrane Fouling Simulator: A practical tool for fouling prediction and control. *J Membrane Sci* **2006,** *281* (1–2), 316-324.

5. Flemming, H. C.; Schaule, G.; Griebe, T.; Schmitt, J.; Tamachkiarowa, A., Biofouling—the Achilles heel of membrane processes. *Desalination* **1997,** *113* (2–3), 215-225.

6. Ridgeway, H. F., *Biological Fouling of Separation Membranes Used in Water Treatment Applications*. AWWA Research Foundation, 2003.

7. Al-Ahmad, M.; Aleem, F. A. A.; Mutiri, A.; Ubaisy, A., Biofuoling in RO membrane systems Part 1: Fundamentals and control. *Desalination* **2000,** *132* (1-3), 173-179.

8. Characklis, W. G. and K. C. Marshall, Eds. *Biofilms*; Wiley: New York, 1990.

9. (a) Saad, M. A., Biofouling prevention in RO polymeric membrane systems. *Desalination* **1992,** *88* (1–3), 85-105; (b) Polanska, M.; Huysman, K.; van Keer, C., Investigation of assimilable organic carbon (AOC) in flemish drinking water. *Water Res* **2005,** *39* (11), 2259-2266.

10. Richardson, S. D., Disinfection by-products and other emerging contaminants in drinking water. *Trac-Trend Anal Chem* **2003,** *22* (10), 666-684.

11. Lehtola, M. J.; Miettinen, I. T.; Vartiainen, T.; Rantakokko, P.; Hirvonen, A.; Martikainen, P. J., Impact of UV disinfection on microbially available phosphorus,

organic carbon, and microbial growth in drinking water. *Water Res* **2003,** *37* (5), 1064-1070.

12.   Loge, F. J.; Darby, J. L.; Tchobanoglous, G., UV disinfection of wastewater: Probabilistic approach to design. *J Environ Eng-Asce* **1996,** *122* (12), 1078-1084.

13.   Xiong, Y. H.; Liu, Y., Biological control of microbial attachment: a promising alternative for mitigating membrane biofouling. *Applied Microbiology and Biotechnology* **2010,** *86* (3), 825-837.

14.   Kim, M.-m.; Lin, N. H.; Lewis, G. T.; Cohen, Y., Surface nano-structuring of reverse osmosis membranes via atmospheric pressure plasma-induced graft polymerization for reduction of mineral scaling propensity. *J Membrane Sci* **2010,** *354* (1-2), 142-149.

15.   An, Q.; Li, F.; Ji, Y.; Chen, H., Influence of polyvinyl alcohol on the surface morphology, separation and anti-fouling performance of the composite polyamide nanofiltration membranes. *J Membrane Sci* **2011,** *367* (1-2), 158-165.

16.   (a) Du, J. R.; Peldszus, S.; Huck, P. M.; Feng, X. S., Modification of poly(vinylidene fluoride) ultrafiltration membranes with poly(vinyl alcohol) for fouling control in drinking water treatment. *Water Res* **2009,** *43* (18), 4559-4568; (b) Ma, X. L.; Su, Y. L.; Sun, Q.; Wang, Y. Q.; Jiang, Z. Y., Enhancing the antifouling property of polyethersulfone ultrafiltration membranes through surface adsorption-crosslinking of poly(vinyl alcohol). *J Membrane Sci* **2007,** *300* (1-2), 71-78; (c) Peng, F. B.; Huang, X. F.; Jawor, A.; Hoek, E. M. V., Transport, structural, and interfacial properties of poly (vinyl alcohol)-polysulfone composite nanofiltration membranes. *J Membrane Sci* **2010,** *353* (1-2), 169-176.

17.   Ba, C.; Ladner, D. A.; Economy, J., Using polyelectrolyte coatings to improve fouling resistance of a positively charged nanofiltration membrane. *J Membrane Sci* **2010,** *347* (1-2), 250-259.

18.   Jeong, B. H.; Hoek, E. M. V.; Yan, Y. S.; Subramani, A.; Huang, X. F.; Hurwitz, G.; Ghosh, A. K.; Jawor, A., Interfacial polymerization of thin film nanocomposites: A new concept for reverse osmosis membranes. *J Membrane Sci* **2007,** *294* (1-2), 1-7.

19.   Subramani, A.; Huang, X. F.; Hoek, E. M. V., Direct observation of bacterial deposition onto clean and organic-fouled polyamide membranes. *J Colloid Interf Sci* **2009,** *336* (1), 13-20.

20.   (a) Kim, S. H.; Kwak, S.-Y.; Sohn, B.-H.; Park, T. H., Design of TiO2 nanoparticle self-assembled aromatic polyamide thin-film-composite (TFC) membrane as an approach to solve biofouling problem. *J Membrane Sci* **2003,** *211* (1), 157-165; (b) Lee, H. S.; Im, S. J.; Kim, J. H.; Kim, H. J.; Kim, J. P.; Min, B. R., Polyamide thin-film nanofiltration membranes containing TiO2 nanoparticles. *Desalination* **2008,** *219* (1-3), 48-56; (c) Liu, L.; Xiao, L.; Yang, F., Terylene membrane modification with Polyrotaxanes, TiO_2 and Polyvinyl alcohol for better antifouling and adsorption property. *J Membrane Sci* **2009,** *333* (1-2), 110-117.

21.   (a) Lee, S. Y.; Kim, H. J.; Patel, R.; Im, S. J.; Kim, J. H.; Min, B. R., Silver nanoparticles immobilized on thin film composite polyamide membrane: characterization, nanofiltration, antifouling properties. *Polymers for Advanced Technologies* **2007,** *18* (7), 562-568; (b) Zodrow, K.; Brunet, L.; Mahendra, S.; Li, D.; Zhang, A.; Li, Q. L.; Alvarez, P. J. J., Polysulfone ultrafiltration membranes impregnated with silver nanoparticles show improved biofouling resistance and virus removal. *Water Res* **2009,** *43* (3), 715-723.

22.   Lind, M. L.; Jeong, B. H.; Subramani, A.; Huang, X. F.; Hoek, E. M. V., Effect of mobile cation on zeolite-polyamide thin film nanocomposite membranes. *J Mater Res* **2009,** *24* (5), 1624-1631.

23.   Marambio-Jones, C.; Hoek, E. M. V., A review of the antibacterial effects of silver nanomaterials and potential implications for human health and the environment. *J Nanopart Res* **2010,** *12* (5), 1531-1551.

24.   Vertelov, G.; Krutyakov, Y.; Efremenkova, O.; Olenin, A.; Lisichkin, G., A versatile synthesis of highly bactericidal Myramistin® stabilized silver nanoparticles. *Nanotechnology* **2008,** *19* (35).

25.   Raffi, M.; Hussain, F.; Bhatti, T.; Akhter, J.; Hameed, A.; Hasan, M., Antibacterial characterization of silver nanoparticles against *E. coli* ATCC-15224. *J Mater Sci Technol* **2008,** *24* (2), 192-196.

26.   Smetana, A.; Klabunde, K.; Marchin, G.; Sorensen, C., Biocidal activity of nanocrystalline silver powders and particles. *Langmuir* **2008,** *24* (14), 7457-7464.

27.   Kvitek, L.; Panacek, A.; Soukupova, J.; Kolar, M.; Vecerova, R.; Prucek, R.; Holecova, M.; Zboril, R., Effect of surfactants and polymers on stability and antibacterial activity of silver nanoparticles (NPs). *J Phys Chem C* **2008,** *112* (15), 5825-5834.

28. Yoon, K.; Byeon, J.; Park, J.; Ji, J.; Bae, G.; Hwang, J., Antimicrobial characteristics of silver aerosol nanoparticles against Bacillus subtilis bioaerosols. *Environ Eng Sci* **2008,** *25* (2), 289-293.

29. Inoue, Y.; Hoshino, M.; Takahashi, H.; Noguchi, T.; Murata, T.; Kanzaki, Y.; Hamashima, H.; Sasatsu, M., Bactericidal activity of Ag-zeolite mediated by reactive oxygen species under aerated conditions. *J Inorg Biochem* **2002,** *92* (1), 37-42.

30. Cowan, M.; Abshire, K.; Houk, S.; Evans, S., Antimicrobial efficacy of a silver-zeolite matrix coating on stainless steel. *J Ind Microbiol Biot* **2003,** *30* (2), 102-106.

31. Balogh, L.; Swanson, D.; Tomalia, D.; Hagnauer, G.; McManus, A., Dendrimer-silver complexes and nanocomposites as antimicrobial agents. *Nano Lett* **2001,** *1* (1), 18-21.

32. Zhang, Y.; Peng, H.; Huang, W.; Zhou, Y.; Yan, D., Facile preparation and characterization of highly antimicrobial colloid Ag or Au nanoparticles. *J Colloid Interf Sci* **2008,** *325* (2), 371-376.

33. Tomsic, B.; Simoncic, B.; Orel, B.; Zerjav, M.; Schroers, H.; Simoncic, A.; Samardzija, Z., Antimicrobial activity of AgCl embedded in a silica matrix on cotton fabric. *Carbohyd Polym* **2009,** *75* (4), 618-626.

34. Kim, K.; Sung, W.; Moon, S.; Choi, J.; Kim, J.; Lee, D., Antifungal effect of silver nanoparticles on dermatophytes. *J Microbiol Biotechn* **2008,** *18* (8), 1482-1484.

35. Kim, K.; Sung, W.; Suh, B.; Moon, S.; Choi, J.; Kim, J.; Lee, D., Antifungal activity and mode of action of silver nano-particles on *Candida albicans*. *Biometals* **2009,** *22* (2), 235-242.

36. Roe, D.; Karandikar, B.; Bonn-Savage, N.; Gibbins, B.; Roullet, J., Antimicrobial surface functionalization of plastic catheters by silver nanoparticles. *J Antimicrob Chemoth* **2008,** *61* (4), 869-876.

37. Kim, J.; Kuk, E.; Yu, K.; Kim, J.; Park, S.; Lee, H.; Kim, S.; Park, Y.; Park, Y.; Hwang, C.; Kim, Y.; Lee, Y.; Jeong, D.; Cho, M., Antimicrobial effects of silver nanoparticles. *Nanomed-Nanotechnol* **2007,** *3* (1), 95-101.

38. Elechiguerra, J.; Burt, J.; Morones, J.; Camacho-Bragado, A.; Gao, X.; Lara, H.; Yacaman, M., Interaction of silver nanoparticles with HIV-1. *J Nanobiotechnol* **2005,** *3* (1477-3155), 6.

39. Sun, L.; Singh, A.; Vig, K.; Pillai, S.; Singh, S., Silver nanoparticles inhibit replication of Respiratory Syncytial Virus. *J Biomed Nanotechnol* **2008,** *4* (2), 149-158.

40. Navarro, E.; Piccapietra, F.; Wagner, B.; Marconi, F.; Kaegi, R.; Odzak, N.; Sigg, L.; Behra, R., Toxicity of Silver Nanoparticles to *Chlamydomonas reinhardtii. Environ Sci Technol* **2008,** *42* (23), 8959-8964.

41. Asharani, P. V.; Mun, G. L. K.; Hande, M. P.; Valiyaveettil, S., Cytotoxicity and Genotoxicity of Silver Nanoparticles in Human Cells. *Acs Nano* **2009,** *3* (2), 279-290.

42. Choi, O.; Deng, K.; Kim, N.; Ross, L.; Surampalli, R.; Hu, Z., The inhibitory effects of silver nanoparticles, silver ions, and silver chloride colloids on microbial growth. *Water Res* **2008,** *42* (12), 3066-3074.

43. (a) Dibrov, P.; Dzioba, J.; Gosink, K.; Hase, C., Chemiosmotic mechanism of antimicrobial activity of Ag$^+$ in *Vibrio cholerae. Antimicrob Agents Ch* **2002,** *46* (8), 2668-2670; (b) Holt, K.; Bard, A., Interaction of silver(I) ions with the respiratory chain of *Escherichia coli*: An electrochemical and scanning electrochemical microscopy study of the antimicrobial mechanism of micromolar Ag. *Biochemistry-US* **2005,** *44* (39), 13214-13223; (c) Lok, C.; Ho, C.; Chen, R.; He, Q.; Yu, W.; Sun, H.; Tam, P.; Chiu, J.; Che, C., Proteomic analysis of the mode of antibacterial action of silver nanoparticles. *J Proteome Res* **2006,** *5* (4), 916-924.

44. Schreurs, W.; Rosenberg, H., Effect of silver ions on transport and retention of phosphate by *Escherichia-coli. J Bacteriol* **1982,** *152* (1), 7-13.

45. Liau, S.; Read, D.; Pugh, W.; Furr, J.; Russell, A., Interaction of silver nitrate with readily identifiable groups: relationship to the antibacterial action of silver ions. *Lett Appl Microbiol* **1997,** *25* (4), 279-283.

46. Yang, W.; Shen, C.; Ji, Q.; An, H.; Wang, J.; Liu, Q.; Zhang, Z., Food storage material silver nanoparticles interfere with DNA replication fidelity and bind with DNA. *Nanotechnology* **2009,** *20* (8).

47. (a) Feng, Q.; Wu, J.; Chen, G.; Cui, F.; Kim, T.; Kim, J., A mechanistic study of the antibacterial effect of silver ions on *Escherichia coli* and *Staphylococcus aureus. J*

Biomed Mater Res **2000,** *52* (4), 662-668; (b) Jung, W.; Koo, H.; Kim, K.; Shin, S.; Kim, S.; Park, Y., Antibacterial activity and mechanism of action of the silver ion in *Staphylococcus aureus* and *Escherichia coli*. *Appl Environ Microb* **2008,** *74* (7), 2171-2178.

48.   Nel, A.; Xia, T.; Madler, L.; Li, N., Toxic potential of materials at the nanolevel. *Science* **2006,** *311* (5761), 622-627.

49.   Mendis, E.; Rajapakse, N.; Byun, H.; Kim, S., Investigation of jumbo squid (Dosidicus gigas) skin gelatin peptides for their in vitro antioxidant effects. *Life Sci* **2005,** *77* (17), 2166-2178.

50.   Stohs, S. J.; Bagchi, D., Oxidative Mechanisms In The Toxicity Of Metal-Ions. *Free Radic Biol Med* **1995,** *18* (2), 321-336.

51.   Carlson, C.; Hussain, S. M.; Schrand, A. M.; Braydich-Stolle, L. K.; Hess, K. L.; Jones, R. L.; Schlager, J. J., Unique Cellular Interaction of Silver Nanoparticles: Size-Dependent Generation of Reactive Oxygen Species. *J Phys Chem B* **2008,** *112* (43), 13608-13619.

52.   Park, H.; Kim, J.; Kim, J.; Lee, J.; Hahn, J.; Gu, M.; Yoon, J., Silver-ion-mediated reactive oxygen species generation affecting bactericidal activity. *Water Res* **2009,** *43* (4), 1027-1032.

53.   Choi, O.; Hu, Z., Size dependent and reactive oxygen species related nanosilver toxicity to nitrifying bacteria. *Environmental Science and Technology.* **2008,** *42* (12), 4583-4588.

54.   (a) Lok, C.; Ho, C.; Chen, R.; He, Q.; Yu, W.; Sun, H.; Tam, P.; Chiu, J.; Che, C., Silver nanoparticles: partial oxidation and antibacterial activities. *J Biol Inorg Chem* **2007,** *12* (4), 527-534; (b) Gupta, A.; Matsui, K.; Lo, J. F.; Silver, S., Molecular basis for resistance to silver cations in *Salmonella*. *Nat Med* **1999,** *5* (2), 183-188.

55.   Sondi, I.; Salopek-Sondi, B., Silver nanoparticles as antimicrobial agent: a case study on E-coli as a model for Gram-negative bacteria. *J Colloid Interf Sci* **2004,** *275* (1), 177-182.

56.   Morones, J.; Elechiguerra, J.; Camacho, A.; Holt, K.; Kouri, J.; Ramirez, J.; Yacaman, M., The bactericidal effect of silver nanoparticles. *Nanotechnology* **2005,** *16* (10), 2346-2353.

57.   Amro, N.; Kotra, L.; Wadu-Mesthrige, K.; Bulychev, A.; Mobashery, S.; Liu, G., High-resolution atomic force microscopy studies of the *Escherichia coli* outer membrane: Structural basis for permeability. *Langmuir* **2000,** *16* (6), 2789-2796.

58.   Xu, X.; Brownlow, W.; Kyriacou, S.; Wan, Q.; Viola, J., Real-time probing of membrane transport in living microbial cells using single nanoparticle optics and living cell imaging. *Biochemistry-US* **2004,** *43* (32), 10400-10413.

59.   Gupta, A.; Silver, S., Molecular genetics - Silver as a biocide: Will resistance become a problem? *Nat Biotechnol* **1998,** *16* (10), 888-888.

60.   (a) Gupta, A.; Phung, L. T.; Taylor, D. E.; Silver, S., Diversity of silver resistance genes in IncH incompatibility group plasmids. *Microbiol-Sgm* **2001,** *147*, 3393-3402; (b) Silver, S.; Phung, L. T.; Silver, G., Silver as biocides in burn and wound dressings and bacterial resistance to silver compounds. *J Ind Microbiol Biot* **2006,** *33* (7), 627-634.

61.   Silver, S., Bacterial silver resistance: molecular biology and uses and misuses of silver compounds. *Fems Microbiol Rev* **2003,** *27* (2-3), 341-353.

62.   Pal, S.; Tak, Y.; Song, J., Does the antibacterial activity of silver nanoparticles depend on the shape of the nanoparticle? A study of the gram-negative bacterium *Escherichia coli*. *Appl Environ Microb* **2007,** *73* (6), 1712-1720.

63.   Martinez-Castanon, G. A.; Nino-Martinez, N.; Martinez-Gutierrez, F.; Martinez-Mendoza, J. R.; Ruiz, F., Synthesis and antibacterial activity of silver nanoparticles with different sizes. *J Nanopart Res* **2008,** *10* (8), 1343-1348.

64.   (a) Teeguarden, J.; Hinderliter, P.; Orr, G.; Thrall, B.; Pounds, J., Particokinetics in vitro: Dosimetry considerations for in vitro nanoparticle toxicity assessments. *Toxicol Sci* **2007,** *95* (2), 300-312; (b) Shrivastava, S.; Bera, T.; Roy, A.; Singh, G.; Ramachandrarao, P.; Dash, D., Characterization of enhanced antibacterial effects of novel silver nanoparticles. *Nanotechnology* **2007,** *18* (22).

65.   Yu, D., Formation of colloidal silver nanoparticles stabilized by Na+-poly(gamma-glutamic acid)-silver nitrate complex via chemical reduction process. *Colloid Surface B* **2007,** *59* (2), 171-178.

66.   Nel, A. E.; Madler, L.; Velegol, D.; Xia, T.; Hoek, E. M. V.; Somasundaran, P.; Klaessig, F.; Castranova, V.; Thompson, M., Understanding biophysicochemical interactions at the nano-bio interface. *Nat Mater* **2009,** *8* (7), 543-557.

67. Gao, J.; Youn, S.; Hovsepyan, A.; Llaneza, V. L.; Wang, Y.; Bitton, G.; Bonzongo, J. C. J., Dispersion and Toxicity of Selected Manufactured Nanomaterials in Natural River Water Samples: Effects of Water Chemical Composition. *Environ Sci Technol* **2009,** *43* (9), 3322-3328.

68. Choi, O.; Cleuenger, T.; Deng, B.; Surampalli, R.; Ross, L.; Hu, Z., Role of sulfide and ligand strength in controlling nanosilver toxicity. *Water Res* **2009,** *43* (7), 1879-1886.

69. Gupta, A.; Maynes, M.; Silver, S., Effects of halides on plasmid-mediated silver resistance in Escherichia coli. *Appl Environ Microb* **1998,** *64* (12), 5042-5045.

70. DeMerlis, C. C.; Schoneker, D. R., Review of the oral toxicity of polyvinyl alcohol (PVA). *Food and Chemical Toxicology* **2003,** *41* (3), 319-326.

71. Zhang, C.-H.; Yang, F.-l.; Wang, W.-J.; Chen, B., Preparation and characterization of hydrophilic modification of polypropylene non-woven fabric by dip-coating PVA (polyvinyl alcohol). *Separation and Purification Technology* **2008,** *61* (3), 276-286.

72. Peng, F. B.; Hoek, E. M. V.; Damoiseaux, R., High-Content Screening for Biofilm Assays. *J Biomol Screen* **2010,** *15* (7), 748-754.

73. Ng, L. Y.; Mohammad, A. W.; Leo, C. P.; Hilal, N., Polymeric membranes incorporated with metal/metal oxide nanoparticles: A comprehensive review. *Desalination* (0).

74. Lind, M. L.; Ghosh, A. K.; Jawor, A.; Huang, X. F.; Hou, W.; Yang, Y.; Hoek, E. M. V., Influence of Zeolite Crystal Size on Zeolite-Polyamide Thin Film Nanocomposite Membranes. *Langmuir* **2009,** *25* (17), 10139-10145.

75. (a) Chou, W. L.; Yu, D. G.; Yang, M. C., The preparation and characterization of silver-loading cellulose acetate hollow fiber membrane for water treatment. *Polymers for Advanced Technologies* **2005,** *16* (8), 600-607; (b) Damm, C.; Muensted, H.; Roesch, A., Long-term antimicrobial polyamide 6/silver-nanocomposites. *Journal of Materials Science* **2007,** *42* (15), 6067-6073; (c) Deng, Y.; Dang, G.; Zhou, H.; Rao, X.; Chen, C., Preparation and characterization of polyimide membranes containing Ag nanoparticles in pores distributing on one side. *Materials Letters* **2008,** *62* (6-7), 1143-1146.

76. (a) Cho, M.; Chung, H.; Choi, W.; Yoon, J., Linear correlation between inactivation of E-coli and OH radical concentration in TiO2 photocatalytic disinfection. *Water Res* **2004,** *38* (4), 1069-1077; (b) Gumy, D.; Morais, C.; Bowen, P.; Pulgarin, C.; Giraldo, S.; Hajdu, R.; Kiwi, J., Catalytic activity of commercial of TiO2 powders for the abatement

of the bacteria (E-coli) under solar simulated light: Influence of the isoelectric point. *Applied Catalysis B-Environmental* **2006,** *63* (1-2), 76-84; (c) Yao, Y.; Ohko, Y.; Sekiguchi, Y.; Fujishima, A.; Kubota, Y., Self-sterilization using silicone catheters coated with Ag and TiO2 nanocomposite thin film. *Journal of Biomedical Materials Research Part B-Applied Biomaterials* **2008,** *85B* (2), 453-460.

77.   Yang, H.-L.; Lin, J. C.-T.; Huang, C., Application of nanosilver surface modification to RO membrane and spacer for mitigating biofouling in seawater desalination. *Water Res* **2009,** *43* (15), 3777-3786.

78.   Nguyen, V.; Hoek, E. M. V., Modifying The Separation Properties of Nanofiltration Membranes by Poly(vinyl alcohol) and TiO_2 Nanomaterials. *Submitted to Journal of Membrane Science* **2011**.

CHAPTER II

EVALUATION OF BACTERIAL ADHESION ON POLYVINYL ALCOHOL

COATING FILMS

2.1   Introduction

Bacteria cells and their extracellular products can attach firmly to almost any surface of man-made or natural origin[1]. Immobilized cells grow, reproduce, and produce extra-cellular polymers, which leads to biofilm formation. Biofilms cause major medical problems since the extracellular matrix probably protect the bacteria from phagocytosis and host immune responses[2]. Biofilms also cause rejection of medical devices and implants[15], hospitalization related infections, contaminate drinking water in the distribution system[3], and cause operational problems for power plant cooling towers, marine vessels, water filters and desalination processes. The generally accepted stages in the development of a biofilm are: (1) initial transport and deposition, (2) more permanent adhesion or release, (3) proliferation and extracellular polymeric substances (EPS) production, and (4) sloughing or trans-location. The unwanted deposition and growth of a biofilm in any system is referred to as biofouling.

Biofouling-resistant surfaces are highly sought after, as are compounds that modulate biofilm formation, where the key step is the initial attachment of bacteria cells to a substrate surface (*a.k.a.*, primary adhesion), which ultimately leads to cells growth, replication, coordination of adhered cells in fully formed biofilms [4]. Primary adhesion is governed by cell-substrate physicochemical interactions and is largely reversible (over short time periods) by simple physical and chemical perturbations (*e.g.*, hydraulic flushing or chemical cleaning). In many systems, primary adhesion of bacteria cells may be preceded by adsorption of dissolved organic matter of biological and geological origins, which alter membrane surface properties possibly making bacterial adhesion more favorable [5].

Hence, truly anti-fouling surfaces must resist primary adhesion of organic matter and bacteria cells [6]. It is well established that non-polar surfaces encourage adsorption of organic and biological matter in water via hydrophobic attraction, whether natural organic compounds such as humic and fulvic acids [7] or microbial matter [8]. The highly polar nature of polyvinyl alcohol (PVA) minimizes fouling in such applications because a great deal of attractive energy is needed to displace adsorbed water molecules strongly bound to PVA. However, because of its hydrophilic nature, PVA must be modified to limit swelling when intended for use in aquatic membrane separations.

A burgeoning literature exists on the stabilization of PVA films for aquatic applications [9]. The stability of cross-linked PVA in highly acidic or highly alkaline environments has been demonstrated [10]. There has been a continuing effort in the biotechnology area to use PVA membranes for protein recovery [11], as well, PVA gels have been studied extensively as biomaterials for artificial kidney and pancreas, glucose sensors, immuno-isolation membranes, artificial cartilage, contact lenses and drug delivery systems[12]. Methods of improving the mechanical integrity of PVA include freezing, heat treatment, irradiation, and chemical cross-linking. Chemically cross-linked PVA films (and membranes) show high physical and chemical stability, and exhibited different surface chemical structure because of different chemical structure of cross-linking agents [13].

This chapter focus on biofilm formation on polymeric films in aquatic media representing freshwater, wastewater and seawater. The impacts of PVA chemistry on hydrophilicity and bacterial adhesion is analyzed. For this, a combinatorial array of dicarboxylic acid cross-linked PVA film compositions were prepared with varying degree

of polymerization, hydrolysis and cross-linking. In addition, PVA films were prepare with cross-linking agents that offer different functional groups with the objective of elucidate how different molecular heterogeneity and specific chemical interactions affect the hydrophilicity of the films and the bacterial attachment. Specifically, eight different dicarboxylic acid cross-linking agents that introduced different functional groups such as -OH, -SH, -NH$_2$ were utilized. Bacterial adhesion assays employed three water matrices, each evaluated with and without a complex mixture of organic macromolecules for both gram-negative and gram-positive bacteria cell types. All film casting and bacterial adhesion tests were performed directly in 384-well microplates enabling high throughput screening (HTS) of the entire combinatorial matrix of cross-linked PVA film compositions, bacteria cell types, and water chemistries.

2.2   Materials and methods

2.2.1   *Aquatic media and bacterial suspension preparation*

Three aquatic matrices were prepared with compositions designed to represent: (1) fresh surface water, (2) secondary wastewater effluent, and (3) seawater. These are three water types often treated with polymeric membranes in practical applications like drinking water treatment, wastewater reclamation and seawater desalination. For each aquatic matrix type, two composition were prepared, the first, "inorganic recipe" contains only inorganic components, shown in Table 2.1. The second, "organic recipe" contains organic matter in addition to the components listed in the table. Specifically, the organic recipe was prepared by adding 17 mg/L alginate acid, 12.8 mg/L bovine serum albumin (BSA) and 12.5 mg/L tannic acid to the inorganic matrix for a total organic carbon content of 20mg/L. The pH value of all water chemistries was adjusted to 7.0 by

41

addition of HCl or NaOH. All chemicals were ACS reagent grade or better and used as received (Fisher Scientific, Pittsburgh, PA).

Table 2.1   Inorganic composition of representative aquatic media

	Freshwater	Wastewater	Seawater
Na^+	14.4	212.6	9624.8
Mg^{2+}	7.0	25.5	1146.6
Ca^{2+}	40.0	78.6	368.0
K^+	2.4	16.0	356.3
NH_4^+	-	20.7	-
Sr^{2+}	-	-	7.2
Cl^-	22.0	239.0	17290.7
SO_4^{2-}	104.0	393.4	2422.9
HCO_3^-	29.0	64.1	112.5
NO_3^-	-	52.5	-
Br^-	-	-	60.1
F^-	-	-	1.2
H_3BO_3	-	-	23.0
Ionic strength (M)	0.0056	0.0235	0.7145
Total dissolved solids	218.9	1049.8	31329.0

Model microorganisms used in this study included *Pseudomonas putida* (provided by Dr. Patricia Holden at UC Santa Barbara), which is a gram-negative aerobic bacterium cultured in tryptic soy broth (TSB), and *Bacillus subtilis*, which is a gram-positive aerobic bacteria cultured in Luria–Bertani broth (LB)[3c]. Pure bacterial cell cultures were suspended in TSB or LB media and shaken at 150 rpm in an incubator at 25 °C. Cells were harvested at mid-exponential phase by centrifugation at 3,800 g. Pelletized cells were washed twice using phosphate buffered saline (PBS) solution and centrifugation, then obtained cells were washed using either freshwater, wastewater, or seawater matrices depending on the experiment and resuspended in the given water matrix. Bacterial suspension then were normalized to 10^9 cells per liter using a hemocytometer following the procedure described previously by Kang *et al.*[14] and immediately utilized in

the adhesion test assay (section 2.2.3). A total of twelve bacterial suspension were prepare in this manner, the 2 bacterial strains *B. subtilis* and *P. putida* in the six aquatic matrices, *i. e.*, freshwater, wastewater and seawater inorganic and organic recipes.

2.2.2 *Polyvinyl alcohol films casting*

Mowiol® PVA 4-88, 5-88, 8-88, 4-98, 6-98 and 10-98,whose properties are shown in Table 2.2, were utilized to cast the PVA films. PVA powders were purchased from Sigma-Aldrich Company (Sigma–Aldrich, St. Louis, Missouri, USA) except Mowiol® PVA 5-88 that was supplied as free sample by Kuraray Co. Ltd (Chiyoda-ku, Tokyo, Japan). Oxalic acid, succinic acid, maleic acid, malic acid, aspartic acid, mercaptosuccinic acid, diglycolic acid, and suberic acid (> 99%, Sigma–Aldrich, St. Louis, Missouri, USA) were used as cross-linking agents.

Table 2.2   Physicochemical properties of PVA used to cast the films

PVA	Viscocity mPa·s*	Hydrolysis degree %	Polymerization degree	Molecular weight (kDa)
Mowiol® 4-88	4.0 ± 1.0	87.7 ± 1.0	630	31
Mowiol® 5-88	5.5 ± 0.5	87.7 ± 1.0	1000	43
Mowiol® 8-88	8.0 ± 1.0	87.7 ± 1.0	1400	67
Mowiol® 4-98	4.5 ± 0.5	98.4 ± 0.4	600	27
Mowiol® 6-98	6.0 ± 1.0	98.4 ± 0.4	1000	47
Mowiol® 10-98	10 ± 1.0	98.4 ± 0.4	1400	61

PVA powder was dissolved under mechanically stirring in deionized water (DI) at 90 °C. Unless otherwise specified, the PVA concentration was 0.10 wt%. Next, PVA solutions were cooled to room temperature and the cross-linking agent was added from a 10% (w/v) solution; subsequently the pH was adjusted to 2.5 using 2M HCl. The resulting solution was then kept under continuous stirring in a wrist shaker for at least 30 min to

produce the PVA casting solution. Cross-linking agent concentration was selected to produce a theoretical cross-linking degree, which was defined by

$$\chi_{CL}[\%] = \frac{W_{CL} \times MW_{PVAunit} \times 2}{W_{PVA} \times MW_{CL}} \times 100 \qquad \qquad 2.1$$

where W_{CL}, W_{PVA}, $MW_{PVA\ unit}$, and MW_{CL} represented the weight of cross-linking agent, the weight of PVA, the molecular weight of one PVA unit (—CHOH–CH$_2$—), and the molecular weight of the cross-linking agent, respectively.

The casting solution was then dispensed in polystyrene black/clear bottom 384 well microplate (Cat # 781091, Greiner Bio One, Frickenhausen, Germany), 50 µL PVA casting solution per well were dispensed using an automated dispenser (Multidrop 384, Thermo Scientific, Williston, VT, USA). Each microplate was designed to content two different films one in the top half of the plate (rows 1 to 8) and one in the bottom half (rows 9 to 16). Then, the aqueous casting solution was air-dried at room temperature for 24 h (in a closed sterile chamber), followed by curing in a laboratory oven at 100 °C for 10 minutes.

2.2.3 High throughput screening adhesion assay

In order to study the bacterial adhesion to the PVA films, the adhesion assay previously discussed by Peng *et. al.* was utilized [13a]. This assay consists in four steps: (1) PVA coating film preparation, (2) biofilm formation, (3) biofilm staining, and (4) imaging and analysis.

Subsequently to the PVA coating film preparation (described in section 2.2.2), step 2 was performed by adding 50 µL of bacterial suspension (see section 2.2.1) to each

well of a 384 well plate using a Biomek FX (Beckman Coulter, Indianapolis, IN). For this, each microplate was designed to contain the 2 bacterial strains and the six water chemistry tested. The microplate design included also control wells where pure aquatic matrices, no bacteria were added.

The microplates were incubated for 24 hours at 30 °C followed by the dyeing process to quantify the total cell adhesion . The molecular probe SYTO-9 from (LIVE/DEAD® BacLightTM Bacterial Viability Kits, Invitrogen, Carlsbad, CA, USA) was dissolved in 30 mL sterile DI water to achieve a concentration of 2μM. Subsequently, a multidrop 384 was utilized to dispense 10 μL of the dye into each well and the microplates were incubated for 20 min at room temperature. To determine total bacterial adhesion, fluorescence imaging was perform of the PVA films located on the bottom of the microplate wells via a Image-Xpress Micro (Molecular Devices, Sunnyvale, CA, USA) using image based focusing. Afterward, each well was washed three times with 100 μL DI water using an ELX405 Microplate Washer (BIO-TEK Instruments, Inc., Winooski, VT, USA) and re-imaged to quantify the irreversible fraction of bacterial adhesion. Images were processed in MetaXpress 1.74R software (Molecular Devices, Sunnyvale, CA, USA) using the "Multiple Wavelength Cell Scoring" module. The total number of adhered cells in the field of view resulted from the SYTO-9 channel. The approximate minimum width was set to 10 μm, and the approximate maximum to 30 μm and the intensity above background was 1,000 gray levels.

2.2.4   Determination of interfacial tension and surface free energy of adhesion and cohesion

Two helpful parameters to characterize the interaction of a material, such a PVA film surface with its surrounding aquatic media and potential biofoulants, i.e. bacterial cells, are the free energy of cohesion ΔG_{131} and adhesion ΔG_{132}. The free energy of cohesion or hydrophilicity indicates the relative attraction between molecules of the same material versus the attraction that this material has for water. If the material has a higher attraction for water molecules than for alike molecules, then the material considered hydrophilic, if it has a higher attraction for itself then is hydrophobic. Typically, hydrophilic materials have been linked to antifouling properties, since in order for a foulant to attach to an hydrophilic surface the energy of hydration needs to be overcame. However, a more suitable indicator of fouling, or specifically biofouling, is the free energy of adhesion ΔG_{132}, since this parameter indicates the relative attraction of a material to the specific fouling agent compared to water (or the aquatic media in which the interaction occurs) If ΔG_{132} is positive . A schematic representation of hydrophilicity and adhesion propensity is depicted

$\Delta G_{131} > 0$ Hydrophilic repulsion
$\Delta G_{131} < 0$ Hydrophobic attraction

$\Delta G_{132} > 0$ No adhesion propensity
$\Delta G_{132} < 0$ Adhesion propensity
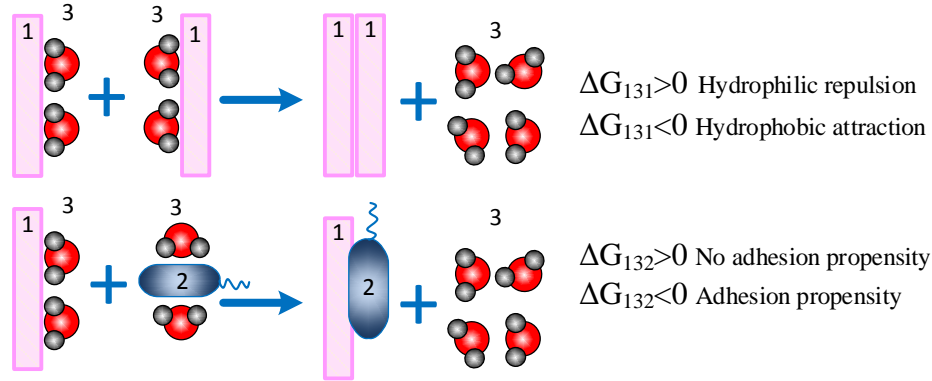
Figure 2.1   Schematic representation of free energy of cohesion and free energy of adhesion. Material 1 represent a surface, 2 presents a foulant, for instance a bacterial cell and 3 the aquatic media, typically water, where 1 and 2 are immerse.

The free energy of adhesion can be estimated based on the interaction forces between the material and the fouling agent surfaces. Specifically, it is required to calculate the work required to maintain the adhesion between the film surface and the bacterial cell . This work depends not only on the materials at interaction but on the media in which the materials are immerse. The subscripts 1, 2, represent, in this case, the PVA film surface and bacterial cells and 3 refers to the aquatic media in which they are immerse.

The free energy of adhesion can be expressed in terms of the interfacial tension (γ_{ij}) by means of Dupre equation [15] as follow,

$$\Delta G_{132} = \gamma_{12} - \gamma_{13} - \gamma_{23} \qquad\qquad 2.2$$

Similarly, the interaction of particles of material 1, immerse in liquid 3, i.e. free energy of cohesion is estimated from equation 2.3

$$\Delta G_{131} = -2\gamma_{13} \qquad\qquad 2.3$$

The interfacial tension γ_{ij} consists of apolar or lifshitz-van der Waals (γ_{ij}^{LW}) and polar acid base (γ_{ij}^{AB}) interactions , which are given by the following expressions:

$$\gamma_{ij} = \gamma_{ij}^{LW} + \gamma_{ij}^{AB}$$

2.4

$$\gamma_{ij}^{LW} = \left(\sqrt{\gamma_i^{LW}} - \sqrt{\gamma_j^{LW}} \right)^2$$

2.5

$$\gamma_{ij}^{AB} = 2\left(\sqrt{\gamma_i^+ \gamma_i^-} + \sqrt{\gamma_j^+ \gamma_j^-} - \sqrt{\gamma_i^+ \gamma_j^-} - \sqrt{\gamma_i^- \gamma_j^+} \right)$$

2.6

$$\Rightarrow \gamma_{ij} = \gamma_{ij}^{LW} + \gamma_{ij}^{AB} = \left(\sqrt{\gamma_i^{LW}} - \sqrt{\gamma_j^{LW}} \right)^2 + 2\left(\sqrt{\gamma_i^+ \gamma_i^-} + \sqrt{\gamma_j^+ \gamma_j^-} - \sqrt{\gamma_i^+ \gamma_j^-} - \sqrt{\gamma_i^- \gamma_j^+} \right)$$

2.7

Where γ_i^+ and γ_i^- are the electron acceptor and electron donor parameters of the surface tension of material i. Then ΔG_{131} and ΔG_{132} can be determined if the apolar and polar components of the films, cells and aquatic media are known. The following expression, find by van Oss replacing Dupré's equation with the interfacial tensions expressions, shows this relationship.

$$\begin{aligned}
\Delta G_{132} = 2[&\sqrt{\gamma_1^{LW} \gamma_3^{LW}} + \sqrt{\gamma_2^{LW} \gamma_3^{LW}} - \sqrt{\gamma_1^{LW} \gamma_2^{LW}} \\
&- \gamma_3^{LW} + \sqrt{\gamma_3^+}\left(\sqrt{\gamma_1^-} + \sqrt{\gamma_2^-} - \sqrt{\gamma_3^-} \right) + \\
&\sqrt{\gamma_3^-}\left(\sqrt{\gamma_1^+} + \sqrt{\gamma_2^+} - \sqrt{\gamma_3^+} \right) - \sqrt{\gamma_1^+ \gamma_2^-} - \sqrt{\gamma_1^- \gamma_2^+}]
\end{aligned}$$

2.8

Similarly the free energy of cohesion is obtained from the following expression,

$$\Delta G_{131} = -2\left(\sqrt{\gamma_1^{LW}} - \sqrt{\gamma_3^{LW}} \right)^2 - 4\left(\sqrt{\gamma_1^+ \gamma_1^-} + \sqrt{\gamma_3^+ \gamma_3^-} - \sqrt{\gamma_1^+ \gamma_3^-} - \sqrt{\gamma_1^- \gamma_3^+} \right)$$

2.9

In order to determine the surface tension's polar and apolar components of PVA films and the bacteria cells, Young-Dupré equation is utilized. Young, in 1805, described the relation between the contact angle θ form by a droplet on a solid surface (see Figure 2.2), with the surface γ_i and interfacial tensions γ_{ij} of the liquid and the solid (equation 2.10). Subsequently, Dupré in 1869 showed that the work of adhesion ΔG_{13} between a liquid and the solid, was a function of their surface and interfacial tensions (equation 2.11) . Combination of these two equations results ins the Young-Dupré equation below (equation 2.12).

$$\gamma_3 \cos\theta = \gamma_1 - \gamma_{13} \tag{2.10}$$

$$\Delta G_{13} = \gamma_{13} - \gamma_1 - \gamma_3 \tag{2.11}$$

$$\Delta G_{13} = -\gamma_3 \left(1 + \cos\theta\right) \tag{2.12}$$
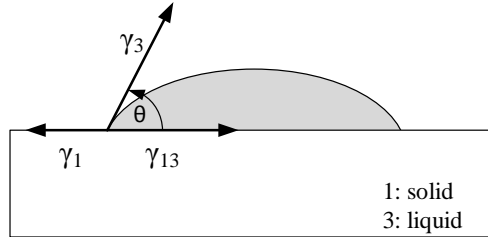
Figure 2.2   Schematic describing Young's equation, depicting liquid's surface tension γ_3, solid's surface tension γ_1 and solid-liquid interfacial tension γ_{13}

An extended version of Young-Dupré equation is obtained as discussed by van Oss when incorporating the polar and apolar components of the liquid surface tension,

$$\left(1 + \cos\theta\right)\gamma_3 = 2\left(\sqrt{\gamma_1^{LW}\gamma_3^{LW}} + \sqrt{\gamma_1^+\gamma_3^-} + \sqrt{\gamma_1^-\gamma_3^+}\right) \tag{2.13}$$

This equation allows the estimation of the polar and apolar components of the solid surface from the contact angles of 3 liquids, with known acid base electron-donor γ_3^-, electron-acceptor γ_3^+, and apolar γ_3^{LW} components, while $\gamma_3 = \gamma_3^{LW} + \gamma_3^{AB} = \gamma_3^{LW} + 2\sqrt{\gamma_3^+ \gamma_3^-}$. One of these liquid probes must be apolar $(\gamma_3 = \gamma_3^{LW})$ and the other 2 must be polar liquids. Once the 3 independents contact angles are measured, equation 2.13 can be used to determine the tension components of the solid, $\gamma_1^{LW}, \gamma_1^+, \gamma_1^-$ by solving a 3 by 3 equation system.

In order to determine the surface and interfacial tension components for the PVA films the contact angle of glycerol, diiodomethane and the aquatic media (see section 2.2.1) were measure on the surface of the films casted on glass slides. A sessile drop method was adopted and an automated contact angle goniometer (DSA10 KRÜSS GmbH, Hamburg, Germany) was utilized to perform the measurements . A minimun of 12 equilibrium contact angles were determined for each liquid and film and the highest and lowest values discarded. The average of the remaining left and right contact angles was taken as the equilibrium contact angle.

2.3   Results and Discussions

2.3.1   *Free energy of cohesion and adhesion of the films in different water chemistries*

Cross-linked PVA films and bacterial cell contact angles of water, glycerol and diiodomethane together with the estimated LW and acid base components of the films surface tensions and wettability are reported in Table 2.3. The contact angle data of all six water matrices (FW inorganics, FW organics, WW inorganics, WW organics, SW

inorganics and SW organics) on the PVA films are reported in appendix 2A. As expected all PVA cross-linked films resulted highly wettable, i.e, ΔG_{13} of all films was higher than 72.8 mJ/m^2, which corresponds to a water contact angle of 90°C. It is well known, that PVA is very wettable due to plenty of hydroxyl groups in PVA polymer chain; the wettability observed in the cross-linked PVA may originate from unreacted, residual PVA hydroxyl and carboxyl groups due to incomplete cross-linking reaction [13b].

The PVA films electron donor components of the surface free energy were significantly higher than the electron acceptor component for all films (refer to Table 2A.3 to A.6 in appendix 3A). This is a positive feature to prevent bacterial attachment because acid base interaction of the films with bacteria, which have mainly electron donor functionalities, are minimized and therefore bacterial adhesion is less favorable.

Table 2.3   Contact angle data, surface tension and wettability of PVA films

Solid/Liquid Substrate	Raw/Measured Values			Intrinsic Substrate Properties					Wettability
	θ_{water} (deg)	$\theta_{glycerol}$ (deg)	$\theta_{diiodomethane}$ (deg)	γ^{LW} (mJ/m^2)	γ^{+} (mJ/m^2)	γ^{-} (mJ/m^2)	γ^{AB} (mJ/m^2)	γ^{TOT} (mJ/m^2)	$-\Delta G_{13}$ (mJ/m^2)
diiodomethane	n/a	n/a	n/a	50.8	0.0	0.0	0.0	50.8	n/a
glycerol	n/a	n/a	n/a	34.0	3.9	57.4	29.9	63.9	n/a
water	n/a	n/a	n/a	21.8	25.5	25.5	51.0	72.8	n/a
P. putida	29.6 ± 3.1	35.9 ± 2.0	42.4 ± 3.9	38.4	0.0	61.9	1.9	40.3	136.1
B. subtilis	20.7 ± 4.2	22.5 ± 0.9	47.2 ± 1.3	35.8	0.2	64.0	6.7	42.5	140.9
4-88 succinic, 20%	31.0 ± 2.2	60.6 ± 0.8	33.0 ± 1.2	42.9	0.8	67.7	14.7	57.7	135.2
5-88 succinic, 20%	20.5 ± 1.1	63.9 ± 0.8	33.9 ± 3.3	42.5	1.9	86.4	25.4	67.9	141.0
8-88 succinic, 20%	27.5 ± 1.6	60.3 ± 1.5	35.8 ± 0.7	41.6	0.8	72.6	15.0	56.6	137.4
4-98 succinic, 20%	44.8 ± 1.9	44.5 ± 2.4	44.2 ± 1.6	37.4	1.1	31.5	11.8	49.3	124.4
6-98 succinic, 10%	41.4 ± 2.6	46.8 ± 3.6	36.3 ± 0.8	41.4	0.3	37.2	6.9	48.3	127.4
6-98 succinic, 20%	42.1 ± 1.8	41.8 ± 0.6	41.1 ± 0.5	39.0	1.1	32.6	12.2	51.2	126.8
6-98 succinic, 40%	42.1 ± 1.3	41.3 ± 1.5	37.2 ± 0.6	41.0	1.0	31.9	11.2	52.2	126.8
6-98 succinic, 80%	37.1 ± 1.9	37.3 ± 1.0	32.6 ± 1.8	43.1	1.0	34.9	11.6	54.7	130.9
6-98 Maleic, 20%	37.9 ± 1.8	43.1 ± 3.4	36.0 ± 0.9	41.5	0.5	38.6	8.9	50.5	130.2
6-98 Malic, 20%	43.8 ± 2.9	44.5 ± 2.6	34.8 ± 2.0	42.1	0.6	31.9	8.6	50.7	125.4
6-98 Aspartic, 20%	30.1 ± 4.4	41.2 ± 1.5	38.8 ± 0.3	40.2	0.5	47.0	9.9	50.2	135.8
6-98 Mercaptosuccinic, 20%	42.9 ± 5.8	40.8 ± 1.0	38.4 ± 0.4	40.4	1.2	30.6	12.0	52.3	126.2
6-98 Dyglycolic, 20%	36.7 ± 1.6	39.5 ± 1.3	37.4 ± 0.4	40.9	0.9	37.4	11.7	52.6	131.2
6-98 Oxalic, 20%	43.9 ± 1.8	42.8 ± 1.6	38.3 ± 1.7	40.4	0.9	30.9	10.8	51.2	125.3
6-98 Suberic, 20%	42.0 ± 1.4	45.3 ± 0.4	36.4 ± 0.6	41.4	0.5	35.1	8.2	49.6	126.9
10-98 Succinic, 20%	42.8 ± 2.7	44.9 ± 2.3	31.1 ± 2.3	43.7	0.4	33.2	7.1	50.8	126.2

(Note: *P. putida* and *B. subtilis* contact angles taken from Subramani [3c, 16]
Surface tension properties of probe liquids data taken from van Oss [15]

Free energies of cohesion and adhesion data for the films in all six aquatic media and water are summarized from Tables 2.4 to 2.6, while the respective LW and acid base surface tension and free energies components are presented in appendix 2A. When the free energy of cohesion is negative a material is considered hydrophilic. Table 2.4 show that all the films, can be classified as hydrophilic ($\Delta G_{131} > 0$) if the immersion liquid is pure water. However, when immerse in the different electrolytes more films behave in a hydrophobic manner. For example the PVA film cross-linked with maleic acid, would be classified hydrophilic material if only water contact angle are considered. However, in every other aquatic media maleic acid shows a negative free energy of cohesion.

When averaging the free energy of cohesion across all the films for an specific aquatic media, it was found that seawater organic recipe holds the lowest ΔG_{131} average followed closely by the seawater inorganic media. Also, in average, the films behaved less hydrophilic in the organic containing aquatic media.

The free energy of adhesion of all films versus both bacterial strains tested was positive in all six aquatic matrices with the exception of the films cross-linked with maleic acid when immersed seawater inorganic, freshwater and wasterwater organic recipes (and in seawater organic media ΔG_{132} value was very small). In the same way as with the hydrophilicities values, free energies of cohesion was on average smaller, when the media contained organics or had high ionic strength. In average the seawater inorganic media produced in average the lowest ΔG_{132}.

52

Table 2.4   Free energy of cohesion (ΔG_{131} (mJ/m^2)) in different water matrices

ΔG_{131} (mJ/m^2)	4-88 20% succinic	5-88 20% succinic	8-88 20% succinic	4-98 20% succinic	6-98 10% succinic	6-98 20% succinic	6-98 40% succinic	6-98 80% succinic	6-98 20% Maleic	6-98 20% Malic acid	6-98 20% Aspartic	6-98 20% Mercaptosuccinic	6-98 20% Dyglycolic	6-98 20% Oxalic	6-98 20% Suberic	10-98 20% succinic
water	45.7	55.7	51.5	4.7	12.5	5.5	3.7	6.7	13.9	3.7	25.6	2.0	11.5	2.6	9.0	5.1
FW inorganics	54.8	53.8	52.4	7.6	7.1	10.7	17.7	2.5	**-5.5**	13.6	**-13.9**	7.6	23.0	9.6	3.6	**-1.9**
WW inorganics	55.2	55.4	51.2	11.4	**-4.8**	14.6	19.6	6.6	**-22.4**	12.5	16.7	2.8	29.7	4.1	4.5	0.8
SW inorganics	46.7	52.0	47.9	8.6	**-1.4**	**-2.5**	17.7	3.2	**-32.2**	**-4.8**	14.3	0.1	19.3	**-7.4**	8.0	**-4.6**
FW organics	51.9	54.5	51.3	5.4	0.3	10.6	16.9	7.4	**-44.8**	3.9	27.2	10.3	27.7	4.7	2.4	**-2.1**
WW organics	51.0	54.9	51.1	9.6	1.8	4.5	6.6	3.6	**-39.8**	9.5	27.2	6.2	25.7	2.0	**-0.5**	**-3.3**
SW organics	47.5	52.5	48.2	**-0.7**	**-5.8**	**-0.4**	**-0.2**	4.1	**-26.5**	6.9	12.4	8.4	21.3	**-0.7**	9.9	**-4.2**

Table 2.5   Free energy of adhesion (ΔG_{132} (mJ/m^2)) for the films and *P. putida* in different water matrices.

ΔG_{132} (mJ/m^2)	4-88 20% succinic	5-88 20% succinic	8-88 20% succinic	4-98 20% succinic	6-98 10% succinic	6-98 20% succinic	6-98 40% succinic	6-98 80% succinic	6-98 20% Maleic	6-98 20% Malic acid	6-98 20% Aspartic	6-98 20% Mercaptosuccinic	6-98 20% Dyglycolic	6-98 20% Oxalic	6-98 20% Suberic	10-98 20% succinic
water	49.0	56.9	52.3	23.6	30.2	24.1	23.5	25.6	30.5	24.6	37.1	22.0	28.3	22.8	27.8	26.1
FW inorganics	55.1	55.4	52.8	25.5	26.9	27.6	32.5	22.8	17.8	30.7	10.2	25.8	35.5	27.5	24.4	21.7
WW inorganics	55.4	56.7	52.1	28.1	19.3	30.1	33.6	25.5	5.1	30.0	31.7	22.5	39.4	23.9	25.0	23.4
SW inorganics	49.6	54.0	50.0	26.2	21.5	18.4	32.4	23.2	**-3.4**	19.0	30.1	20.7	33.2	15.9	27.2	19.9
FW organics	53.1	56.0	52.1	24.0	22.6	27.5	31.9	26.0	**-16.2**	24.7	38.0	27.5	38.3	24.3	23.6	21.6
WW organics	52.5	56.3	52.0	26.9	23.6	23.4	25.4	23.5	**-10.8**	28.2	38.0	24.9	37.1	22.5	21.8	20.8
SW organics	50.1	54.4	50.2	19.8	18.6	20.0	20.8	23.8	1.7	26.6	28.9	26.3	34.5	20.6	28.3	20.2

Table 2.6   Free energy of adhesion (ΔG_{132} (mJ/m^2))for the films and *B. subtilis* in different water matrices.

ΔG_{132} (mJ/m^2)	4--88 20% succinic	5--88 20% succinic	8--88 20% succinic	4--98 20% succinic	6--98 10% succinic	6--98 20% succinic	6--98 40% succinic	6--98 80% succinic	6--98 20% Maleic	6--98 20% Malic acid	6--98 20% Aspartic	6--98 20% Mercaptosuccinic	6--98 20% Dyglycolic	6--98 20% Oxalic	6--98 20% Suberic	10--98 20% succinic
water	49.0	56.2	52.1	24.9	31.5	25.5	24.9	27.0	31.7	26.1	37.9	23.5	29.5	24.3	29.2	27.7
FW inorganics	54.6	54.8	52.6	26.8	28.4	28.8	33.5	24.3	19.6	31.9	12.3	27.1	36.4	28.7	25.9	23.5
WW inorganics	54.9	56.0	51.9	29.2	21.1	31.1	34.6	26.9	7.5	31.3	32.7	24.0	40.1	25.3	26.5	25.1
SW inorganics	49.6	53.5	50.0	27.4	23.2	20.0	33.5	24.7	**-0.6**	20.8	31.2	22.2	34.2	17.7	28.6	21.8
FW organics	52.8	55.3	52.0	25.3	24.3	28.7	33.0	27.3	**-12.8**	26.2	38.7	28.8	39.0	25.7	25.2	23.4
WW organics	52.2	55.6	51.8	28.1	25.2	24.8	26.8	25.0	**-7.7**	29.6	38.7	26.2	37.9	24.0	23.4	22.6
SW organics	50.1	53.9	50.2	21.3	20.5	21.5	22.4	25.3	4.2	28.0	30.1	27.6	35.4	22.2	29.7	22.1

2.3.2   *Effect of cross-linking degree on bacterial adhesion*

Succinic acid was used as the cross-linking agent in the following investigation of the impact of cross-linking degree on the bacteria adhesion properties of PVA films. Four different films were prepared utilizing Mowiol 6-98 PVA (Refer to Table 2.2) and cross-linked with succinic acid to obtain theoretical cross-linking degrees of 10%, 20%, 40% and 80%.

Total adhesion and irreversible adhesion of *P. putida* and *B. subtilis* was analyzed for the four different films in fresh, waste and seawater inorganic and organic aquatic media. Most of the initially adhered bacteria either in inorganic or organic water matrices was removed after a simple water rinse, what shows that the films are not too prone to biofouling. The study showed that in most cases both total and irreversible bacterial adhesion increased as cross-linking degree increased from 10% to 80%. The exceptions were *B. subtilis* irreversible bacterial adhesion in freshwater organic media and *P. putida*

total adhesion in seawater organic media (Figure 2.3), what could be explained by experimental variability. The increase trend of bacterial attachment as cross-linked degree increased was more pronounced in freshwater and wastewater than in seawater. In seawater, this positive correlation existed but it was less strong than in the other two cases.
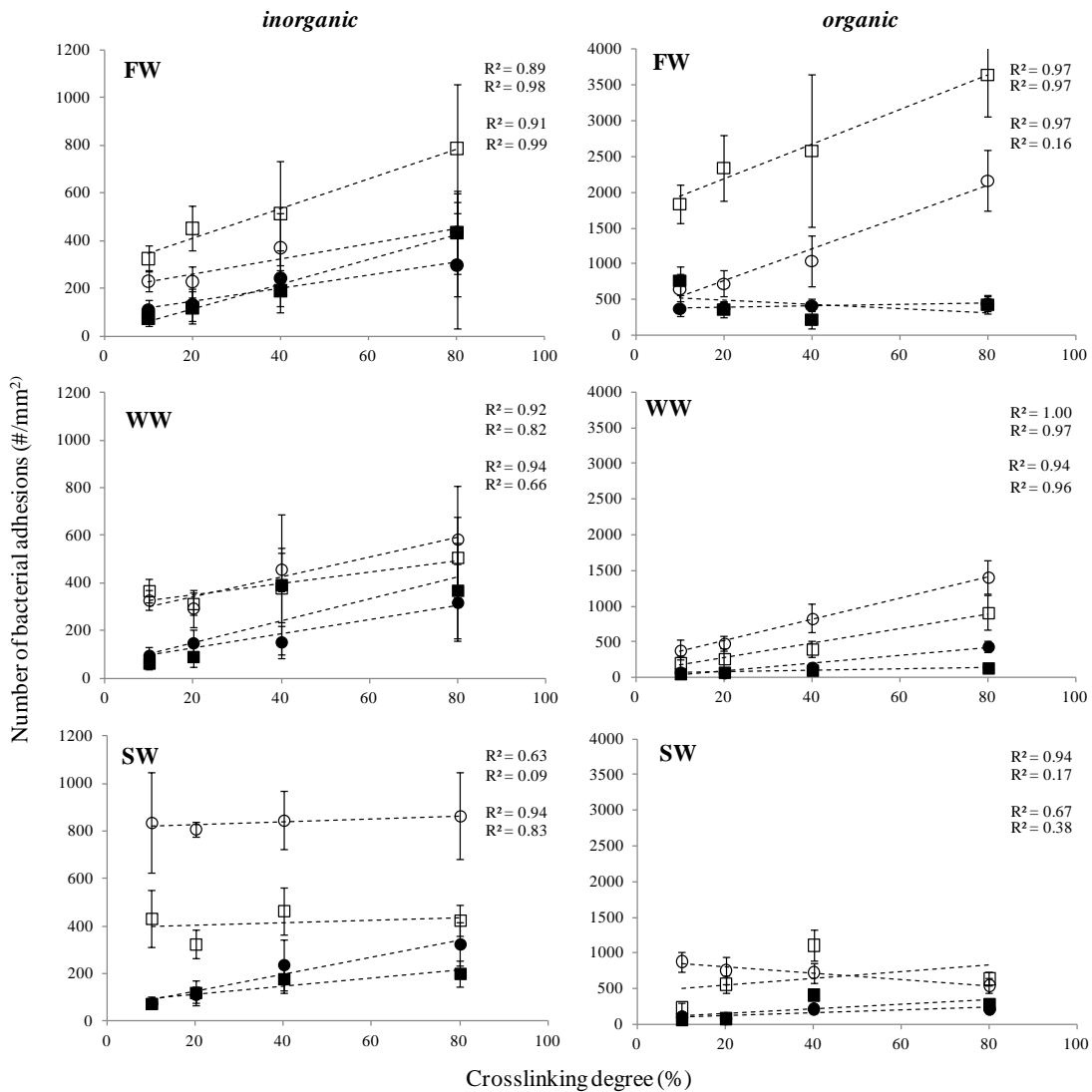
Figure 2.3 Impacts of PVA degree of crosslinking on bacterial adhesion on freshwater (FW), wastewater (WW) and seawater (SW) inorganic and organic matrices. Total adhesion (white symbols) and irreversible (black symbols) for *P. putida* (circles) and *B. subtilis* (squares).

55

2.3.3   *Effect of PVA molecular weight and hydrolysis degree on bacterial adhesion*

Figure 2.4 and Figure 2.5 show the bacterial adhesion on PVA films casted using 600, 1000, 1400 degrees of polymerization, which produce average molecular weights of 30, 45 and 60 kDa, for two different degrees of hydrolysis 87.7% and 98.4 %. Previous research showed that lower molecular weight PVA produced more hydrophilic surfaces and more hydrophilic surfaces would be more fouling resistance [13b] . However, based on the contact angle analysis in this study lower molecular weights did not always translated in higher hydrophilicity nor higher free energy of adhesions. Moreover, differences in %PVA molecular weight did not play an strong impact on bacterial attachment.

On the other hand, the PVA hydrolysis degree seems to have a more strong impact in the number of adhesions. Apparently, lower PVA hydrolysis degree (87.7%) produced less total adhesion and, especially, very small irreversible bacteria adhesion when compared to films made from 98.4% hydrolysis degree PVA. However, the presence of organics in the water matrices had a higher influence in the bacterial adhesion behavior, decreasing the difference of bacterial attachment between low and high hydrolysis.

Polyvinyl alcohol that is 87.7% hydrolyzed has residual acetyl content of $10.8\pm0.8\%$ w/w and ester value 140 ± 10 mg-KOH/g, while 98.4% hydrolyzed PVA has $1.5\pm0.4\%$ w/w and 20 ± 5 mg-KOH/g respectively[17]. Therefore, less hydrolyzed PVA has less functionality to form hydrogen bonds than more hydrolyzed PVA. At first, this may appear counter-intuitive because hydrophilicity is often associated with hydrogen bonding ability. However, previous research [13b] and the contact angle analysis performed in this research showed that electron donor functionality decreased with PVA

56

hydrolysis state. In another words the difference between electron donor and electron acceptor components in films of 87.7% hydrolysis is higher than in films with 98.4% , thus the first ones are closer to a monopolar electron-donor functionality. Mixed electron-donor/electron-acceptor functionality can produce a type of "hydrophobic attraction," whereas monopolar electron-donor functionality gives rise to the most fouling resistant interfaces as previously described by van Oss, Whitesides and others [15] [18].
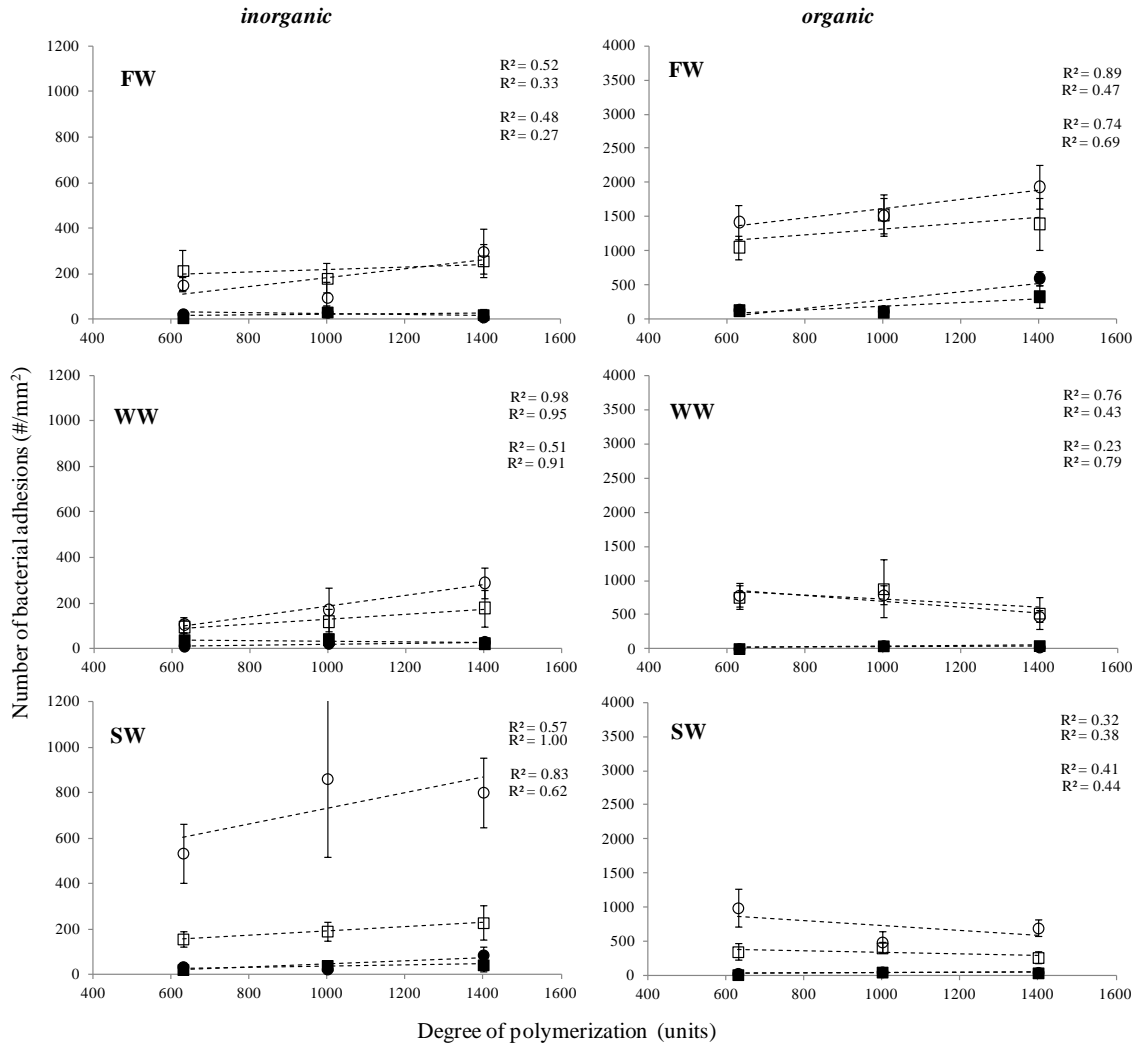
Figure 2.4   Impacts of PVA degree of polymerization (i.e., molecular weight) on bacterial adhesion on films with 87.7% hydrolysis degree for freshwater (FW), wastewater (WW) and seawater (SW) inorganic and organic matrices. Total adhesion (white symbols) and irreversible (black symbols) for *P. putida* (circles) and *B. subtilis* (squares).
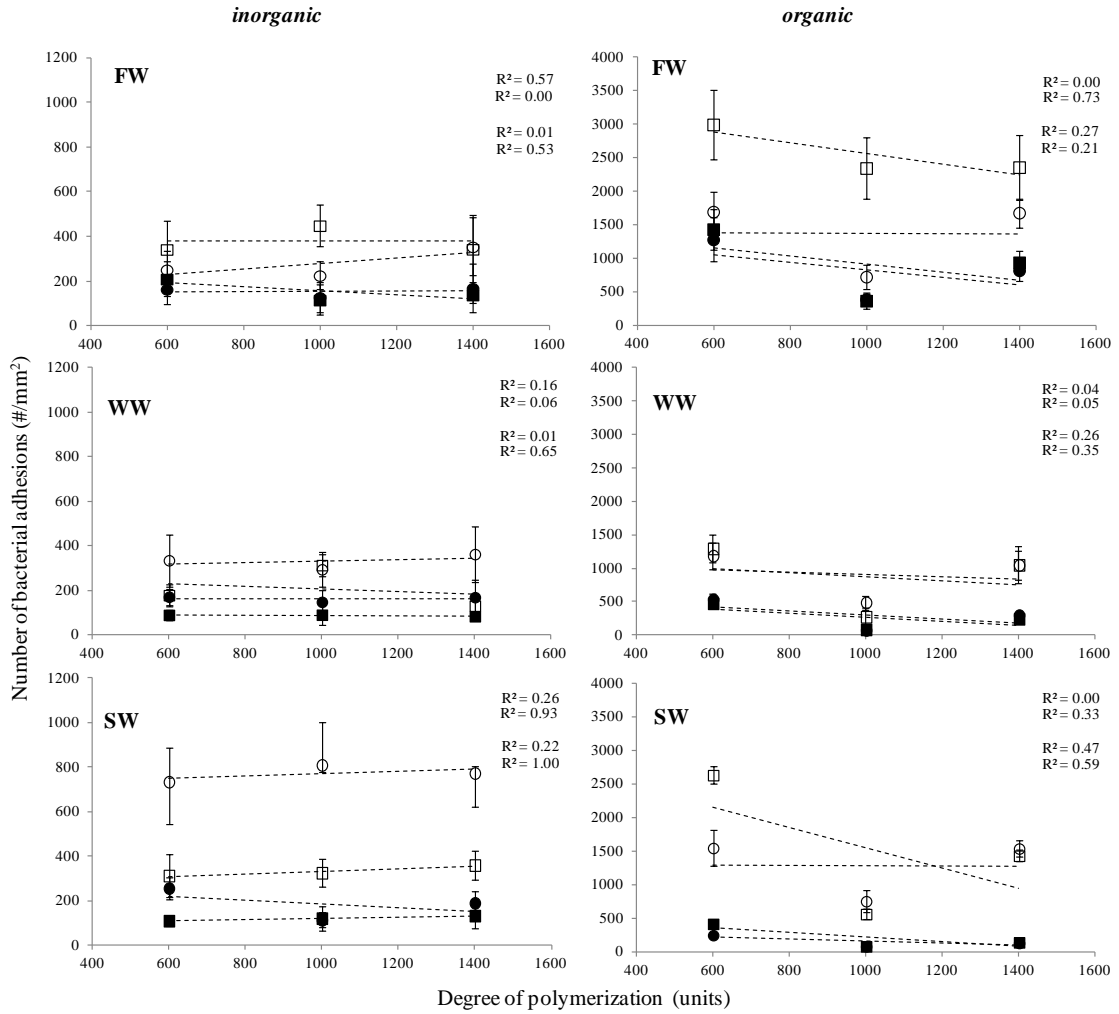
Figure 2.5   Impacts of PVA degree of polymerization (i.e., molecular weight) on
bacterial adhesion on films with 98.4% hydrolysis degree for freshwater
(FW), wastewater (WW) and seawater (SW) inorganic and organic matrices.
Total adhesion (white symbols) and irreversible (black symbols) for *P. putida*
(circles) and *B. subtilis* (squares).

2.3.4   Effect of cross-linking agent on bacterial adhesion

Cross-linked PVA (Mowiol 6-98) films were prepared with eight different cross-linking agents (oxalic, succinic, maleic, malic, aspartic, mercaptosuccinic, diglycolic, and suberic acid) at a cross-linking degree of 20%. The cross-linking agents were selected to present different lengths (i.e., number of carbon atoms) and functional groups. Oxalic, succinic, and suberic acids contain 2, 4, and 8 carbon atoms, respectively. Maleic acid (-C=C-), malic acid (-OH), aspartic acid ($-NH_2$), mercaptosuccinic acid (-SH) and diglycolic acid (-O-) have the same carbon atom number as succinic acid, but offer new functional groups with different polarity or charge.

The length of the cross- linking agent did not correlate with the number of bacterial attachment in inorganic water matrices. However, in organic water matrices, the bacterial adhesions increased as the number of carbon atoms of the cross-linker increased. The films prepared with suberic acid showed the highest bacterial adhesions in the organic aquatic media   (Figure 2.6).

The impacts of cross-linker with different functionalities is presented in Figure 2.8. As shown a large variability of adhesion is observed, two observations can be made. The films cross-linked with maleic acid, which is more hydrophobic than the other acids due to the –C=C- group, produced higher total and irreversible bacterial adhesion. Additionally, higher total and irreversible adhesion is observed in organic containing aquatic media.

A correlation between ΔG_{132} and the number of bacterial attachment was performed to understand better the impacts of different functionalities. It was found that

60

total bacterial adhesions did not correlate with the films ΔG_{132} but irreversible adhesions showed a moderated correlation with it, as shown in Figure 2.8. Overall, PVA films cross-linked by maleic acid had lower ΔG_{132}, and as commented earlier showed high bacterial attachment
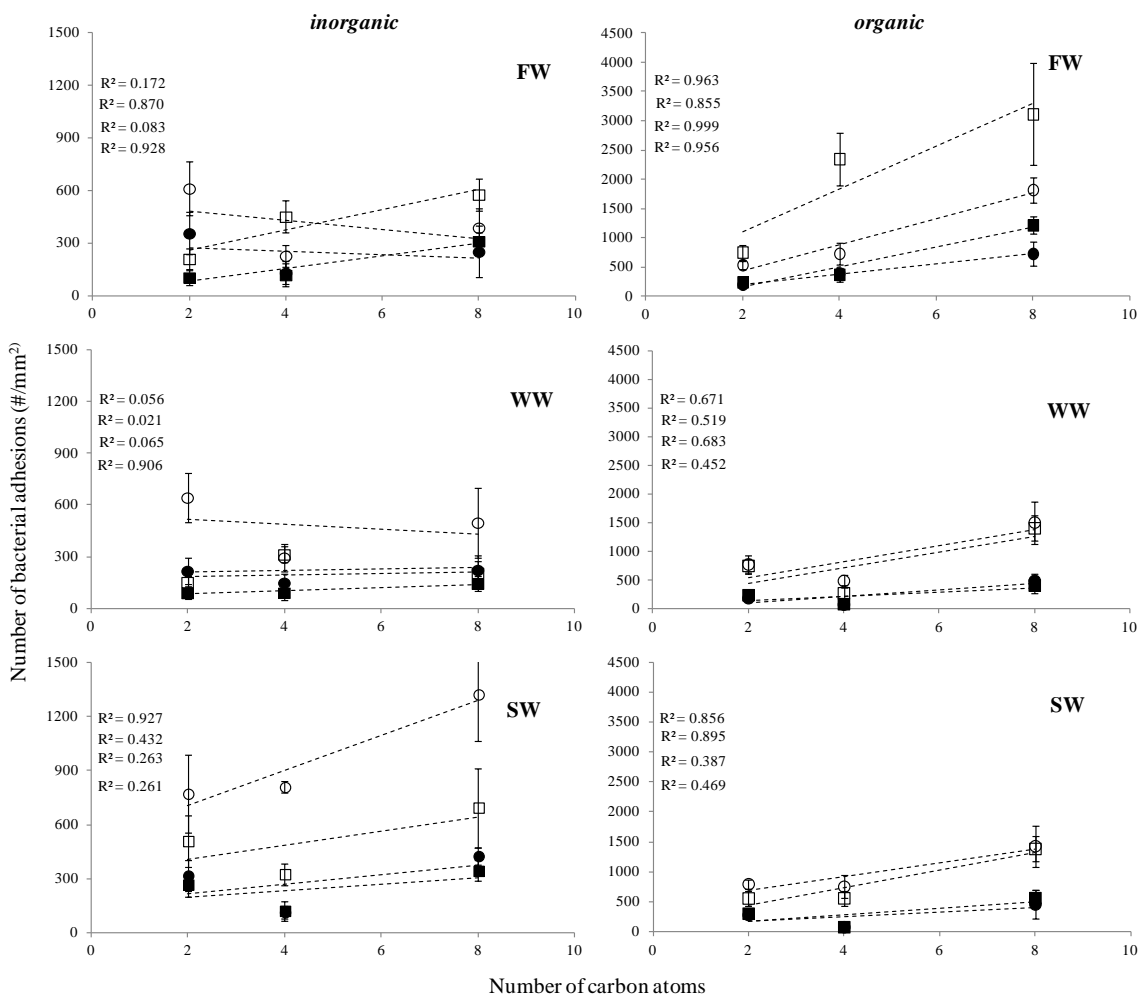
Figure 2.6   Impacts of cross-linking molecule length (i.e., number of carbon atoms) on bacterial adhesion for freshwater (FW), wastewater (WW) and seawater (SW) inorganic and organic matrices. Total adhesion (white symbols) and irreversible (black symbols) for *P. putida* (circles) and *B. subtilis* (squares).
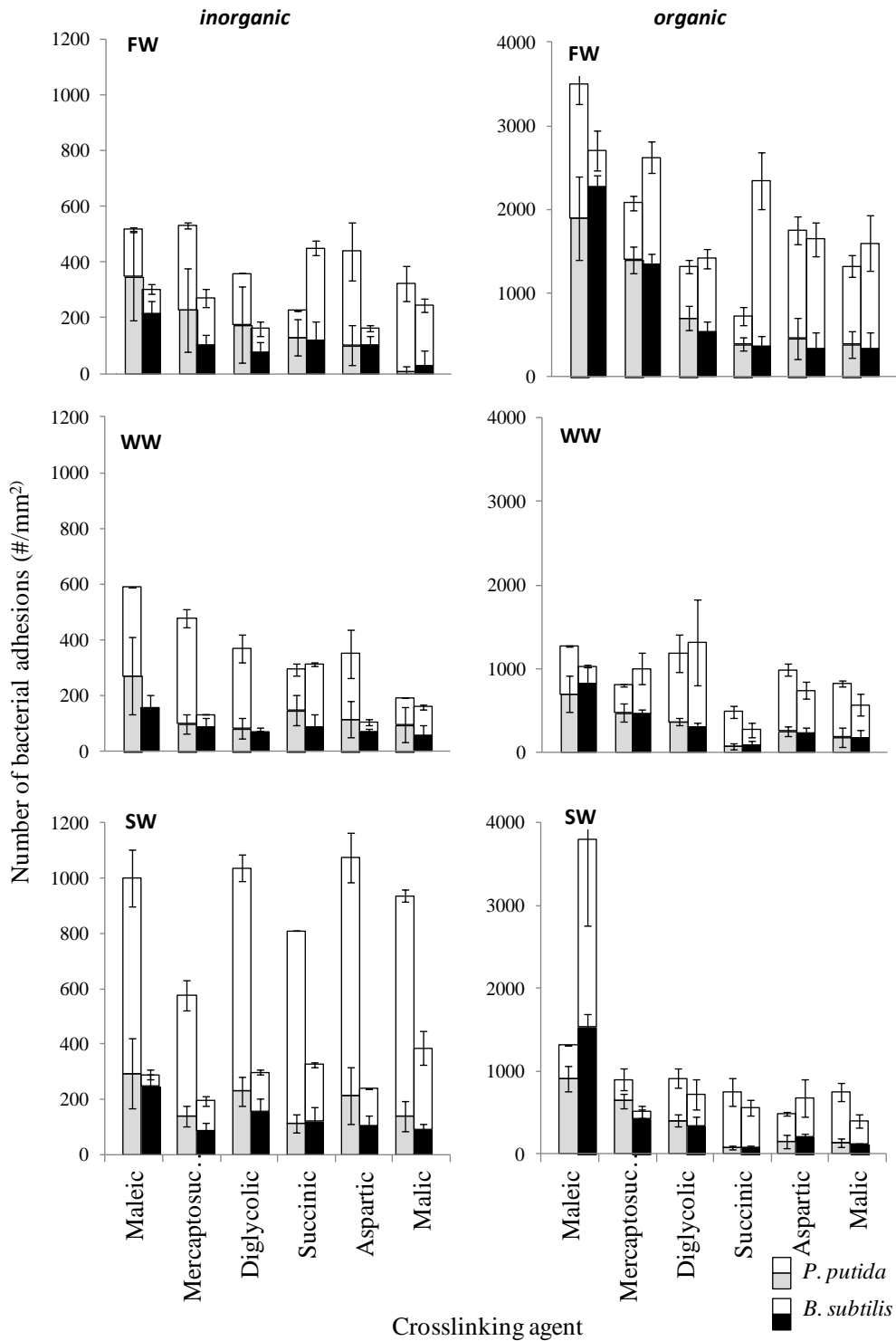
Figure 2.7   Impacts of specific chemical functionality introduced by the cross-linking
agent on bacterial adhesion for freshwater (FW), wastewater (WW) and
seawater (SW). Column height represents total number of adhesions and
shaded areas correspond to irreversible adhesions.
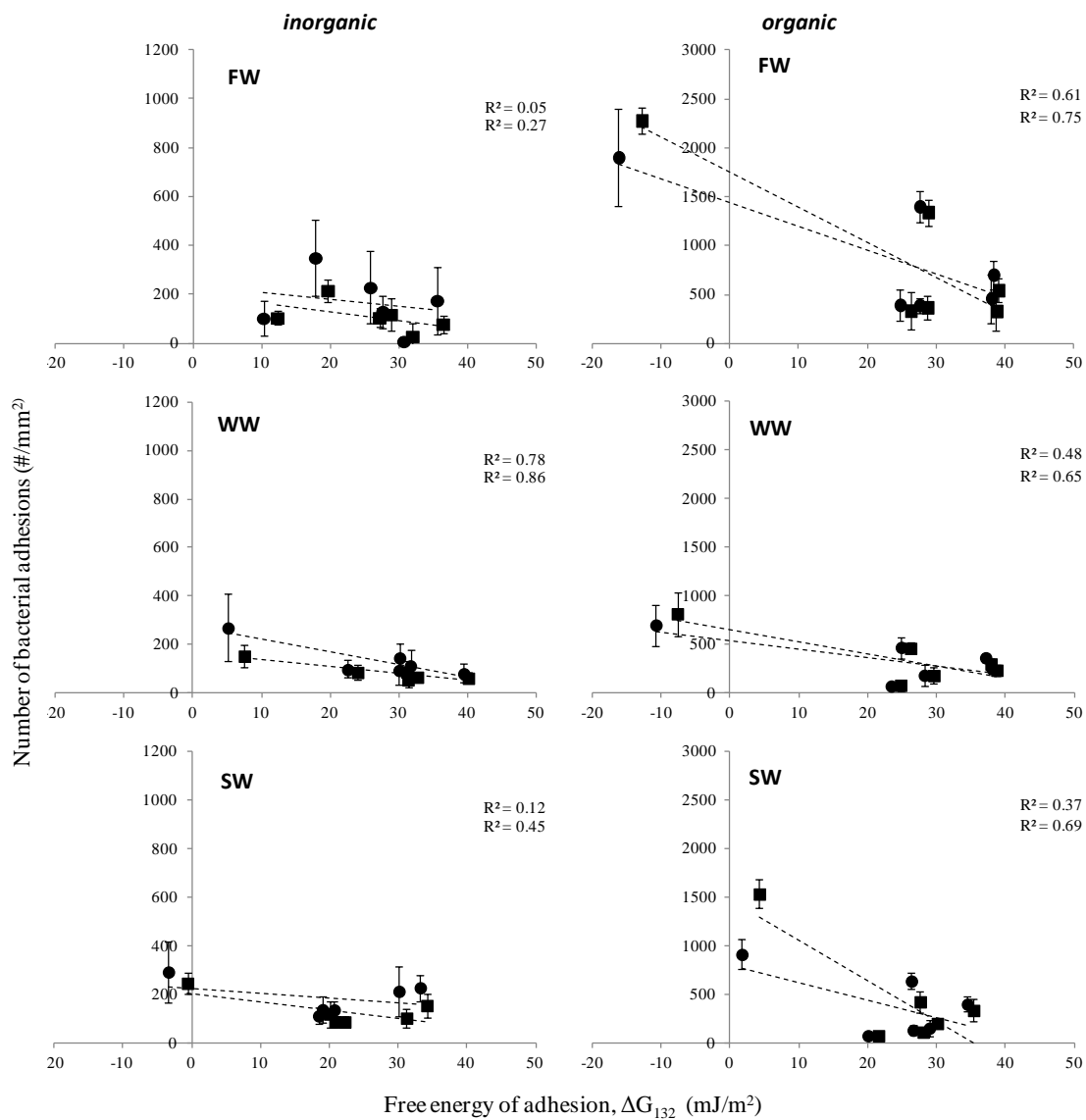
Figure 2.8 Relationship between surface energy and irreversible bacterial adhesion on
PVA films with cross-linking agents offering different functionalities.
Irreversible adhesions for *P. putida* (circles) and *B. subtilis* (squares) in
inorganic and organic aquatic media.

2.3.5 *Overall bacterial adhesion trends*

Considering all conditions tested, some general trends emerge. The content of dissolved/macromolecular organic material strongly influences bacterial adhesion, regardless of the coating film chemistry. As shown in Figure 2.10, higher number of total and irreversible bacterial adhesion (in average) occurred for aquatic media containing organics than in inorganic media. Potentially, the presence of organics may affect the films physical heterogeneity, for example with the formation of nano-scale features, and changes on the average surface chemistry, induced by the adsorbed macromolecules [3c, 5, 16], that leads to higher propensity to biofouling.

Additionally, within the cases containing organic matter, films exposed to wastewater and seawater were less prone to irreversible biofouling than in freshwater. It has been previously published [19] that water chemistry affects surface properties of the membranes such as surface charge, zeta potential and hydrophilicity. For example, divalent cations such as Ca^{2+}, Ba^{2+}, Sr^{2+} increase wettability of polymeric membranes by higher structuring of water at the interface[19a]. The content of divalent cations in wastewater and seawater is much larger than fresh water, what could cause some of those effects.

The higher ionic strength of the seawater and wastewater media may offer more insights. It is well known that, mixed electron-donor/electron-acceptor functionality can produce a type of "hydrophobic attraction," whereas monopolar electron-donor functionality gives rise to the most fouling resistant interfaces as previously described by van Oss, Whitesides and [15, 18a, 18c] High ionic strength has been reported to greatly affect surface functionality by increasing the electron donor components while decreasing the

64

electron acceptor component [19a]. Therefore, in seawater and wastewater the films may behave closer to monopolar electron donor functionality than in freshwater. This would translate to lower propensity to bacterial attachment whose have typically large electron donor components.

Another trend that seem to emerge is the effectivity on the cleaning of films with different functionalities. It is noted that after hydraulic washing, the films cross-linked with agents containing only carboxylic acid functionalities, were more effectively cleaned than the films with other functionality. For instance, on average malic acid and succinic cross-linked films had lower irreversible adhesions than the films cross-linked with agents containing other functionalities such as maleic($-C=C-$), aspartic ($-NH_2$), diglycolic ($-O-$), mercaptosuccinic ($-SH$) under similar conditions of cross-linking degree. Residual carboxylic functionalities have been previously observed to provide negative surface charge and moderate hydrophilicity to PVA films and RO membranes [3c], these features may lead to the observed lower irreversible adhesions.
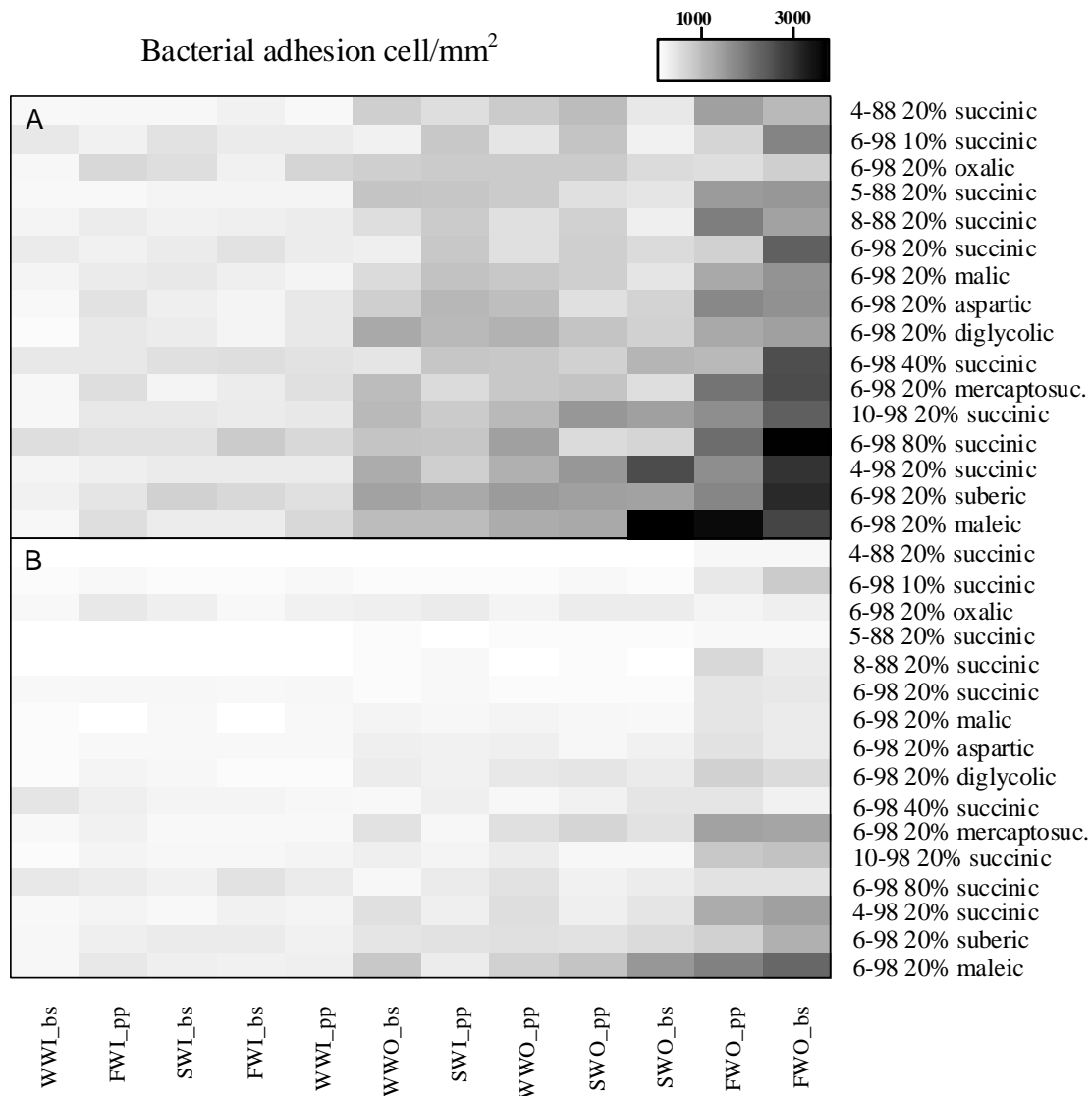
Figure 2.9   Heatmaps of bacterial adhesion for all the conditions discussed in text.
Total adhesion (A), irreversible adhesion (B). Dark areas represent conditions
prone to biofouling while light areas represent conditions more biofouling
resistant.

It is well accepted that interfacial free energies of cohesion and adhesion
correlate strongly with bacterial adhesion and depend on the ionic composition of the
surrounding liquid [3c, 5]; in the following paragraphs the relation obtained between total
and irreversible adhesion to the free energies of adhesion obtained from the contact angle
analysis for the PVA films in the different water matrices is discussed. Figure 2.10 shows
that most of the adhesion data is concentrated between $\Delta G_{132} = 15 \text{mJ/m}^2$ and ΔG_{132}

=35mJ/m^2 , while a second cluster is located for ΔG_{132} values in the vicinity of 50-55 mJ/m^2 and the rest of the data is distributed in the lowest end of ΔG_{132} .

Overall lower number of adhesion, and specially irreversible adhesions, are observed for the largest ΔG_{132} values and the largest number of adhesion occur for the lowest values of ΔG_{132}. Therefore, a slight trends emerges following the expected behavior where films with higher ΔG_{132} are less prone to adhesion and films with negative ΔG_{132} are more prone to have biofouling. However, in the intermediate range a large dispersion of total and irreversible adhesion exists what produces only a poor linear correlation fit.

In the same way, as observed in the heatmap above, in Figure 2.10 is possible to distinguish between adhesions occurring in media with and without organics; overall biofouling was more intense, higher number of bacterial adhesions, in aquatic media containing organics (shades of blue). Although, this behavior was more evident for total adhesion than in irreversible adhesions. In the figure, linear fittings are provided for organics (solid line) and inorganic (dashed line) trends, even though the correlation is poor it can be seen from the trend that more biofouling occur for the organic containing media.

However, in despite that organic matter seem to strongly affect biofouling in these films, Figure 2.11 does not seem to support that the increase on biofouling is only due to a change in the surface chemistry of the films, leading perhaps to mixed electron donor-electron acceptor functionalities and a "hydrophobic type" of attraction. Since, if this were the case, it would be expected to observe an accumulation of high adhesion data

points towards the lower end of the ΔG_{132} axis and not the widespread distribution observed along the x axis. Therefore, the higher number of bacterial attachments in organic aquatic media must be originated at least in part by other mechanism, for example the change in the films physical heterogeneity, such as the formation of nanoscale features.
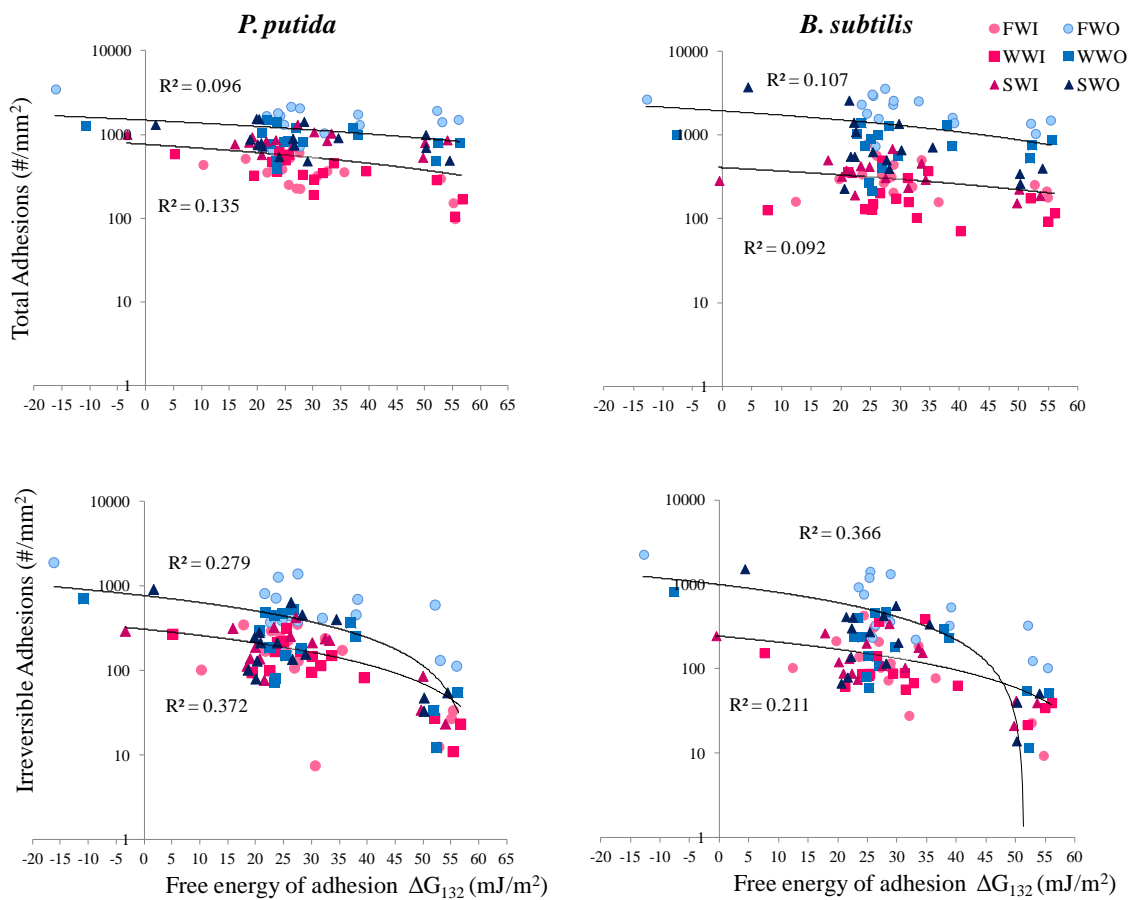
Figure 2.10 Total and irreversible adhesion versus free energy of adhesion for all PVA films and bacterial cells in the different aquatic media. Linear fitting has been traced for the inorganic and organic recipes and their respective linear correlation coefficients are annotated.

2.4   Conclusions

A combinatorial matrix of cross-linked polyvinyl alcohol thin films were synthesized directly in 384-well microplates, and then bacterial adhesion, viability, and removal were quantitatively assessed using high throughput screening biofouling assays. The use of high throughput screening permitted simultaneous investigation of bacterial adhesion for two different bacteria cells – *P. putida* and *B. subtilis* – in six different assay systems representing practical water chemistries in which bacterial adhesion and biofilm formation actually occur.

Generally, less cross-linked PVA films prepared from less hydrolyzed PVA produced more adhesion resistant films. Even though previous literature indicates that lower molecular weights PVA produce more hydrophilic films, this was not observed in this study and lower molecular weights PVA did not significantly influenced the bacterial adhesion in the tested conditions. Although the optimal cross-linked PVA film chemistry was a function of bacteria cell type and water chemistry, in general, cross-linking agents offering pendant hydrophilic functional groups produced better adhesion resistance for both bacteria in all water matrices tested.

Contact angle analysis for all the combination of water chemistry and PVA films and the subsequent determination of free energy of cohesion and adhesion allowed to see that even when films can be classified as hydrophilic when at interaction with pure water, they may as well behave in a hydrophobic manner depending on the water chemistry, thus information based only on pure water may be misleading.

Overall, general free energy of adhesion was inversely correlated with bacterial adhesions. However for medium values of free energy of adhesion a large dispersion of bacterial attachment was observed. Moreover, free energy of adhesion was not able to solely account for the higher biofouling observed in organic aquatic medias. This leads to conclude that in addition to free energy of adhesion, physical heterogeneity of the films, for instance formation of nanoscale features, are significant in the propensity to biofouling of the studied PVA films.

Appendix 2A

Table 2A.1   Contact angle data of simulated freshwater (FW), wastewater (WW) and seawater (SW) inorganic and organic recipes. Values represent the average and standard deviation of at least 10 independent measurements.

Contact angle θ (deg)		4-88 20% succinic	5-88 20% succinic	8-88 20% succinic	4-98 20% succinic	6-98 10% succinic	6-98 20% succinic	6-98 40% succinic	6-98 80% succinic	6-98 20% Maleic	6-98 20% Malic acid	6-98 20% Aspartic	6-98 20% Mercaptosuccinic	6-98 20% Dyglycolic	6-98 20% Oxalic	6-98 20% Suberic	10-98 20% succinic
water	average	31.0	20.5	27.5	44.8	41.4	42.1	42.1	37.1	37.9	43.8	30.1	42.9	36.7	43.9	42.0	42.8
	stdev	2.2	1.0	1.6	1.9	2.6	1.8	1.3	1.9	1.8	2.9	4.4	5.8	1.6	1.8	1.4	2.7
glycerol	average	60.6	63.9	60.3	44.5	46.8	41.8	41.3	37.3	43.1	44.5	41.2	40.8	39.5	42.8	45.3	44.9
	stdev	0.8	0.8	1.5	2.4	3.6	0.6	1.5	1.0	3.4	2.6	1.5	1.0	1.3	1.6	0.4	2.3
diiodomethane	average	33.0	33.9	35.8	44.2	36.3	41.1	37.2	32.6	36.0	34.8	38.8	38.4	37.4	38.3	36.4	31.1
	stdev	1.2	3.3	0.7	1.6	0.8	0.5	0.6	1.8	0.9	2.0	0.3	0.4	0.4	1.7	0.6	2.3
FW inorganics	average	21.3	23.4	26.6	43.4	43.9	39.4	34.6	39.4	47.6	39.0	51.5	39.9	29.9	40.3	44.6	46.1
	stdev	1.4	0.4	2.3	2.1	1.5	2.3	1.6	3.5	3.6	1.8	3.6	3.3	2.3	1.7	5.0	1.5
WW inorganics	average	20.7	21.0	27.7	41.4	49.4	37.3	33.5	37.1	56.0	39.5	35.3	42.5	25.6	43.1	44.1	44.8
	stdev	1.7	1.5	1.4	1.3	4.6	1.8	3.1	1.6	7.1	3.0	4.8	2.6	1.8	1.6	3.1	1.9
SW inorganics	average	30.1	25.7	30.7	42.9	47.8	46.3	34.6	39.0	61.2	47.8	36.7	43.9	32.2	48.8	42.5	47.4
	stdev	2.6	1.1	3.3	2.2	1.3	1.2	1.4	2.0	9.5	3.0	2.7	3.2	3.2	2.5	1.5	1.6
FW organics	average	24.9	22.4	27.6	44.5	47.1	39.4	35.0	36.7	68.5	43.7	29.2	38.5	26.9	42.8	45.1	46.2
	stdev	1.3	1.9	1.0	1.2	1.5	2.0	2.5	1.6	6.4	3.2	1.8	0.5	1.3	1.4	3.8	1.8
WW organics	average	25.9	21.8	27.8	42.4	46.4	42.7	40.5	38.8	65.5	41.0	29.1	40.7	28.2	44.1	46.5	46.7
	stdev	1.8	1.9	3.1	1.2	1.6	1.7	2.7	2.1	6.9	2.0	1.8	1.9	2.0	2.2	2.1	1.3
SW organics	average	29.4	25.1	30.4	47.6	49.8	45.2	44.1	38.5	58.1	42.3	37.7	39.5	31.0	45.5	41.6	47.2
	stdev	1.4	0.6	1.8	1.3	3.5	0.9	2.4	3.5	6.0	1.3	2.7	1.9	1.5	1.8	3.5	1.2

Table 2A.2   Free energy of cohesion, adhesion and wettability in distilled water

Solid/Liquid Substrate	Raw/Measured Values			Intrinsic Substrate Properties					Wettability	Hydrophilicity				Adhesional Propensity				
														P. putida		B. subtilis		
	θ_{water}	$\theta_{glycerol}$	$\theta_{diiodomethane}$	γ^{LW}	γ^{+}	γ^{-}	γ^{AB}	γ^{TOT}	$-\Delta G_{13}$	ΔG_{131}^{LW}	ΔG_{131}^{AB}	ΔG_{131}^{TOT}	ΔG_{132}^{LW}	ΔG_{132}^{AB}	ΔG_{132}^{TOT}	ΔG_{132}^{LW}	ΔG_{132}^{AB}	ΔG_{132}^{TOT}
	(deg)	(deg)	(deg)	(mJ/m²)	(mJ/m²)	(mJ/m²)	(mJ/m²)	(mJ/m²)	(mJ/m²)	(mJ/m²)	(mJ/m²)	(mJ/m²)	(mJ/m²)	(mJ/m²)	(mJ/m²)	(mJ/m²)	(mJ/m²)	(mJ/m²)
diiodomethane	n/a	n/a	n/a	50.8	0.0	0.0	0.0	50.8	n/a	n/a	n/a	n/a	n/a	n/a	n/a	n/a	n/a	n/a
glycerol	n/a	n/a	n/a	34.0	3.9	57.4	29.9	63.9	n/a	n/a	n/a	n/a	n/a	n/a	n/a	n/a	n/a	n/a
water	n/a	n/a	n/a	21.8	25.5	25.5	51.0	72.8	n/a	n/a	n/a	n/a	n/a	n/a	n/a	n/a	n/a	n/a
P. putida	29.6 ± 3.1	35.9 ± 2.0	42.4 ± 3.9	38.4	0.0	61.9	1.9	40.3	136.1	-4.7	55.6	50.9	-4.7	55.6	50.9	n/a	n/a	n/a
B. subtilis	20.7 ± 4.2	22.5 ± 0.9	47.2 ± 1.3	35.8	0.2	64.0	6.7	42.5	140.9	-3.5	54.7	51.2	n/a	n/a	n/a	-3.5	54.7	51.2
4--88 succinic, 20%	31.0 ± 2.2	60.6 ± 0.8	33.0 ± 1.2	42.9	0.8	67.7	14.7	57.7	135.2	-7.1	52.8	45.7	-5.7	54.8	49.0	-5.0	54.0	49.0
5--88 succinic, 20%	20.5 ± 1.1	63.9 ± 0.8	33.9 ± 3.3	42.5	1.9	86.4	25.4	67.9	141.0	-6.9	62.5	55.7	-5.7	62.6	56.9	-4.9	61.1	56.2
8--88 succinic, 20%	27.5 ± 1.6	60.3 ± 1.5	35.8 ± 0.7	41.6	0.8	72.6	15.0	56.6	137.4	-6.4	57.8	51.5	-5.4	57.7	52.3	-4.7	56.8	52.1
4--98 succinic, 20%	44.8 ± 1.9	44.5 ± 2.4	44.2 ± 1.6	37.4	1.1	31.5	11.8	49.3	124.4	-4.2	8.9	4.7	-4.4	28.0	23.6	-3.8	28.7	24.9
6-98 succinic, 10%	41.4 ± 2.6	46.8 ± 3.6	36.3 ± 0.8	41.4	0.3	37.2	6.9	48.3	127.4	-6.3	18.8	12.5	-5.4	35.6	30.2	-4.7	36.2	31.5
6--98 succinic, 20%	42.1 ± 1.8	41.8 ± 0.6	41.1 ± 0.5	39.0	1.1	32.6	12.2	51.2	126.8	-5.0	10.5	5.5	-4.8	28.9	24.1	-4.2	29.6	25.5
6--98 succinic, 40%	42.1 ± 1.3	41.3 ± 1.5	37.2 ± 0.6	41.0	1.0	31.9	11.2	52.2	126.8	-6.0	9.7	3.7	-5.3	28.8	23.5	-4.6	29.5	24.9
6--98 succinic, 80%	37.1 ± 1.9	37.3 ± 1.0	32.6 ± 1.8	43.1	1.0	34.9	11.6	54.7	130.9	-7.2	13.9	6.7	-5.8	31.4	25.6	-5.0	31.9	27.0
6--98 Maleic, 20%	37.9 ± 1.8	43.1 ± 3.4	36.0 ± 0.9	41.5	0.5	38.6	8.9	50.5	130.2	-6.3	20.2	13.9	-5.4	35.9	30.5	-4.7	36.4	31.7
6--98 Malic, 20%	43.8 ± 2.9	44.5 ± 2.6	34.8 ± 2.0	42.1	0.6	31.9	8.6	50.7	125.4	-6.6	10.3	3.7	-5.6	30.1	24.6	-4.8	30.9	26.1
6--98 Aspartic, 20%	30.1 ± 4.4	41.2 ± 1.5	38.8 ± 0.3	40.2	0.5	47.0	9.9	50.2	135.8	-5.6	31.2	25.6	-5.1	42.2	37.1	-4.4	42.3	37.9
6--98 Mercaptosuccinic, 20%	42.9 ± 5.8	40.8 ± 1.0	38.4 ± 0.4	40.4	1.2	30.6	12.0	52.3	126.2	-5.7	7.7	2.0	-5.1	27.2	22.0	-4.4	27.9	23.5
6--98 Dyglycolic, 20%	36.7 ± 1.6	39.5 ± 1.3	37.4 ± 0.4	40.9	0.9	37.4	11.7	52.6	131.2	-5.9	17.5	11.5	-5.3	33.6	28.3	-4.5	34.0	29.5
6--98 Oxalic, 20%	43.9 ± 1.8	42.8 ± 1.6	38.3 ± 1.7	40.4	0.9	30.9	10.8	51.2	125.3	-5.7	8.3	2.6	-5.2	28.0	22.8	-4.4	28.8	24.3
6--98 Suberic, 20%	42.0 ± 1.4	45.3 ± 0.4	36.4 ± 0.6	41.4	0.5	35.1	8.2	49.6	126.9	-6.2	15.2	9.0	-5.4	33.2	27.8	-4.6	33.8	29.2
10--98 Succinic, 20%	42.8 ± 2.7	44.9 ± 2.3	31.1 ± 2.3	43.7	0.4	33.2	7.1	50.8	126.2	-7.6	12.7	5.1	-5.9	32.1	26.1	-5.1	32.8	27.7

73

Table 2A.3　　Free energy of cohesion, adhesion and wettability in FW inorganics

Solid/Liquid Substrate	Raw/Measured Values			Intrinsic Substrate Properties					Hydrophilicity				Adhesional Propensity				
													P. putida			*B. subtilis*	
	$\theta_{FW\ inorganics}$	$\theta_{glycerol}$	$\theta_{diiodomethane}$	γ^{LW}	γ^{+}	γ^{-}	γ^{AB}	γ^{TOT}	ΔG_{131}^{LW}	ΔG_{131}^{AB}	ΔG_{131}^{TOT}	ΔG_{132}^{LW}	ΔG_{132}^{AB}	ΔG_{132}^{TOT}	ΔG_{132}^{LW}	ΔG_{132}^{AB}	ΔG_{132}^{TOT}
	(deg)	(deg)	(deg)	(mJ/m²)	(mJ/m²)	(mJ/m²)	(mJ/m²)	(mJ/m²)	(mJ/m²)	(mJ/m²)	(mJ/m²)	(mJ/m²)	(mJ/m²)	(mJ/m²)	(mJ/m²)	(mJ/m²)	(mJ/m²)
diiodomethane	n/a	n/a	n/a	50.8	0.0	0.0	0.0	50.8	n/a	n/a	n/a	n/a	n/a	n/a	n/a	n/a	n/a
glycerol	n/a	n/a	n/a	34.0	3.9	57.4	29.9	63.9	n/a	n/a	n/a	n/a	n/a	n/a	n/a	n/a	n/a
water	n/a	n/a	n/a	21.8	25.5	25.5	51.0	72.8	n/a	n/a	n/a	n/a	n/a	n/a	n/a	n/a	n/a
P. putida	29.6 ± 3.1	35.9 ± 2.0	42.4 ± 3.9	38.4	0.0	61.9	1.9	40.3	-4.7	55.6	50.9	-4.7	55.6	50.9	n/a	n/a	n/a
B. subtilis	20.7 ± 4.2	22.5 ± 0.9	47.2 ± 1.3	35.8	0.2	64.0	6.7	42.5	-3.5	54.7	51.2	n/a	n/a	n/a	-3.5	54.7	51.2
4-88 succinic, 20%	21.3 ± 1.4	60.6 ± 0.8	33.0 ± 1.2	42.9	1.2	80.1	19.4	62.3	-7.1	61.9	54.8	-5.7	60.8	55.1	-5.0	54.5	49.6
5-88 succinic, 20%	23.4 ± 0.4	63.9 ± 0.8	33.9 ± 3.3	42.5	1.7	83.0	24.0	66.6	-6.9	60.6	53.8	-5.7	61.1	55.4	-4.9	59.7	54.8
8-88 succinic, 20%	26.6 ± 2.3	60.3 ± 1.5	35.8 ± 0.7	41.6	0.8	73.7	15.4	57.1	-6.4	58.7	52.4	-5.4	58.3	52.8	-4.7	54.7	50.0
4-98 succinic, 20%	43.4 ± 2.1	44.5 ± 2.4	44.2 ± 1.6	37.4	1.0	33.4	11.7	49.1	-4.2	11.8	7.6	-4.4	30.0	25.5	-3.8	31.2	27.4
6-98 succinic, 10%	43.9 ± 1.5	46.8 ± 3.6	36.3 ± 0.8	41.4	0.4	33.7	7.4	48.9	-6.3	13.4	7.1	-5.4	32.3	26.9	-4.7	27.9	23.2
6-98 succinic, 20%	39.4 ± 2.3	41.8 ± 0.6	41.1 ± 0.5	39.0	1.0	36.2	11.9	50.9	-5.0	15.7	10.7	-4.8	32.4	27.6	-4.2	24.2	20.0
6-98 succinic, 40%	34.6 ± 1.6	41.3 ± 1.5	37.2 ± 0.6	41.0	0.6	41.5	10.1	51.1	-6.0	23.7	17.7	-5.3	37.7	32.5	-4.6	38.0	33.5
6-98 succinic, 80%	39.4 ± 3.5	37.3 ± 1.0	32.6 ± 1.8	43.1	1.1	32.0	11.9	55.0	-7.2	9.7	2.5	-5.8	28.5	22.8	-5.0	29.7	24.7
6-98 Maleic, 20%	47.6 ± 3.6	43.1 ± 3.4	36.0 ± 0.9	41.5	1.0	26.0	10.3	51.8	-6.3	0.8	-5.5	-5.4	23.2	17.8	-4.7	4.1	-0.6
6-98 Malic, 20%	39.0 ± 1.8	44.5 ± 2.6	34.8 ± 2.0	42.1	0.4	38.3	7.6	49.8	-6.6	20.2	13.6	-5.6	36.2	30.7	-4.8	25.6	20.8
6-98 Aspartic, 20%	51.5 ± 3.6	41.2 ± 1.5	38.8 ± 0.3	40.2	1.8	20.1	12.0	52.3	-5.6	-8.3	-13.9	-5.1	15.4	10.2	-4.4	35.6	31.2
6-98 Mercaptosuccinic, 20%	39.9 ± 3.3	40.8 ± 1.0	38.4 ± 0.4	40.4	1.0	34.5	11.7	52.0	-5.7	13.3	7.6	-5.1	31.0	25.8	-4.4	26.7	22.2
6-98 Dyglycolic, 20%	29.9 ± 2.3	39.5 ± 1.3	37.4 ± 0.4	40.9	0.6	45.6	10.7	51.6	-5.9	29.0	23.0	-5.3	40.8	35.5	-4.5	38.7	34.2
6-98 Oxalic, 20%	40.3 ± 1.7	42.8 ± 1.6	38.3 ± 1.7	40.4	0.7	35.6	10.3	50.7	-5.7	15.3	9.6	-5.2	32.6	27.5	-4.4	22.2	17.7
6-98 Suberic, 20%	44.6 ± 5.0	45.3 ± 0.4	36.4 ± 0.6	41.4	0.6	31.6	8.7	50.1	-6.2	9.8	3.6	-5.4	29.8	24.4	-4.6	33.2	28.6
10-98 Succinic, 20%	46.1 ± 1.5	44.9 ± 2.3	31.1 ± 2.3	43.7	0.5	28.9	7.7	51.4	-7.6	5.6	-1.9	-5.9	27.6	21.7	-5.1	26.9	21.8

Table 2A.4 Free energy of cohesion, adhesion and wettability in WW inorganics

Solid/Liquid Substrate	Raw/Measured Values			Intrinsic Substrate Properties					Hydrophilicity			Adhesional Propensity — *P. putida*			Adhesional Propensity — *B. subtilis*		
	$\theta_{WW\,inorganics}$ (deg)	$\theta_{glycerol}$ (deg)	$\theta_{diiodomethane}$ (deg)	γ^{LW} (mJ/m²)	γ^{+} (mJ/m²)	γ^{-} (mJ/m²)	γ^{AB} (mJ/m²)	γ^{TOT} (mJ/m²)	ΔG_{131}^{LW} (mJ/m²)	ΔG_{131}^{AB} (mJ/m²)	ΔG_{131}^{TOT} (mJ/m²)	ΔG_{132}^{LW} (mJ/m²)	ΔG_{132}^{AB} (mJ/m²)	ΔG_{132}^{TOT} (mJ/m²)	ΔG_{132}^{LW} (mJ/m²)	ΔG_{132}^{AB} (mJ/m²)	ΔG_{132}^{TOT} (mJ/m²)
diiodomethane	n/a	n/a	n/a	50.8	0.0	0.0	0.0	50.8	n/a	n/a	n/a	n/a	n/a	n/a	n/a	n/a	n/a
glycerol	n/a	n/a	n/a	34.0	3.9	57.4	29.9	63.9	n/a	n/a	n/a	n/a	n/a	n/a	n/a	n/a	n/a
water	n/a	n/a	n/a	21.8	25.5	25.5	51.0	72.8	n/a	n/a	n/a	n/a	n/a	n/a	n/a	n/a	n/a
P. putida	29.6 ± 3.1	35.9 ± 2.0	42.4 ± 3.9	38.4	0.0	61.9	1.9	40.3	-4.7	55.6	50.9	-4.7	55.6	50.9	n/a	n/a	n/a
B. subtilis	20.7 ± 4.2	22.5 ± 0.9	47.2 ± 1.3	35.8	0.2	64.0	6.7	42.5	-3.5	54.7	51.2	n/a	n/a	n/a	-3.5	54.7	51.2
4-88 succinic, 20%	20.7 ± 1.7	60.6 ± 0.8	33.0 ± 1.2	42.9	1.2	80.7	19.6	62.6	-7.1	62.3	55.2	-5.7	61.1	55.4	-5.0	59.8	54.9
5-88 succinic, 20%	21.0 ± 1.5	63.9 ± 0.8	33.9 ± 3.3	42.5	1.8	85.8	25.2	67.7	-6.9	62.2	55.4	-5.7	62.4	56.7	-4.9	60.8	56.0
8-88 succinic, 20%	27.7 ± 1.4	60.3 ± 1.5	35.8 ± 0.7	41.6	0.8	72.2	14.9	56.5	-6.4	57.6	51.2	-5.4	57.5	52.1	-4.7	56.6	51.9
4-98 succinic, 20%	41.4 ± 1.3	44.5 ± 2.4	44.2 ± 1.6	37.4	0.9	36.0	11.4	48.9	-4.2	15.6	11.4	-4.4	32.5	28.1	-3.8	33.0	29.2
6-98 succinic, 10%	49.4 ± 4.6	46.8 ± 3.6	36.3 ± 0.8	41.4	0.7	26.4	8.4	49.8	-6.3	1.5	-4.8	-5.4	24.7	19.3	-4.7	25.8	21.1
6-98 succinic, 20%	37.3 ± 1.8	41.8 ± 0.6	41.1 ± 0.5	39.0	0.9	38.9	11.6	50.7	-5.0	19.5	14.6	-4.8	34.9	30.1	-4.2	35.3	31.1
6-98 succinic, 40%	33.5 ± 3.1	41.3 ± 1.5	37.2 ± 0.6	41.0	0.6	42.8	9.9	50.9	-6.0	25.6	19.6	-5.3	38.9	33.6	-4.6	39.2	34.6
6-98 succinic, 80%	37.1 ± 1.6	37.3 ± 1.0	32.6 ± 1.8	43.1	1.0	34.8	11.6	54.7	-7.2	13.8	6.6	-5.8	31.3	25.5	-5.0	31.9	26.9
6-98 Maleic, 20%	56.0 ± 7.1	43.1 ± 3.4	36.0 ± 0.9	41.5	1.7	15.8	10.4	51.9	-6.3	-16.1	-22.4	-5.4	10.6	5.1	-4.7	12.2	7.5
6-98 Malic, 20%	39.5 ± 3.0	44.5 ± 2.6	34.8 ± 2.0	42.1	0.4	37.6	7.8	49.9	-6.6	19.1	12.5	-5.6	35.6	30.0	-4.8	36.1	31.3
6-98 Aspartic, 20%	35.3 ± 4.8	41.2 ± 1.5	38.8 ± 0.3	40.2	0.7	40.7	10.8	51.1	-5.6	22.3	16.7	-5.1	36.8	31.7	-4.4	37.1	32.7
6-98 Mercaptosuccinic, 20%	42.5 ± 2.6	40.8 ± 1.0	38.4 ± 0.4	40.4	1.1	31.1	11.9	52.3	-5.7	8.5	2.8	-5.1	27.7	22.5	-4.4	28.4	24.0
6-98 Dyglycolic, 20%	25.6 ± 1.8	39.5 ± 1.3	37.4 ± 0.4	40.9	0.5	50.4	10.0	50.8	-5.9	35.6	29.7	-5.3	44.7	39.4	-4.5	44.6	40.1
6-98 Oxalic, 20%	43.1 ± 1.6	42.8 ± 1.6	38.3 ± 1.7	40.4	0.9	31.9	10.7	51.1	-5.7	9.8	4.1	-5.2	29.0	23.9	-4.4	29.8	25.3
6-98 Suberic, 20%	44.1 ± 3.1	45.3 ± 0.4	36.4 ± 0.6	41.4	0.6	32.2	8.6	50.0	-6.2	10.8	4.5	-5.4	30.4	25.0	-4.6	31.1	26.5
10-98 Succinic, 20%	44.8 ± 1.9	44.9 ± 2.3	31.1 ± 2.3	43.7	0.5	30.6	7.5	51.2	-7.6	8.4	0.8	-5.9	29.4	23.4	-5.1	30.3	25.1

Table 2A.5 Free energy of cohesion, adhesion and wettability in SW inorganics

Solid/Liquid Substrate	Raw/Measured Values			Intrinsic Substrate Properties					Hydrophilicity			Adhesional Propensity — P. putida			Adhesional Propensity — B. subtilis		
	$\theta_{SW\,inorganics}$ (deg)	$\theta_{glycerol}$ (deg)	$\theta_{diiodomethane}$ (deg)	γ^{LW} (mJ/m²)	γ^{+} (mJ/m²)	γ^{-} (mJ/m²)	γ^{AB} (mJ/m²)	γ^{TOT} (mJ/m²)	ΔG_{131}^{LW} (mJ/m²)	ΔG_{131}^{AB} (mJ/m²)	ΔG_{131}^{TOT} (mJ/m²)	ΔG_{132}^{LW} (mJ/m²)	ΔG_{132}^{AB} (mJ/m²)	ΔG_{132}^{TOT} (mJ/m²)	ΔG_{132}^{LW} (mJ/m²)	ΔG_{132}^{AB} (mJ/m²)	ΔG_{132}^{TOT} (mJ/m²)
diiodomethane	n/a	n/a	n/a	50.8	0.0	0.0	0.0	50.8	n/a	n/a	n/a	n/a	n/a	n/a	n/a	n/a	n/a
glycerol	n/a	n/a	n/a	34.0	3.9	57.4	29.9	63.9	n/a	n/a	n/a	n/a	n/a	n/a	n/a	n/a	n/a
water	n/a	n/a	n/a	21.8	25.5	25.5	51.0	72.8	n/a	n/a	n/a	n/a	n/a	n/a	n/a	n/a	n/a
P. putida	29.6 ± 3.1	35.9 ± 2.0	42.4 ± 3.9	38.4	0.0	61.9	1.9	40.3	-4.7	55.6	50.9	-4.7	55.6	50.9	n/a	n/a	n/a
B. subtilis	20.7 ± 4.2	22.5 ± 0.9	47.2 ± 1.3	35.8	0.2	64.0	6.7	42.5	-3.5	54.7	51.2	n/a	n/a	n/a	-3.5	54.7	51.2
4-88 succinic, 20%	30.1 ± 2.6	60.6 ± 0.8	33.0 ± 1.2	42.9	0.8	68.9	15.2	58.1	-7.1	53.8	46.7	-5.7	55.4	49.6	-5.0	54.5	49.6
5-88 succinic, 20%	25.7 ± 1.1	63.9 ± 0.8	33.9 ± 3.3	42.5	1.6	80.1	22.8	65.4	-6.9	58.9	52.0	-5.7	59.7	54.0	-4.9	58.4	53.5
8-88 succinic, 20%	30.7 ± 3.3	60.3 ± 1.5	35.8 ± 0.7	41.6	0.7	68.0	13.4	55.0	-6.4	54.2	47.9	-5.4	55.4	50.0	-4.7	54.7	50.0
4-98 succinic, 20%	42.9 ± 2.2	44.5 ± 2.4	44.2 ± 1.6	37.4	1.0	34.1	11.6	49.1	-4.2	12.8	8.6	-4.4	30.6	26.2	-3.8	31.2	27.4
6-98 succinic, 10%	47.8 ± 1.3	46.8 ± 3.6	36.3 ± 0.8	41.4	0.6	28.4	8.2	49.6	-6.3	4.8	-1.4	-5.4	26.9	21.5	-4.7	27.9	23.2
6-98 succinic, 20%	46.3 ± 1.2	41.8 ± 0.6	41.1 ± 0.5	39.0	1.4	27.1	12.5	51.5	-5.0	2.4	-2.5	-4.8	23.3	18.4	-4.2	24.2	20.0
6-98 succinic, 40%	34.6 ± 1.4	41.3 ± 1.5	37.2 ± 0.6	41.0	0.6	41.5	10.1	51.1	-6.0	23.7	17.7	-5.3	37.7	32.4	-4.6	38.0	33.5
6-98 succinic, 80%	39.0 ± 2.0	37.3 ± 1.0	32.6 ± 1.8	43.1	1.1	32.5	11.8	54.9	-7.2	10.4	3.2	-5.8	29.0	23.2	-5.0	29.7	24.7
6-98 Maleic, 20%	61.2 ± 9.5	43.1 ± 3.4	36.0 ± 0.9	41.5	2.2	10.4	9.7	51.2	-6.3	-25.9	-32.2	-5.4	2.0	-3.4	-4.7	4.1	-0.6
6-98 Malic, 20%	47.8 ± 3.0	44.5 ± 2.6	34.8 ± 2.0	42.1	0.8	26.6	9.1	51.3	-6.6	1.9	-4.8	-5.6	24.6	19.0	-4.8	25.6	20.8
6-98 Aspartic, 20%	36.7 ± 2.7	41.2 ± 1.5	38.8 ± 0.3	40.2	0.8	39.0	11.0	51.3	-5.6	19.9	14.3	-5.1	35.2	30.1	-4.4	35.6	31.2
6-98 Mercaptosuccinic, 20%	43.9 ± 3.2	40.8 ± 1.0	38.4 ± 0.4	40.4	1.2	29.4	12.0	52.4	-5.7	5.8	0.1	-5.1	25.9	20.7	-4.4	26.7	22.2
6-98 Dyglycolic, 20%	32.2 ± 3.2	39.5 ± 1.3	37.4 ± 0.4	40.9	0.7	42.9	11.1	51.9	-5.9	25.2	19.3	-5.3	38.5	33.2	-4.5	38.7	34.2
6-98 Oxalic, 20%	48.8 ± 2.5	42.8 ± 1.6	38.3 ± 1.7	40.4	1.3	24.4	11.2	51.6	-5.7	-1.6	-7.4	-5.2	21.1	15.9	-4.4	22.2	17.7
6-98 Suberic, 20%	42.5 ± 1.5	45.3 ± 0.4	36.4 ± 0.6	41.4	0.5	34.4	8.3	49.7	-6.2	14.2	8.0	-5.4	32.6	27.2	-4.6	33.2	28.6
10-98 Succinic, 20%	47.4 ± 1.6	44.9 ± 2.3	31.1 ± 2.3	43.7	0.6	27.3	7.9	51.6	-7.6	2.9	-4.6	-5.9	25.9	19.9	-5.1	26.9	21.8

Table 2A.6   Free energy of cohesion, adhesion and wettability in FW organics

Solid/Liquid Substrate	Raw/Measured Values			Intrinsic Substrate Properties					Hydrophilicity			Adhesional Propensity					
													P. putida			*B. subtilis*	
	$\theta_{FWorganics}$	$\theta_{glycerol}$	$\theta_{diiodomethane}$	γ^{LW}	γ^{+}	γ^{-}	γ^{AB}	γ^{TOT}	ΔG_{131}^{LW}	ΔG_{131}^{AB}	ΔG_{131}^{TOT}	ΔG_{132}^{LW}	ΔG_{132}^{AB}	ΔG_{132}^{TOT}	ΔG_{132}^{LW}	ΔG_{132}^{AB}	ΔG_{132}^{TOT}
	(deg)	(deg)	(deg)	(mJ/m²)	(mJ/m²)	(mJ/m²)	(mJ/m²)	(mJ/m²)	(mJ/m²)	(mJ/m²)	(mJ/m²)	(mJ/m²)	(mJ/m²)	(mJ/m²)	(mJ/m²)	(mJ/m²)	(mJ/m²)
diiodomethane	n/a	n/a	n/a	50.8	0.0	0.0	0.0	50.8	n/a	n/a	n/a	n/a	n/a	n/a	n/a	n/a	n/a
glycerol	n/a	n/a	n/a	34.0	3.9	57.4	29.9	63.9	n/a	n/a	n/a	n/a	n/a	n/a	n/a	n/a	n/a
water	n/a	n/a	n/a	21.8	25.5	25.5	51.0	72.8	n/a	n/a	n/a	n/a	n/a	n/a	n/a	n/a	n/a
P. putida	29.6 ± 3.1	35.9 ± 2.0	42.4 ± 3.9	38.4	0.0	61.9	1.9	40.3	-4.7	55.6	50.9	-4.7	55.6	50.9	n/a	n/a	n/a
B. subtilis	20.7 ± 4.2	22.5 ± 0.9	47.2 ± 1.3	35.8	0.2	64.0	6.7	42.5	-3.5	54.7	51.2	n/a	n/a	n/a	-3.5	54.7	51.2
4-88 succinic, 20%	24.9 ± 1.3	60.6 ± 0.8	33.0 ± 1.2	42.9	1.0	75.9	17.8	60.7	-7.1	59.0	51.9	-5.7	58.8	53.1	-5.0	57.7	52.8
5-88 succinic, 20%	22.4 ± 1.9	63.9 ± 0.8	33.9 ± 3.3	42.5	1.8	84.2	24.5	67.0	-6.9	61.3	54.5	-5.7	61.6	56.0	-4.9	60.2	55.3
8-88 succinic, 20%	27.6 ± 1.0	60.3 ± 1.5	35.8 ± 0.7	41.6	0.8	72.3	14.9	56.6	-6.4	57.7	51.3	-5.4	57.6	52.1	-4.7	56.6	52.0
4-98 succinic, 20%	44.5 ± 1.2	44.5 ± 2.4	44.2 ± 1.6	37.4	1.1	31.9	11.8	49.2	-4.2	9.6	5.4	-4.4	28.4	24.0	-3.8	29.2	25.3
6-98 succinic, 10%	47.1 ± 1.5	46.8 ± 3.6	36.3 ± 0.8	41.4	0.5	29.5	8.0	49.5	-6.3	6.5	0.3	-5.4	28.0	22.6	-4.7	28.9	24.3
6-98 succinic, 20%	39.4 ± 2.0	41.8 ± 0.6	41.1 ± 0.5	39.0	1.0	36.1	11.9	50.9	-5.0	15.6	10.6	-4.8	32.3	27.5	-4.2	32.8	28.7
6-98 succinic, 40%	35.0 ± 2.5	41.3 ± 1.5	37.2 ± 0.6	41.0	0.6	40.9	10.2	51.2	-6.0	22.9	16.9	-5.3	37.2	31.9	-4.6	37.6	33.0
6-98 succinic, 80%	36.7 ± 1.6	37.3 ± 1.0	32.6 ± 1.8	43.1	0.9	35.3	11.6	54.7	-7.2	14.6	7.4	-5.8	31.8	26.0	-5.0	32.3	27.3
6-98 Maleic, 20%	68.5 ± 6.4	43.1 ± 3.4	36.0 ± 0.9	41.5	3.2	4.4	7.5	49.1	-6.3	-38.5	-44.8	-5.4	-10.8	-16.2	-4.7	-8.1	-12.8
6-98 Malic, 20%	43.7 ± 3.2	44.5 ± 2.6	34.8 ± 2.0	42.1	0.6	32.1	8.6	50.7	-6.6	10.6	3.9	-5.6	30.3	24.7	-4.8	31.0	26.2
6-98 Aspartic, 20%	29.2 ± 1.8	41.2 ± 1.5	38.8 ± 0.3	40.2	0.5	48.1	9.8	50.0	-5.6	32.8	27.2	-5.1	43.1	38.0	-4.4	43.1	38.7
6-98 Mercaptosuccinic, 20%	38.5 ± 0.5	40.8 ± 1.0	38.4 ± 0.4	40.4	0.9	36.3	11.5	51.9	-5.7	16.0	10.3	-5.1	32.7	27.5	-4.4	33.2	28.8
6-98 Dyglycolic, 20%	26.9 ± 1.3	39.5 ± 1.3	37.4 ± 0.4	40.9	0.5	48.9	10.2	51.1	-5.9	33.6	27.7	-5.3	43.5	38.3	-4.5	43.5	39.0
6-98 Oxalic, 20%	42.8 ± 1.4	42.8 ± 1.6	38.3 ± 1.7	40.4	0.9	32.3	10.6	51.1	-5.7	10.4	4.7	-5.2	29.4	24.3	-4.4	30.2	25.7
6-98 Suberic, 20%	45.1 ± 3.8	45.3 ± 0.4	36.4 ± 0.6	41.4	0.6	30.9	8.8	50.1	-6.2	8.6	2.4	-5.4	29.0	23.6	-4.6	29.8	25.2
10-98 Succinic, 20%	46.2 ± 1.8	44.9 ± 2.3	31.1 ± 2.3	43.7	0.5	28.8	7.7	51.4	-7.6	5.5	-2.1	-5.9	27.5	21.6	-5.1	28.5	23.4

Table 2A.7   Free energy of cohesion, adhesion and wettability in WW organics

Solid/Liquid Substrate	Raw/Measured Values			Intrinsic Substrate Properties					Hydrophilicity				Adhesional Propensity				
													$P.\ putida$			$B.\ subtilis$	
	$\theta_{WW\,organics}$	$\theta_{glycerol}$	$\theta_{diiodomethane}$	γ^{LW}	γ^{+}	γ^{-}	γ^{AB}	γ^{TOT}	ΔG_{131}^{LW}	ΔG_{131}^{AB}	ΔG_{131}^{TOT}	ΔG_{132}^{LW}	ΔG_{132}^{AB}	ΔG_{132}^{TOT}	ΔG_{132}^{LW}	ΔG_{132}^{AB}	ΔG_{132}^{TOT}
	(deg)	(deg)	(deg)	(mJ/m²)	(mJ/m²)	(mJ/m²)	(mJ/m²)	(mJ/m²)	(mJ/m²)	(mJ/m²)	(mJ/m²)	(mJ/m²)	(mJ/m²)	(mJ/m²)	(mJ/m²)	(mJ/m²)	(mJ/m²)
diiodomethane	n/a	n/a	n/a	50.8	0.0	0.0	0.0	50.8	n/a	n/a	n/a	n/a	n/a	n/a	n/a	n/a	n/a
glycerol	n/a	n/a	n/a	34.0	3.9	57.4	29.9	63.9	n/a	n/a	n/a	n/a	n/a	n/a	n/a	n/a	n/a
water	n/a	n/a	n/a	21.8	25.5	25.5	51.0	72.8	n/a	n/a	n/a	n/a	n/a	n/a	n/a	n/a	n/a
$P.\ putida$	29.6 ± 3.1	35.9 ± 2.0	42.4 ± 3.9	38.4	0.0	61.9	1.9	40.3	-4.7	55.6	50.9	-4.7	55.6	50.9	n/a	n/a	n/a
$B.\ subtilis$	20.7 ± 4.2	22.5 ± 0.9	47.2 ± 1.3	35.8	0.2	64.0	6.7	42.5	-3.5	54.7	51.2	n/a	n/a	n/a	-3.5	54.7	51.2
4-88 succinic, 20%	25.9 ± 1.8	60.6 ± 0.8	33.0 ± 1.2	42.9	1.0	74.6	17.3	60.2	-7.1	58.1	51.0	-5.7	58.2	52.5	-5.0	57.1	52.2
5-88 succinic, 20%	21.8 ± 1.9	63.9 ± 0.8	33.9 ± 3.3	42.5	1.8	84.9	24.8	67.3	-6.9	61.7	54.9	-5.7	61.9	56.3	-4.9	60.5	55.6
8-88 succinic, 20%	27.8 ± 3.1	60.3 ± 1.5	35.8 ± 0.7	41.6	0.8	72.1	14.8	56.5	-6.4	57.5	51.1	-5.4	57.4	52.0	-4.7	56.5	51.8
4-98 succinic, 20%	42.4 ± 1.2	44.5 ± 2.4	44.2 ± 1.6	37.4	1.0	34.8	11.6	49.0	-4.2	13.8	9.6	-4.4	31.3	26.9	-3.8	31.9	28.1
6-98 succinic, 10%	46.4 ± 1.6	46.8 ± 3.6	36.3 ± 0.8	41.4	0.5	30.4	7.9	49.3	-6.3	8.0	1.8	-5.4	29.0	23.6	-4.7	29.9	25.2
6-98 succinic, 20%	42.7 ± 1.7	41.8 ± 0.6	41.1 ± 0.5	39.0	1.2	31.9	12.3	51.3	-5.0	9.4	4.5	-4.8	28.2	23.4	-4.2	28.9	24.8
6-98 succinic, 40%	40.5 ± 2.7	41.3 ± 1.5	37.2 ± 0.6	41.0	0.9	33.9	11.0	52.0	-6.0	12.7	6.6	-5.3	30.7	25.4	-4.6	31.4	26.8
6-98 succinic, 80%	38.8 ± 2.1	37.3 ± 1.0	32.6 ± 1.8	43.1	1.1	32.8	11.8	54.9	-7.2	10.8	3.6	-5.8	29.3	23.5	-5.0	30.0	25.0
6-98 Maleic, 20%	65.5 ± 6.9	43.1 ± 3.4	36.0 ± 0.9	41.5	2.8	6.6	8.6	50.1	-6.3	-33.5	-39.8	-5.4	-5.4	-10.8	-4.7	-3.0	-7.7
6-98 Malic, 20%	41.0 ± 2.0	44.5 ± 2.6	34.8 ± 2.0	42.1	0.5	35.7	8.1	50.2	-6.6	16.2	9.5	-5.6	33.8	28.2	-4.8	34.4	29.6
6-98 Aspartic, 20%	29.1 ± 1.8	41.2 ± 1.5	38.8 ± 0.3	40.2	0.5	48.1	9.8	50.0	-5.6	32.8	27.2	-5.1	43.1	38.0	-4.4	43.1	38.7
6-98 Mercaptosuccinic, 20%	40.7 ± 1.9	40.8 ± 1.0	38.4 ± 0.4	40.4	1.0	33.5	11.7	52.1	-5.7	11.9	6.2	-5.1	30.0	24.9	-4.4	30.6	26.2
6-98 Dyglycolic, 20%	28.2 ± 2.0	39.5 ± 1.3	37.4 ± 0.4	40.9	0.6	47.5	10.4	51.3	-5.9	31.7	25.7	-5.3	42.4	37.1	-4.5	42.4	37.9
6-98 Oxalic, 20%	44.1 ± 2.2	42.8 ± 1.6	38.3 ± 1.7	40.4	1.0	30.5	10.8	51.2	-5.7	7.7	2.0	-5.2	27.6	22.5	-4.4	28.4	24.0
6-98 Suberic, 20%	46.5 ± 2.1	45.3 ± 0.4	36.4 ± 0.6	41.4	0.7	29.1	9.0	50.3	-6.2	5.8	-0.5	-5.4	27.2	21.8	-4.6	28.1	23.4
10-98 Succinic, 20%	46.7 ± 1.3	44.9 ± 2.3	31.1 ± 2.3	43.7	0.5	28.1	7.8	51.5	-7.6	4.3	-3.3	-5.9	26.8	20.8	-5.1	27.8	22.6

Table 2A.8   Free energy of cohesion, adhesion and wettability in SW organics

Solid/Liquid Substrate	Raw/Measured Values			Intrinsic Substrate Properties					Hydrophilicity				Adhesional Propensity				
													P. putida		B. subtilis		
	$\theta_{SW\,organics}$ (deg)	$\theta_{glycerol}$ (deg)	$\theta_{diiodomethane}$ (deg)	γ^{LW} (mJ/m²)	γ^{+} (mJ/m²)	γ^{-} (mJ/m²)	γ^{AB} (mJ/m²)	γ^{TOT} (mJ/m²)	ΔG_{131}^{LW} (mJ/m²)	ΔG_{131}^{AB} (mJ/m²)	ΔG_{131}^{TOT} (mJ/m²)	ΔG_{132}^{LW} (mJ/m²)	ΔG_{132}^{AB} (mJ/m²)	ΔG_{132}^{TOT} (mJ/m²)	ΔG_{132}^{LW} (mJ/m²)	ΔG_{132}^{AB} (mJ/m²)	ΔG_{132}^{TOT} (mJ/m²)
diiodomethane	n/a	n/a	n/a	50.8	0.0	0.0	0.0	50.8	n/a	n/a	n/a	n/a	n/a	n/a	n/a	n/a	n/a
glycerol	n/a	n/a	n/a	34.0	3.9	57.4	29.9	63.9	n/a	n/a	n/a	n/a	n/a	n/a	n/a	n/a	n/a
water	n/a	n/a	n/a	21.8	25.5	25.5	51.0	72.8	n/a	n/a	n/a	n/a	n/a	n/a	n/a	n/a	n/a
P. putida	29.6 ± 3.1	35.9 ± 2.0	42.4 ± 3.9	38.4	0.0	61.9	1.9	40.3	-4.7	55.6	50.9	-4.7	55.6	50.9	n/a	n/a	n/a
B. subtilis	20.7 ± 4.2	22.5 ± 0.9	47.2 ± 1.3	35.8	0.2	64.0	6.7	42.5	-3.5	54.7	51.2	n/a	n/a	n/a	-3.5	54.7	51.2
4-88 succinic, 20%	29.4 ± 1.4	60.6 ± 0.8	33.0 ± 1.2	42.9	0.9	70.0	15.6	58.5	-7.1	54.6	47.5	-5.7	55.9	50.1	-5.0	55.0	50.1
5-88 succinic, 20%	25.1 ± 0.6	63.9 ± 0.8	33.9 ± 3.3	42.5	1.7	80.8	23.1	65.7	-6.9	59.3	52.5	-5.7	60.1	54.4	-4.9	58.7	53.9
8-88 succinic, 20%	30.4 ± 1.8	60.3 ± 1.5	35.8 ± 0.7	41.6	0.7	68.4	13.5	55.1	-6.4	54.6	48.2	-5.4	55.6	50.2	-4.7	54.8	50.2
4-98 succinic, 20%	47.6 ± 1.3	44.5 ± 2.4	44.2 ± 1.6	37.4	1.3	27.8	12.1	49.5	-4.2	3.5	-0.7	-4.4	24.2	19.8	-3.8	25.1	21.3
6-98 succinic, 10%	49.8 ± 3.5	46.8 ± 3.6	36.3 ± 0.8	41.4	0.7	25.8	8.4	49.9	-6.3	0.4	-5.8	-5.4	24.0	18.6	-4.7	25.1	20.5
6-98 succinic, 20%	45.2 ± 0.9	41.8 ± 0.6	41.1 ± 0.5	39.0	1.4	28.6	12.4	51.5	-5.0	4.6	-0.4	-4.8	24.8	20.0	-4.2	25.7	21.5
6-98 succinic, 40%	44.1 ± 2.4	41.3 ± 1.5	37.2 ± 0.6	41.0	1.1	29.3	11.4	52.4	-6.0	5.8	-0.2	-5.3	26.1	20.8	-4.6	27.0	22.4
6-98 succinic, 80%	38.5 ± 3.5	37.3 ± 1.0	32.6 ± 1.8	43.1	1.0	33.1	11.8	54.9	-7.2	11.3	4.1	-5.8	29.6	23.8	-5.0	30.3	25.3
6-98 Maleic, 20%	58.1 ± 6.0	43.1 ± 3.4	36.0 ± 0.9	41.5	1.9	13.5	10.1	51.7	-6.3	-20.2	-26.5	-5.4	7.1	1.7	-4.7	8.9	4.2
6-98 Malic, 20%	42.3 ± 1.3	44.5 ± 2.6	34.8 ± 2.0	42.1	0.5	34.0	8.3	50.4	-6.6	13.5	6.9	-5.6	32.1	26.6	-4.8	32.8	28.0
6-98 Aspartic, 20%	37.7 ± 2.7	41.2 ± 1.5	38.8 ± 0.3	40.2	0.8	37.7	11.2	51.4	-5.6	18.0	12.4	-5.1	34.0	28.9	-4.4	34.5	30.1
6-98 Mercaptosuccinic, 20%	39.5 ± 1.9	40.8 ± 1.0	38.4 ± 0.4	40.4	1.0	35.0	11.6	52.0	-5.7	14.1	8.4	-5.1	31.5	26.3	-4.4	32.0	27.6
6-98 Dyglycolic, 20%	31.0 ± 1.5	39.5 ± 1.3	37.4 ± 0.4	40.9	0.7	44.3	10.9	51.8	-5.9	27.2	21.3	-5.3	39.7	34.5	-4.5	39.9	35.4
6-98 Oxalic, 20%	45.5 ± 1.8	42.8 ± 1.6	38.3 ± 1.7	40.4	1.0	28.7	10.9	51.4	-5.7	5.0	-0.7	-5.2	25.8	20.6	-4.4	26.7	22.2
6-98 Suberic, 20%	41.6 ± 3.5	45.3 ± 0.4	36.4 ± 0.6	41.4	0.5	35.7	8.1	49.5	-6.2	16.1	9.9	-5.4	33.7	28.3	-4.6	34.3	29.7
10-98 Succinic, 20%	47.2 ± 1.2	44.9 ± 2.3	31.1 ± 2.3	43.7	0.6	27.5	7.9	51.6	-7.6	3.4	-4.2	-5.9	26.2	20.2	-5.1	27.2	22.1

References

1.   (a) Costerton, J. W.; Lewandowski, Z.; Caldwell, D. E.; Korber, D. R.; Lappinscott, H. M., Microbial Biofilms. *Annu Rev Microbiol* **1995,** *49*, 711-745; (b) Costerton, J. W.; Stewart, P. S.; Greenberg, E. P., Bacterial biofilms: A common cause of persistent infections. *Science* **1999,** *284* (5418), 1318-1322; (c) Donlan, R. M.; Costerton, J. W., Biofilms: Survival mechanisms of clinically relevant microorganisms. *Clin Microbiol Rev* **2002,** *15* (2), 167-193.

2.   Guenther, F.; Stroh, P.; Wagner, C.; Obst, U.; Hansch, G. M., Phagocytosis of staphylococci biofilms by polymorphonuclear neutrophils: S. aureus and S. epidermidis differ with regard to their susceptibility towards the host defense. *Int J Artif Organs* **2009,** *32* (9), 565-573.

3.   (a) Al-Halbouni, D.; Traber, J.; Lyko, S.; Wintgens, T.; Melin, T.; Tacke, D.; Janot, A.; Dott, W.; Hollender, J., Correlation of EPS content in activated sludge at different sludge retention times with membrane fouling phenomena. *Water Res* **2008,** *42* (6-7), 1475-1488; (b) Kulakov, L. A.; McAlister, M. B.; Ogden, K. L.; Larkin, M. J.; O'Hanlon, J. F., Analysis of bacteria contaminating ultrapure water in industrial systems. *Appl Environ Microb* **2002,** *68* (4), 1548-1555; (c) Subramani, A.; Hoek, E. M. V., Direct observation of initial microbial deposition onto reverse osmosis and nanofiltration membranes. *J Membrane Sci* **2008,** *319* (1-2), 111-125.

4.   (a) Bos, R.; van der Mei, H. C.; Busscher, H. J., Physico-chemistry of initial microbial adhesive interactions - its mechanisms and methods for study. *Fems Microbiol Rev* **1999,** *23* (2), 179-230; (b) Chen, G.; Strevett, K. A., Microbial surface thermodynamics and interactions in aqueous media. *J Colloid Interf Sci* **2003,** *261* (2), 283-290.

5.   Subramani, A.; Huang, X. F.; Hoek, E. M. V., Direct observation of bacterial deposition onto clean and organic-fouled polyamide membranes. *J Colloid Interf Sci* **2009,** *336* (1), 13-20.

6.   Brant, J. A.; Childress, A. E., Colloidal adhesion to hydrophilic membrane surfaces. *J Membrane Sci* **2004,** *241* (2), 235-248.

7.   Carroll, T.; Booker, N. A.; Meier-Haack, J., Polyelectrolyte-grafted microfiltration membranes to control fouling by natural organic matter in drinking water. *J Membrane Sci* **2002,** *203* (1-2), 3-13.

8. Knoell, T.; Safarik, J.; Cormack, T.; Riley, R.; Lin, S. W.; Ridgway, H., Biofouling potentials of microporous polysulfone membranes containing a sulfonated polyether-ethersulfone/polyethersulfone block copolymer: correlation of membrane surface properties with bacterial attachment. *J Membrane Sci* **1999,** *157* (1), 117-138.

9. Immelman, E.; Sanderson, R. D.; Jacobs, E. P.; Vanreenen, A. J., Poly(Vinyl Alcohol) Gel Sublayers for Reverse-Osmosis Membranes .1. Insolubilization by Acid-Catalyzed Dehydration. *J Appl Polym Sci* **1993,** *50* (6), 1013-1034.

10. Peter, S.; Hese, N.; Stefan, R., Phenol-Selective, Highly Resistant Ro-Membranes Made from Pva for Purification of Toxic Industrial-Wastes. *Desalination* **1976,** *19* (1-3), 161-167.

11. (a) Kim, K. J.; Fane, A. G.; Fell, C. J. D., The Performance of Ultrafiltration Membranes Pretreated by Polymers. *Desalination* **1988,** *70* (1-3), 229-249; (b) Li, R. H.; Barbari, T. A., Performance of Poly(Vinyl) Alcohol Thin-Gel Composite Ultrafiltration Membranes. *J Membrane Sci* **1995,** *105* (1-2), 71-78.

12. Amanda, A.; Mallapragada, S. K., Comparison of protein fouling on heat-treated poly(vinyl alcohol), poly(ether sulfone) and regenerated cellulose membranes using diffuse reflectance infrared Fourier transform spectroscopy. *Biotechnol Progr* **2001,** *17* (5), 917-923.

13. (a) Peng, F. B.; Hoek, E. M. V.; Damoiseaux, R., High-Content Screening for Biofilm Assays. *J Biomol Screen* **2010,** *15* (7), 748-754; (b) Peng, F. B.; Huang, X. F.; Jawor, A.; Hoek, E. M. V., Transport, structural, and interfacial properties of poly (vinyl alcohol)-polysulfone composite nanofiltration membranes. *J Membrane Sci* **2010,** *353* (1-2), 169-176; (c) Peng, F. B.; Jiang, Z. Y.; Hoek, E. M. V., Tuning the molecular structure, separation performance and interfacial properties of poly(vinyl alcohol)-polysulfone interfacial composite membranes. *J Membrane Sci* **2011,** *368* (1-2), 26-33.

14. Kang, S. T.; Subramani, A.; Hoek, E. M. V.; Deshusses, M. A.; Matsumoto, M. R., Direct observation of biofouling in cross-flow microfiltration: mechanisms of deposition and release. *J Membrane Sci* **2004,** *244* (1-2), 151-165.

15. Van Oss, C. J., Acid—base interfacial interactions in aqueous media. *Colloids and Surfaces A: Physicochemical and Engineering Aspects* **1993,** *78* (0), 1-49.

16.   Subramani, A.; Hoek, E. M. V., Biofilm formation, cleaning, re-formation on polyamide composite membranes. *Desalination* **2010,** *257* (1-3), 73-79.

17.   www.kremer-pigmente.com/media/files_public/67700-67790e.pdf.   Retrieved September 28, 2012

18.   (a) Chapman, R. G.; Ostuni, E.; Liang, M. N.; Meluleni, G.; Kim, E.; Yan, L.; Pier, G.; Warren, H. S.; Whitesides, G. M., Polymeric thin films that resist the adsorption of proteins and the adhesion of bacteria. *Langmuir* **2001,** *17* (4), 1225-1233; (b) Ostuni, E.; Chapman, R. G.; Holmlin, R. E.; Takayama, S.; Whitesides, G. M., A survey of structure-property relationships of surfaces that resist the adsorption of protein. *Langmuir* **2001,** *17* (18), 5605-5620; (c) Ostuni, E.; Grzybowski, B. A.; Mrksich, M.; Roberts, C. S.; Whitesides, G. M., Adsorption of proteins to hydrophobic sites on mixed self-assembled monolayers. *Langmuir* **2003,** *19* (5), 1861-1872.

19.   (a) Hurwitz, G.; Guillen, G. R.; Hoek, E. M. V., Probing polyamide membrane surface charge, zeta potential, wettability, and hydrophilicity with contact angle measurements. *J Membrane Sci* **2010,** *349* (1-2), 349-357; (b) Jin, X.; Huang, X. F.; Hoek, E. M. V., Role of Specific Ion Interactions in Seawater RO Membrane Fouling by Alginic Acid. *Environ Sci Technol* **2009,** *43* (10), 3580-3587.

CHAPTER III

ANTIBACTERIAL PROPERTIES OF SILVER NANOPARTICLES AND

SILVER-EXCHANGED ZEOLITE NANOCRYSTALS AND ITS POTENTIAL

USE IN ANTIBACTERIAL COATING FILMS

3.1 Introduction

It is well know that silver nanomaterials such as metallic silver nanoparticles AgNP [1] have strong antibacterial properties. Although, the antibacterial mechanisms are not completely elucidated, possible mechanisms by which AgNPs inhibit microorganisms are (1) silver ions release followed by cellular uptake and a cascade of intracellular reactions; (2) interactions with cell membrane, impacting protein function, disrupting proton gradient, and increasing permeability; (3) penetration into the cell where nanoparticles can generate reactive oxygen species (ROS) directly and release silver ions – both potentially impacting DNA replication [2]. Additionally, previous nanotoxicology studies have indicated that their impact is size-and shape-dependent [3] and both their dispersibility and antibacterial efficacy depend on the aquatic media were they are disperse[4].

In the past years, silver nanoparticles have been incorporated, as an antibacterial agent, into a number of products such as households water filters, detergents, dietary supplements, cutting boards, socks, shoes, cell phones, and children toys, among others. Moreover, silver nanoparticles have find their way into membrane technologies for water treatment. Here silver nanoparticles among other nanomaterials are being analyzed as possible control for biofouling. For example, silver nanoparticles have been immobilized into polyamide thin-film layer forming thin film composite membranes with antifouling properties [5]. Silver nanoparticles have been covalent bonded to the surface of polyamide membranes [6] creating a thinfilm nanocomposite with anti-biofouling properties. In another study, silver nanopartices weren introduced on sulfonated polyethersulfone membrane by using vita-min C as a reducing agent[7].

83

Zodrow *et al.*[8] incorporated silver nanoparticles in polysulfone membranes and as result the membrane was able to produce a 2 log reduction of *Escherichia coli* growth and to reduced the attachment of the same bacteria during the wet phase inversion process. The authors observed that in terms of morphology, permeability and surface charge, the membranes containing silver nanoparticles were similar to the unmodified membranes. However, the membranes containing silver were 10% more hydrophilic, which could grant the membrane some fouling resistance. Furthermore, the membrane showed antibacterial properties, specifically reducing by 2 log *E. coli* growth after filtration and decreasing by 94% the bacterial attachment tested in membrane coupons immersed in an *E. coli* suspension. The membrane was also able to inactivate *Pseudomonas mendocina*, a prolific biofilm formation organism. However, the main drawback of the application was that the antibacterial effect was lost quickly due to the depletion of the nanoparticle content.

In this regard, an alternative to silver nanoparticles for surface modifications, is the use of antibacterial ions loaded in zeolites. Zeolites can be use to deliver the antibacterial ions and potentially after depletion they could be reloaded. An illustration describing this concept is shown below.
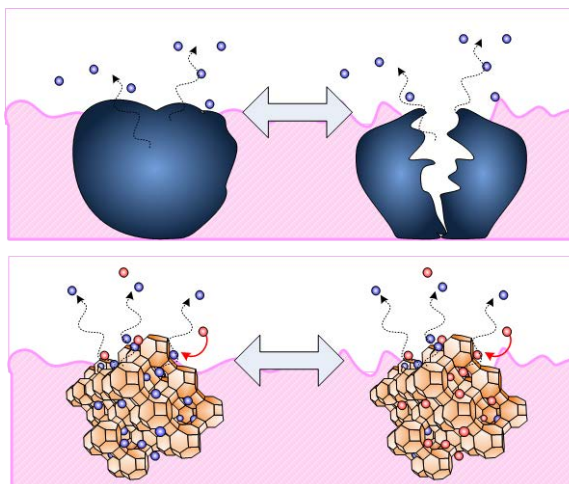
Figure 3.1 Conceptual illustration of silver nanoparticles (top) and zeolite nanoparticles (bottom) embedded in a film and their silver ions release.

Zeolites are crystalline alumino-silicates containing pores and cavities of molecular dimensions and are formed by tetrahedral units of SiO_4 and AlO_4, which are connected by sharing their oxygen atoms [9]. Zeolites, have a negative charge in their structure because of the incorporation of Al; this charge is balanced by extra-framework cations in their pores and cavities. Additionally zeolites are super hydrophilic what make them even better candidates for antifouling purposes.

The zeolite extra-framework cations can be replace with another cation by an ionic exchange process. Silver ions incorporated into the zeolites in this way wills grant zeolites with antibacterial properties [10].

The aim in this paper is to evaluate the antibacterial efficacy of silver-zeolites (Ag-LTA) versus the antibacterial efficacy of silver nanoparticles, in order to decide what antibacterial form is more suitable for future surface modification in the form of antibacterial agent-poly(vinyl) alcohol nanocomposites. To achieve this task a bacterial

viability test will be performed for both nanomaterials, considering two model bacteria a Gram positive and a Gram negative model bacteria and four different water chemistries. Additionally, the antibacterial potency of other 2 metallic nanoparticles, CuNP and ZnNP will be estimated for comparison.

3.2   Materials and methods

3.2.1   Aquatic media

Four aquatic matrices were prepared with compositions designed to represent fresh surface water (FW) and seawater (SW). For each aquatic freshwater matrix type, three composition were prepared, simple electrolyte or "FWNaCl" , complex inorganic recipe (FWI), and complex inorganic plus organic recipe (FWO). The organic recipe was prepared by adding 17 mg/L alginate acid, 12.8 mg/L bovine serum albumin (BSA) and 12.5 mg/L tannic acid to the inorganic matrix for a total organic carbon content of 20mg/L. Additionally, a water chemistry resembling seawater was utilized with the composition presented in Table 3.1. All chemicals were ACS reagent grade or better and used as received (Fisher Scientific, Pittsburgh, PA).

Table 3.1   Composition of representative aquatic media

(mg/L)	FWNaCl	FWI	FWO	SWI
Na+	128.2	14.4	14.4	9624.8
Mg^{2+}		7	7	1146.6
Ca^{2+}		40	40	368.0
K+		2.4	2.4	356.3
NH_4^+		-	-	0.0
Sr^{2+}		-	-	7.2
Cl-	198.2	22	22	17290.7
SO_4^{2-}		104	104	2422.9
HCO_3-		29	29	112.5
NO_3^-		-	-	0.0
Br^-		-	-	60.1
F^-		-	-	1.2
H_3BO_3		-	-	23.0
Ionic strength (M)	0.0056	0.0056	0.0056	0.630
Total dissolved solids	326.424	218.9	218.9	31413.3
pH	7.0	7.0	7.0	7.0
TOC (mg/L)	0	0	20.0	0

3.2.2   *Zeolite nanocrystals preparation and characterization*

Zeolite nanocrystals (Na-LTA) were purchased from NanoScape Company (Munich, Germany). These zeolites have a nominal size of 150 nm, a characteristic pore size of 4Å and an empirical formula of NaAlSiO4. These zeolites have extra-framework Na^+ cations in their internal channels, neutralizing the net charge of the aluminosilicate structure. In order to load the zeolites with silver ions the originally present Na^+ must be exchanged with the antibacterial cation.

Initially, the commercial zeolite was washed with distilled water at least 5 times to remove the excess of NaOH from the manufacturing process. Each step included vortexing the zeolite with distilled water followed by centrifugation (10 min at 4000rpm) and disposal of the supernatant. Then, the washed zeolite was immersed in 1M solution of either $AgNO_3$ and shaked overnight in a wrist action shaker (Burrel Scientific, Pittsburgh) protected from light. Subsequently, the Ag^+ loaded zeolites (Ag-LTA) was

washed three times with distillated water and the resulting zeolite pellets were freeze-dried for 48 hrs and stored in a dessicator. Subsequently, the antibacterial content in the zeolites was determined from an elemental analysis performed in ICP-OES. For this purpose Na-LTA and Ag-LTA samples were acid digested with HNO_3 following standard method 3030E, section 2 [11].

Na-LTA and Ag-LTA were imaged in by scanning electron microscopy (SEM, JEOL JSM-6700F FE-SEM). The SEM settings utilized were 10-13 kV voltage, a working distance of 7.5 mm and a SEI detector. Sample preparation consisted in air dry of 1 drop on the sample holder of either Ag-LTA or Na-LTA.

3.2.3 Preparation and characterization of Ag nanoparticles suspensions

A commercial nanoparticle manufacturer (QuantumSphere Inc.; Santa Ana, California, USA) provided the silver , copper and zinc nanoparticles used in this study. All particles were used as received. Nanoparticle suspensions were prepared in ultrapure sterile water by ultrasonication (FS30H, Fisher Scientific, 1050W, 42kHz) for 10 min. The hydrodynamic diameters of silver nanoparticle in different aquatic electrolytes were determined by dynamic light scattering (BI 90Plus, Brookhaven Instruments Corp.; Holtsville, New York, USA); zeta potential was computed from the measured electrophoretic mobility (ZetaPALS, Brookhaven Instruments Corp.).

3.2.4 Preparation of bacterial cultures

Bacillus subtilis and *Pseudomonas putida* were used as model bacteria to assess toxicity of silver nanoparticles and Ag-LTA in various solution chemistries. Both genera are commonly found in the environment [12]. *P. putida* is a Gram-negative, aerobic bacteria

cultured in trypticase soy broth (TSB). *B. subtilis* is a Gram-positive, aerobic bacteria cultured in Luria–Bertani broth (LB). Pure bacterial cell cultures were grown at 25 °C in incubator with rotary shaking at 150 rpm and harvested at mid-exponential growth phase. Cells were washed twice with phosphate buffered saline (PBS) and re-suspended in the specific solution (FWI, FWO, etc) to achieve an initial cell concentration of 10^8 cells/mL before exposure to the antibacterial agent.

3.2.5   *Bacterial viability assay*

To assess the bacterial toxicity in different aquatic media, a high throughput bactericidal assay previously described[4] was utilized. This assay is a dose response experiment, performed in 384 well microplates, where bacteria viability is determined after exposure to increasing concentration of nanoparticles.

In this assay bacterial membrane integrity is used as a indicator of bacterial viability.   which is determine utilizing the Live/Dead Baclight^{TM} viability kit (Molecular Probes, Eugene, Oregon, USA). This kit consists of two stain solutions a green fluorochrome, SYTO9   that stains all cells, live or dead and a red fluorochrome, propidium iodide, PI, that stains only bacteria with damaged membranes. Simultaneous application of both dyes results in green fluorescence of viable cells with an intact membrane and red fluorescence of dead cells, because of a compromised membrane.

The experiments were performed as follow, 25 μl of silver nanoparticle suspension at 16 different concentrations (from 7.6 μg/L to 250 mg/L) and 25 μl of bacterial suspensions were automatically dispensed into specific wells of a 384-well clear bottom polysterene microplate (Greiner Bio-One; Monroe, North Carolina, USA). Each

combination was tested with four replicates. The plates were incubated for 24 hours at 35

°C. After incubation 10μL of SYTO9 and PI solution (at a concentration of 2μM of

SYTO9 and 10μM PI) were added per well and left to react for 15min. Then, the green to

red fluorescence ratio was   measure by a fluorescence microreader (Flexstation,

Molecular Devices; Sunnyvale, California, USA). This ratio provided the live bacterial

percentage in each well (excitation at 485 nm and emission at 630 nm and 530 nm)

according to a calibration curve previously obtained. This calibration curve consisted in

green to red fluorescence ratios of know percentage of live to dead bacteria, which were

prepare by blending different ratios of live bacteria with bacteria that had been exposed to

70% isopropanol.

Control wells contained either bacteria or silver nanoparticles. The percentage of

live bacteria cells was calculated from the live bacterial percentage for each silver

nanoparticle concentration normalized to the live bacterial percentage for silver-free

controls. Data were fitted by a "dose–response model" using a non-linear regression with

four-parameter logistic equation (Prism 4, GraphPad Software, San Diego, California,

USA), which was used to calculate the IC_{50} values and 95% confidence intervals.

3.3   Results and Discussions

3.3.1   *Characterization of LTA zeolites nanomaterials*

The following figure shows a SEM image of Na-LTA in the left and Ag-

LTA in the right. It can be observed that both Ag-LTA and Na-LTA tended to

agglomerate in the sample. The primary particle size in the 150 nm range is confirmed in the Ag-LTA sample (bottom right).
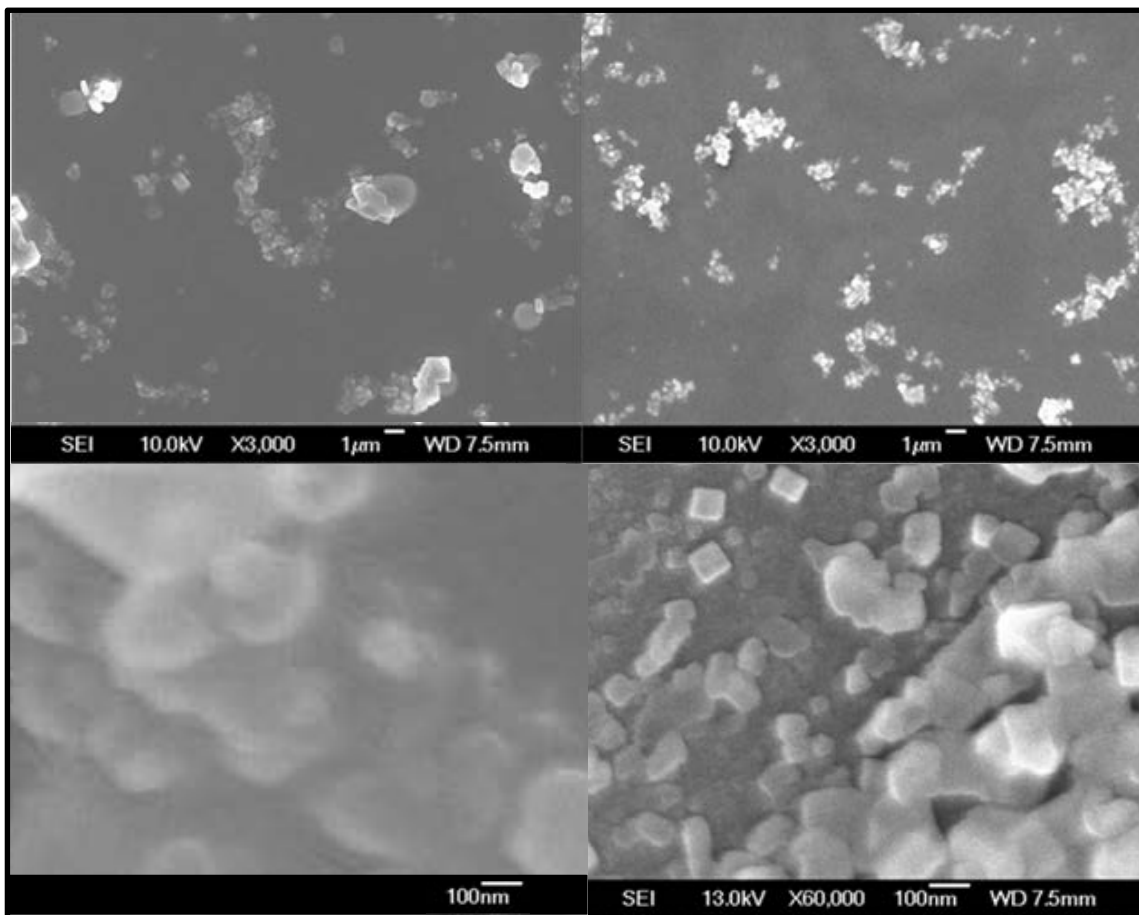

Figure 3.2 SEM images of Na-LTA (Left) and Ag-LTA(right). Na-LTA image is a zoom of a image obtained at 19000X, which was enlarged to met scale bar of Ag-LTA.

Table 3.2 presents the elemental composition of the zeolites in percentage by weight of the particles, obtained from measurements done in ICP-OES. From this the molar ratios were calculated. The elemental composition of the prepared cation-exchanged zeolites showed Si/Al molar ratios close to 1, while the average ratio Al to exchange- cation resulted on 1.2, 1.1, for Na-LTA and Ag-LTA respectively. This

indicates that most of extra frame sodium ions were exchange for silver ions (one silver ion for each).

Table 3.2   Elemental composition by weight of Ag-LTA and Na-LTA

	Si % (w/w)	Al % (w/w)	Na^+ % (w/w)	Ag^+% (w/w)
Na-LTA	20.3 ± 0.9	19.2 ± 3.0	14.1 ± 0.8	-
Ag-LTA	13.3 ± 0.3	11.6 ± 1.5	0.7 ± 0.1	44.1 ± 2.7

LTA and Ag-LTA zeta potential in FWI was calculated from electrophoretic mobility measurements via Smoluchowski equation (Figure 3.2). Both zeolites had, as expected a negative surface charge. Na-LTA showed a higher zeta potential than LTA-Ag, possible due to residual OH^- associated to Na-LTA from the manufacture process.
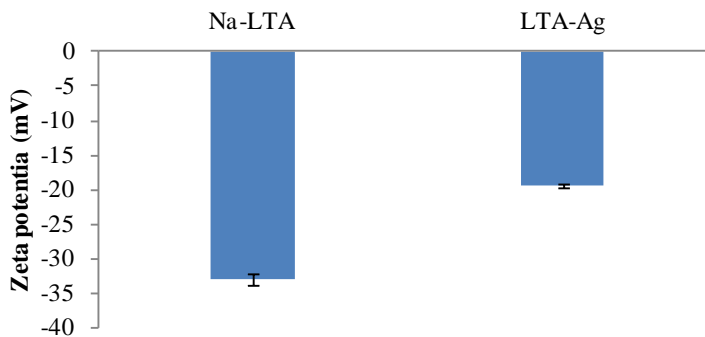
Figure 3.3 Zeta potential (mV) for LTA and Ag-LTA in FWI

3.3.2   *Characterization of silver nanoparticles*

AgNP size was dependent on the water chemistry (Figure 3.3). In the figure both the effective diameter and mean diameter are plotted. The effective diameter is a representation of average diameter of the sample weighted by mass, while the mean diameter is weighted by number. It is observed that the particle size increases from

FWNaCl to SWI. This is explained by the suppression of surface charge as the ionic strength of the medium increases, as shown in   Figure 3.4. The change in size from FWNaCl to FWI, is consistent with Shulze-Hardy rule and previous observations[13]. Both water chemistries have the same ionic strength, but the divalent cations in FWI have a stronger impact in the nanoparticle aggregation.
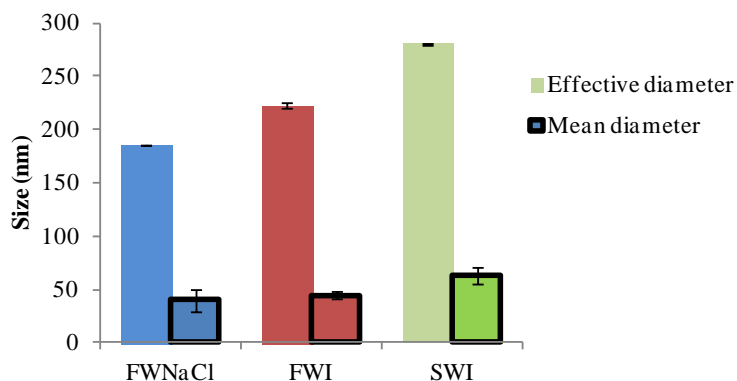

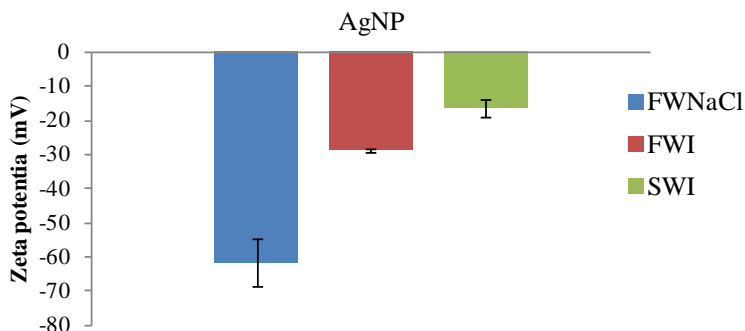Figure 3.4 AgNP particle size in different water chemistries

Figure 3.5 Zeta potential (mV) for AgNP in various water chemistries.

3.3.3   Bacterial inactivation results

The following plots summarize the bacterial inactivation results for *B. subtilis* and *P. putida* exposed to Ag-LTA, AgNP in the 4 different water chemistries. In the plots the antibacterial effectivity, expressed as the inhibitory concentration 50%, IC_{50}, is displayed. This parameter is the concentration of the antibacterial agent at which 50% of

the bacteria population is killed. Therefore, a lower IC_{50} value means a higher antibacterial potency.
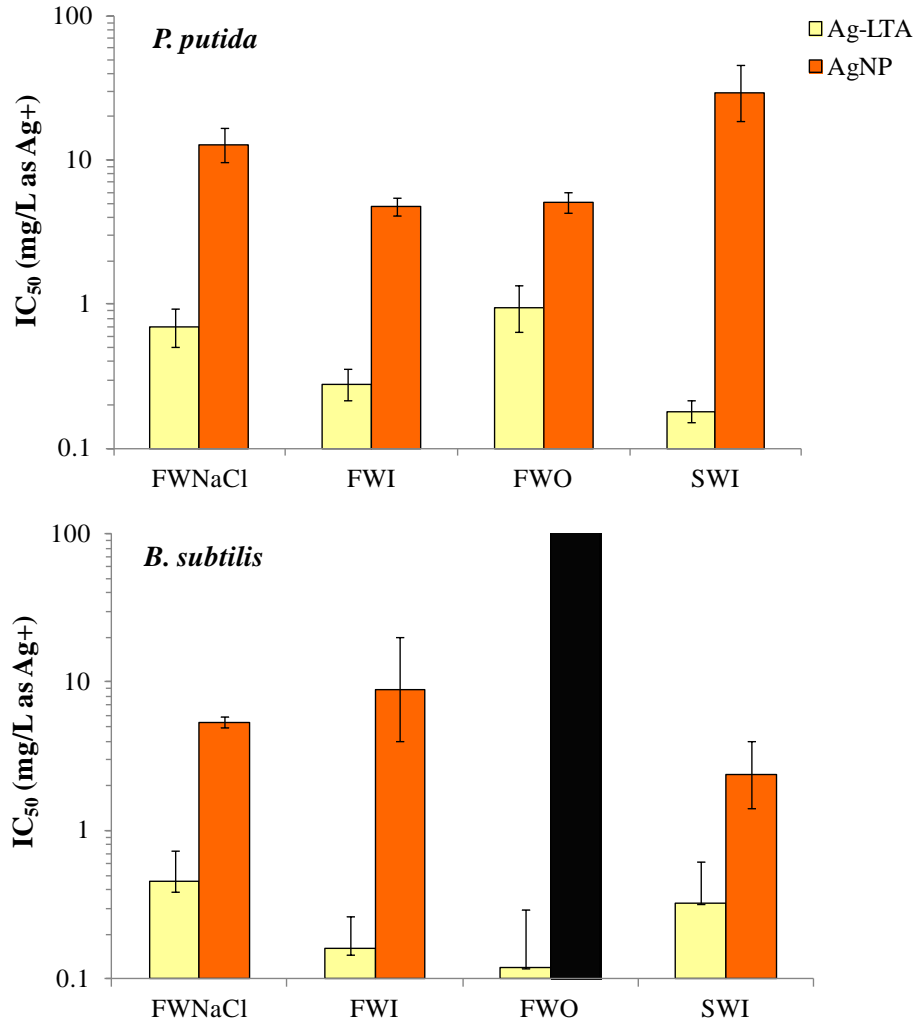

Figure 3.6 Summary of Ag-LTA and AgNP IC_{50} values for *B. subtilis* and *P. putida* in freshwater and seawater resembling solutions. (Black column indicates that $IC_{50}>125mg/L$)

Overall it was observed that Ag-LTA was at least 5 times more effective than AgNP to inactivate *P. putida* and *B subtilis* for all water chemistries tested. For all the water chemistries Ag-LTA IC_{50}s ranged between 0.1 and 1mg/L as Ag. Additionally, Ag-LTA was slightly better at inactivating *B. subtilis* than *P. putida*.

To confirm that the antibacterial activity of Ag-LTA originates in its extra framework Ag ions a bacterial viability test was performed with Na-LTA and compared to the results with Ag-LTA; Figure 3.6 shows that Na-LTA did not exert any antibacterial activity.
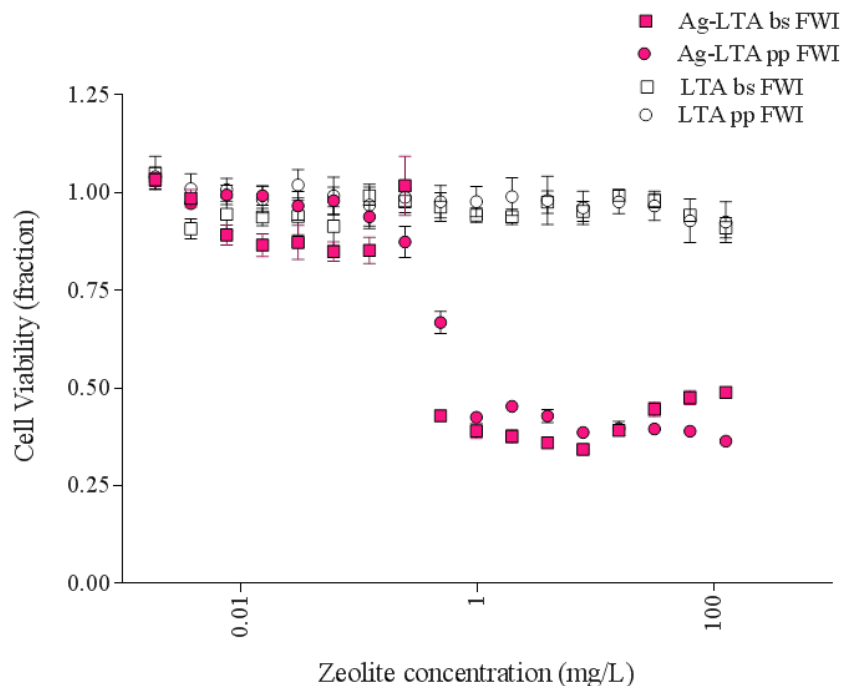

Figure 3.7 Cell viability of *B. subtilis* and *P. putida* in FWI in the presence of Ag-LTA or Na-LTA. Cell viability of 1 means 100% of bacteria is alive with respect to the control group.

3.3.4 Comparison of the antibacterial potency of Ag-LTA to other known antibacterial nanoparticles and salts

Additional viability tests were performed utilizing as antibacterial agent copper and zinc nanoparticles (CuNP, ZnNP) and three known antibacterial salts $AgNO_3$, $Cu(NO_3)_2$ and $Zn(NO_3)_2$ (Figure 3.7). These viability test were performed in FWI. The results suggest that Ag-LTA was the most effective antibacterial (although, likely not

significantly different than AgNO$_3$) to inactivate both *P. putida* and *B. subtilis*. The copper and zinc salts and the ZnNP when similarly effective at inactivating *B. subtilis* were less potent to inactivate *P. putida,* what is not completely unexpected since it is known that *P. putida* is very resistant to heavy metals and other toxicants[14]. AgNP and CuNP were the least effective against both bacteria.
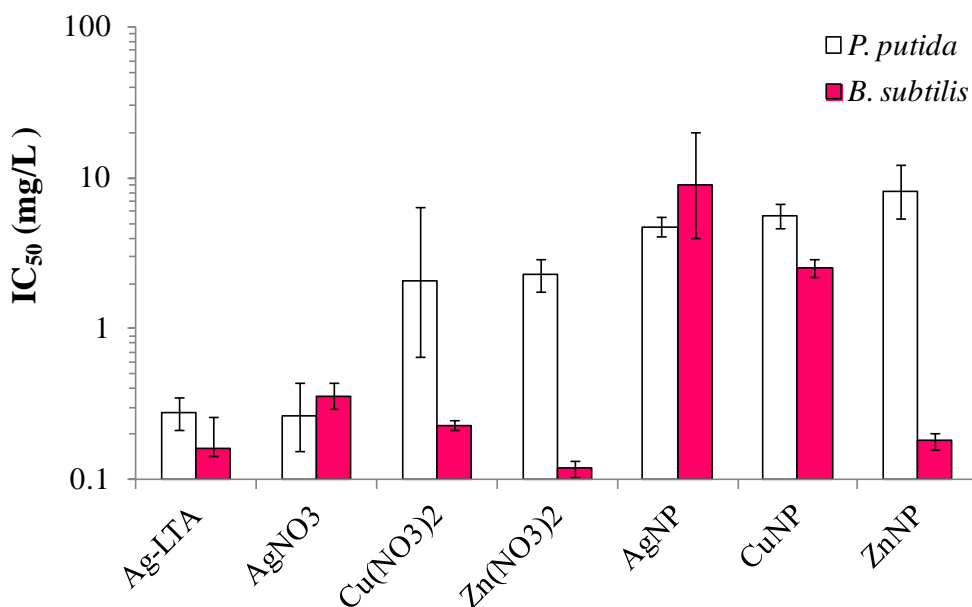

Figure 3.8 Comparing the antibacterial activity of Ag-LTA nanocrystals to antibacterial metallic nanoparticles and salts

3.4 Conclusions

The antibacterial activity of Ag-LTA against model Gram negative and Gram positive bacteria was evaluated in oligothropic simulated freshwater and seawater aquatic matrices. It was observed than under this conditions Ag-LTA exhibits a higher antibacterial potency than commercially available metallic nanoparticles. Indeed, Ag-

LTA's IC_{50} were comparable to those of silver nitrate solution. Moreover, Ag-LTA was able to inactivate at almost the same low dose *B. subtilis* and *P. putida,* while at that low dose copper and zinc salt were only able to inactivate *B. subtilis.* Considering these results and the concepts that zeolites are very hydrophilic and that will not affect the integrity of a poly(vinyl) by leaving a hole after the depletion of its antibacterial ions, it seems that LTA-Ag or LTA loaded with other antibacterial ions might be a good candidate to incorporate in PVA films to form LTA-PVA nanocomposites.
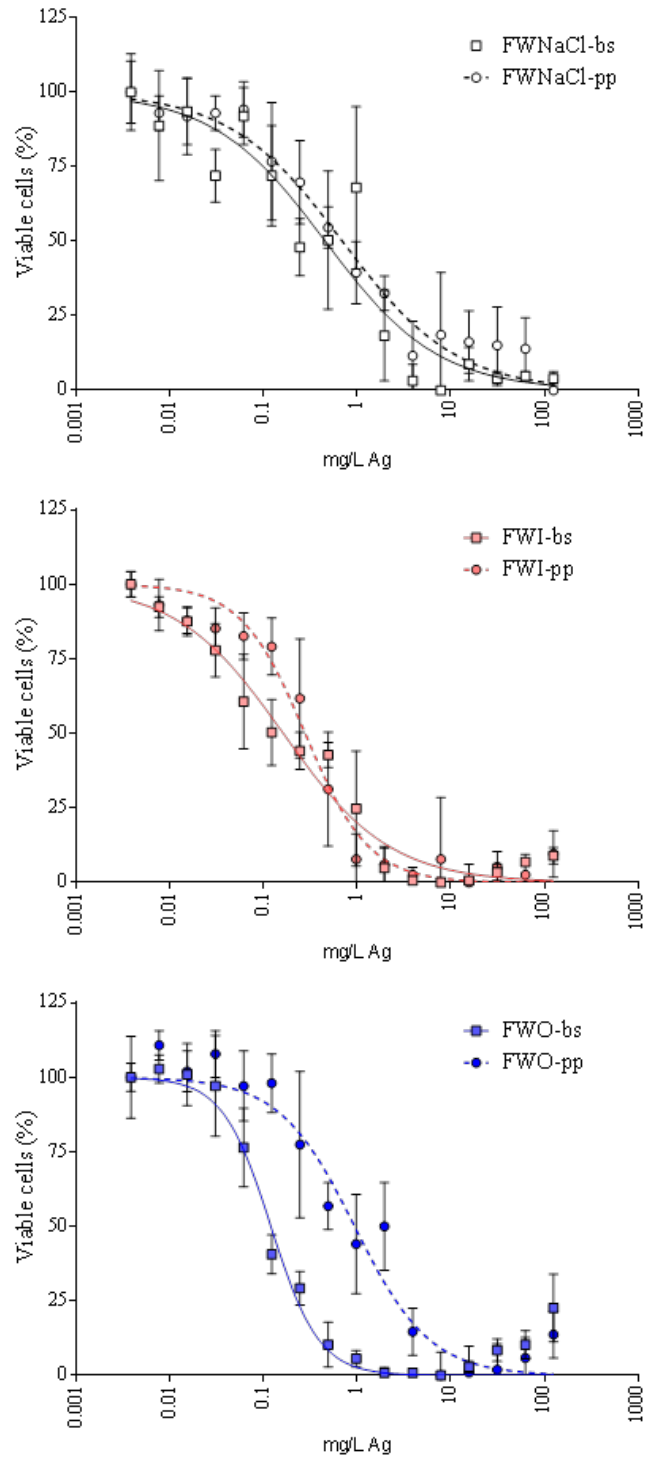
Figure 3A.1   Dose response curves for Ag-LTA in fresh water resembling solutions for
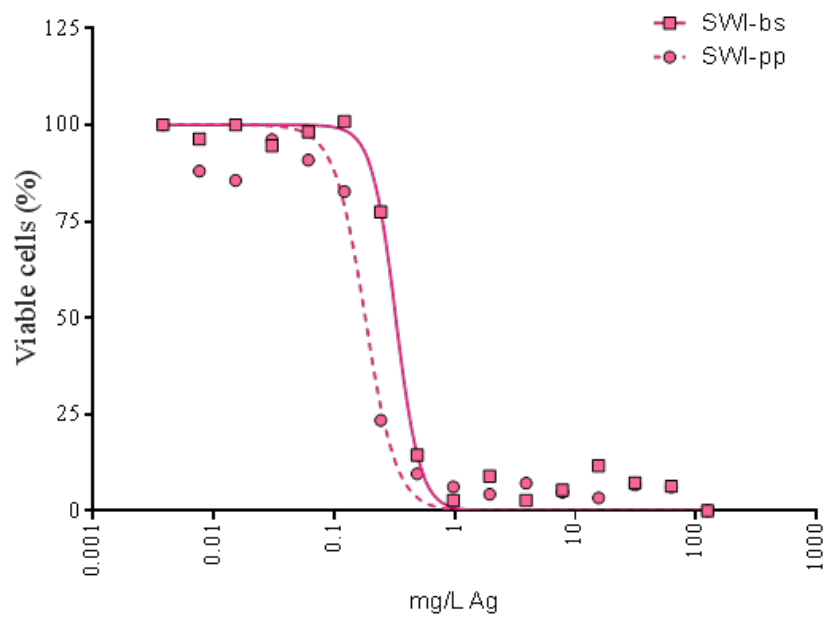*B. subtilis* (squares) and *P. putida* (circles)

Figure 3A.2   Dose response curves for Ag-LTA in seawater resembling solutions for
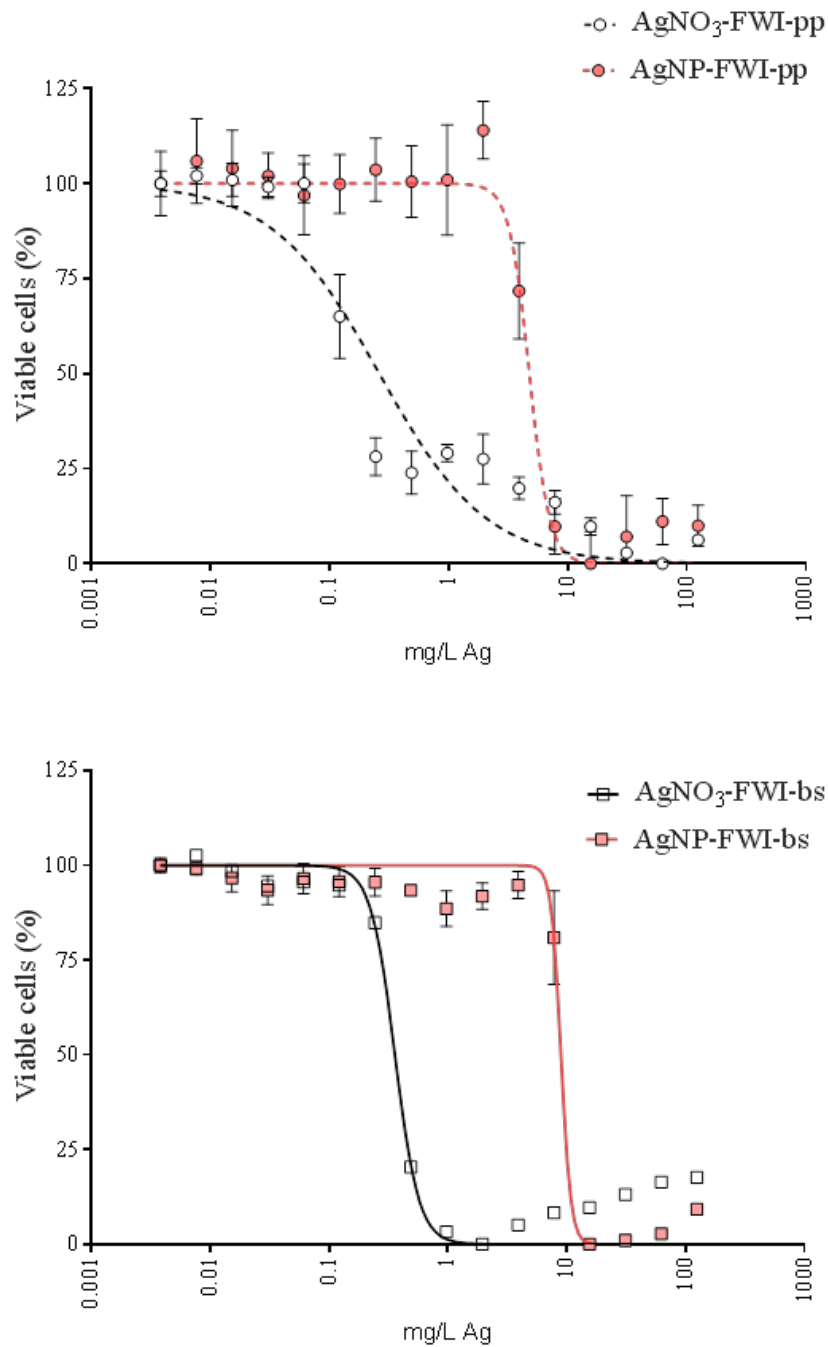*B. subtilis* (bs) and *P. putida* (pp)

Figure 3A.3   Dose response curves for silver nanoparticles (AgNP) and silver nitrate in seawater resembling solutions for *B. subtilis* (bs) and *P. putida* (pp)
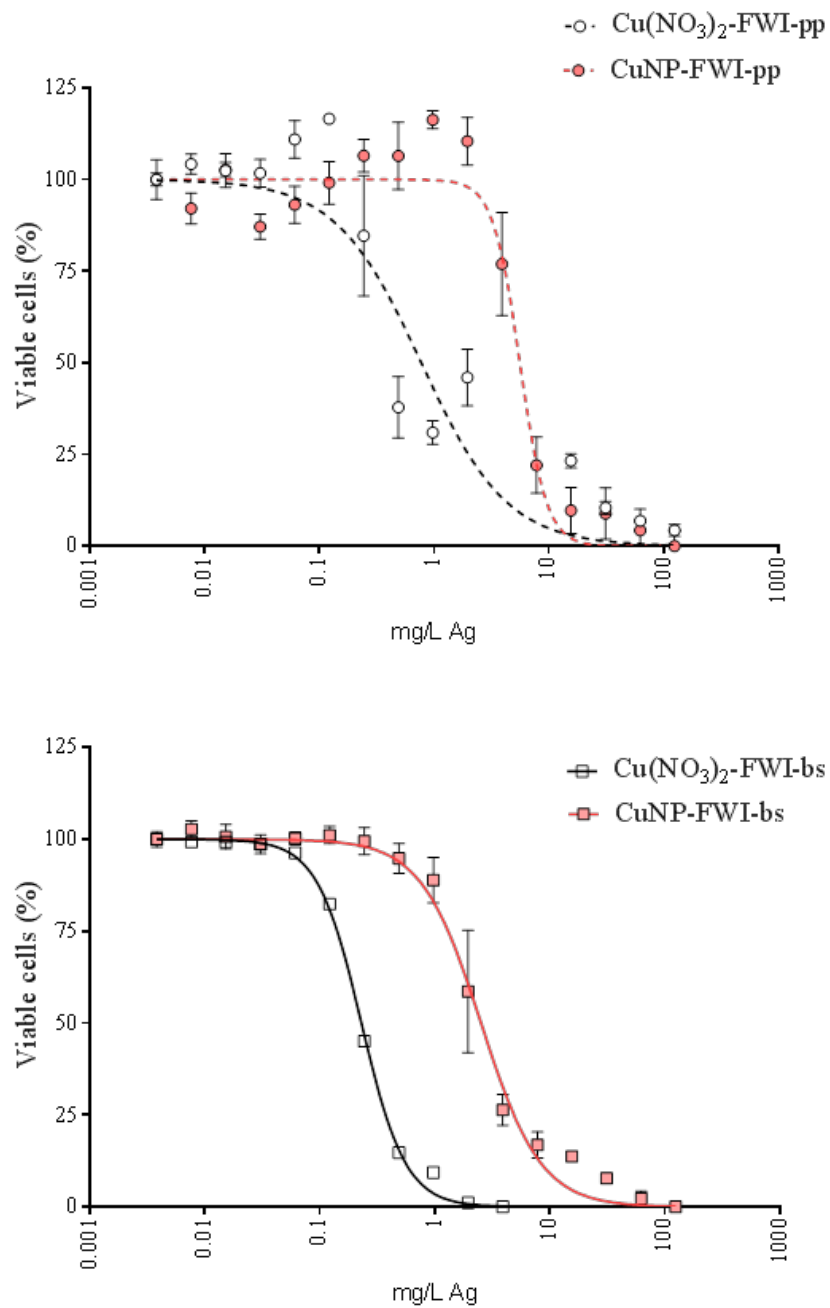
Figure 3A.4   Dose response curves for copper nanoparticles (CuNP) and copper nitrate in FWI solutions for *B. subtilis* (bs) and *P. putida* (pp)
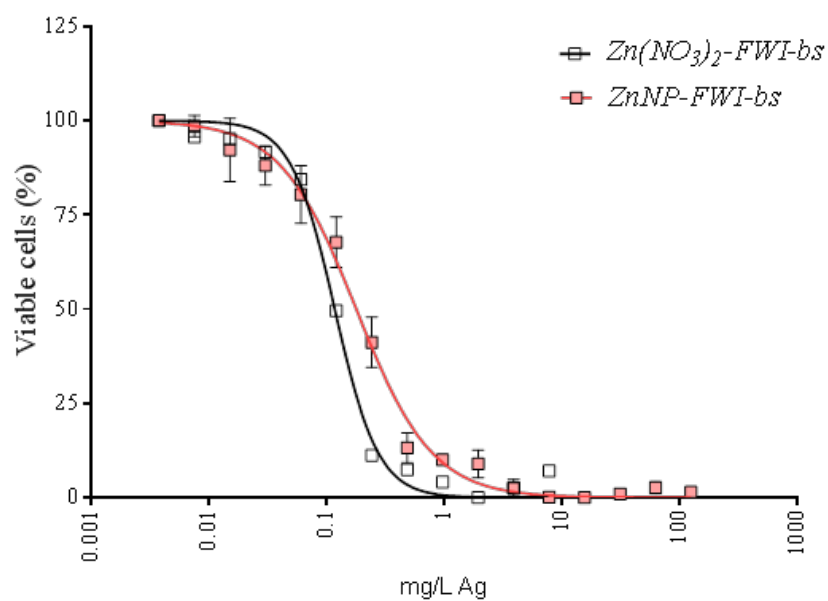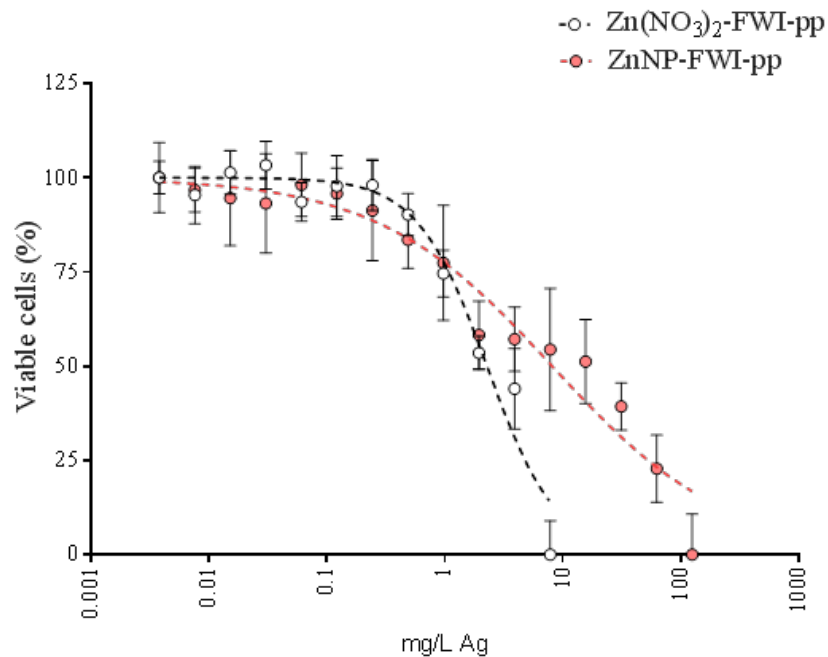
Figure 3A.5   Dose response curves for zinc nanoparticles (ZnNP) and zinc nitrate in FWI solutions for *B. subtilis* (bs) and *P. putida* (pp)

References

1.   (a) Vertelov, G.; Krutyakov, Y.; Efremenkova, O.; Olenin, A.; Lisichkin, G., A versatile synthesis of highly bactericidal Myramistin® stabilized silver nanoparticles. *Nanotechnology* **2008,** *19* (35); (b) Raffi, M.; Hussain, F.; Bhatti, T.; Akhter, J.; Hameed, A.; Hasan, M., Antibacterial characterization of silver nanoparticles against *E. coli* ATCC-15224. *J Mater Sci Technol* **2008,** *24* (2), 192-196; (c) Smetana, A.; Klabunde, K.; Marchin, G.; Sorensen, C., Biocidal activity of nanocrystalline silver powders and particles. *Langmuir* **2008,** *24* (14), 7457-7464; (d) Yoon, K.; Byeon, J.; Park, J.; Ji, J.; Bae, G.; Hwang, J., Antimicrobial characteristics of silver aerosol nanoparticles against Bacillus subtilis bioaerosols. *Environ Eng Sci* **2008,** *25* (2), 289-293.

2.   Marambio-Jones, C.; Hoek, E. M. V., A review of the antibacterial effects of silver nanomaterials and potential implications for human health and the environment. *J Nanopart Res* **2010,** *12* (5), 1531-1551.

3.   Pal, S.; Tak, Y.; Song, J., Does the antibacterial activity of silver nanoparticles depend on the shape of the nanoparticle? A study of the gram-negative bacterium *Escherichia coli*. *Appl Environ Microb* **2007,** *73* (6), 1712-1720.

4.   Jin, X.; Li, M. H.; Wang, J. W.; Marambio-Jones, C.; Peng, F. B.; Huang, X. F.; Damoiseaux, R.; Hoek, E. M. V., High-Throughput Screening of Silver Nanoparticle Stability and Bacterial Inactivation in Aquatic Media: Influence of Specific Ions. *Environ Sci Technol* **2010,** *44* (19), 7321-7328.

5.   (a) Kim, E. S.; Hwang, G.; El-Din, M. G.; Liu, Y., Development of nanosilver and multi-walled carbon nanotubes thin-film nanocomposite membrane for enhanced water treatment. *J Membrane Sci* **2012,** *394*, 37-48; (b) Lee, S. Y.; Kim, H. J.; Patel, R.; Im, S. J.; Kim, J. H.; Min, B. R., Silver nanoparticles immobilized on thin film composite polyamide membrane: characterization, nanofiltration, antifouling properties. *Polymers for Advanced Technologies* **2007,** *18* (7), 562-568.

6.   Yin, J.; Yang, Y.; Hu, Z.; Deng, B., Attachment of silver nanoparticles (AgNPs) onto thin-film composite (TFC) membranes through covalent bonding to reduce membrane biofouling. *J Membrane Sci* **2013,** *441*, 73-82.

7.   Cao, X. L.; Tang, M.; Liu, F.; Nie, Y. Y.; Zhao, C. S., Immobilization of silver nanoparticles onto sulfonated polyethersulfone membranes as antibacterial materials. *Colloid Surface B* **2010,** *81* (2), 555-562.

8.   Zodrow, K.; Brunet, L.; Mahendra, S.; Li, D.; Zhang, A.; Li, Q. L.; Alvarez, P. J. J., Polysulfone ultrafiltration membranes impregnated with silver nanoparticles show improved biofouling resistance and virus removal. *Water Res* **2009,** *43* (3), 715-723.

9.   Breck, D. W., *Zeolite Molecular Sieves: Structure, Chemistry, and Use;* Wiley: New York, 1974.

10.   (a) Inoue, Y.; Hoshino, M.; Takahashi, H.; Noguchi, T.; Murata, T.; Kanzaki, Y.; Hamashima, H.; Sasatsu, M., Bactericidal activity of Ag-zeolite mediated by reactive oxygen species under aerated conditions. *J Inorg Biochem* **2002,** *92* (1), 37-42; (b) Cowan, M.; Abshire, K.; Houk, S.; Evans, S., Antimicrobial efficacy of a silver-zeolite matrix coating on stainless steel. *J Ind Microbiol Biot* **2003,** *30* (2), 102-106.

11.   Clesceri, L. S.; Greenberg, A. E.; Eaton, A. D.; Franson, M. A. H.; American Public Health Association; American Water Works Association; Water Environment Federation, *Standard Methods for the Examination of Water and Wastewater*. 20th ed.; American Public Health Association: Washington, DC 1998; p 1220.

12.   Subramani, A.; Hoek, E. M. V., Direct observation of initial microbial deposition onto reverse osmosis and nanofiltration membranes. *J Membrane Sci* **2008,** *319* (1-2), 111-125.

13.   Elimelech, M.; Omelia, C. R., Effect of Electrolyte Type on the Electrophoretic Mobility of Polystyrene Latex Colloids. *Colloid Surface* **1990,** *44*, 165-178.

14.   (a) Ansari, M. I.; Malik, A., Biosorption of nickel and cadmium by metal resistant bacterial isolates from agricultural soil irrigated with industrial wastewater. *Bioresource Technol* **2007,** *98* (16), 3149-3153; (b) Haritash, A. K.; Kaushik, C. P., Biodegradation aspects of Polycyclic Aromatic Hydrocarbons (PAHs): A review. *J Hazard Mater* **2009,** *169* (1-3), 1-15.

CHAPTER IV

EVALUATION OF BACTERIAL ADHESION AND INACTIVATION ON

POLYVINYL ALCOHOL -ZEOLITES NANOCOMPOSITES

4.1   Introduction

One of the main drawbacks in membranes technologies is biofouling, which is defined as   the unwanted biofilm formation on the membrane surfaces that leads to operational problems such as increasing pressure requirements, flux decline and shortened membrane life[1]. It has been reported that up to 50% of plant operational costs are associated to biofouling[2].

While other forms of fouling such as scaling or colloidal fouling can be controlled by pretreatment such as anti-scalants and ultrafiltration, biofouling problems have not been totally solved. The key steps of biofilm formation are[3]: 1) Membrane modification where organic matter adsorbs to the surface, 2) reversible bacterial adhesion, where bacterial cells are deposited on the membrane surface by hydrodynamic forces, 3). irreversible bacterial adhesion, where adhered microbial cells anchor themselves more permanently to the membranes through the production and excretion of extra-cellular polymeric substances (EPS) and finally biofilm formation, where the adhere cells growth and reproduce using organics and other nutrients from the feed water.

Current research trends to control biofouling include surface modifications that change the membrane material to have a low affinity for bacteria. These surface modifications can be done by polymer blending , grafting, coatings or adding antimicrobial additives[4]. Some antimicrobial additives are polymers containing quaternary[5], cooper [6], silver nanoparticles [7], fullerenes, TiO_2 nanoparticles [8], silver and silver-zeolites[9].

Silver zeolites are very attractive because their incorporate two desired features, they are antibacterial and they are very hydrophilic. In this study, the reversible and irreversible bacterial adhesion on zeolite-PVA nanocomposites, prepared with embedded silver-zeolite (LTA-Ag), cooper-zeolite (Cu-LTA) and zinc-zeolites nanoparticles, is analyzed systematically. The effect of bacterial type, solution chemistry, antibacterial ion utilized on reversible and irreversible adhesions is considered.

4.2   Materials and methods

4.2.1   *Water chemistry preparation*

Three simulated version of seawater were prepared with compositions in increasing complexity (Table 4.1) . In addition to the two seawater solutions utilized in chapter 2, *i. e.*, seawater inorganics (SWI) and seawater organics (SWO) a simple electrolyte consisting of NaCl solution at the same ionic strength was utilized.

Table 4.1   Water chemistry composition (mg/L)

	SWNaCl	SWI	SWO
Na^+	14473.1	9624.8	9624.8
Mg^{2+}	-	1146.6	1146.6
Ca^{2+}	-	368.0	368.0
K^+	-	356.3	356.3
$Sr2+$	-	7.2	7.2
Cl^-	22326.9	17290.7	17290.7
SO_4^{2-}	-	2422.9	2422.9
HCO_3^-	-	112.5	112.5
NO_3^-	-	0.0	0.0
Br-	-	60.1	60.1
F-	-	1.2	1.2
H_3BO_3	-	23.0	23.0
Ionic strength (M)	0.63	0.630	0.63
Total dissolved solids	36800.0	31413.3	31413.3
pH	7.0	7.0	7.0
TOC (mg/L)	0.0	0.0	20.0

The pH of the solution was adjusted to 7 using HCl or NaOH. All chemicals were ACS reagent grade or better and used as received (Fisher Scientific, Pittsburgh, PA). Seawater NaCl, seawater inorganics and the seawater organic recipe (before adding of organics) were sterilized in an autoclaved at 121°C for 20 min and let cool to room temperature. After the sterile solution for seawater organic had reach room temperature 17 mg/L of alginic acid, 12.8 mg/L of BSA and 12.5 mg/L of tannic acid were added to this solution through a 0.2 μm syringe filter to reach 20 mg/L of TOC.

4.2.2   *Bacterial suspension preparation*

The model microorganisms used in this study, as in chapter 2, included *Pseudomonas putida* (provided by Dr. Patricia Holden at UC Santa Barbara), which is a gram-negative aerobic bacterium, and *Bacillus subtilis*, which is a gram-positive aerobic bacteria. Additionally, a third strain was utilized *Halomonas pacifica,* a non motile, rod-shaped, Gram-negative, marine bacteria[10], known to cause severe biofouling in marine environments [11].   Bacterial growth followed the protocol described previously by Subramani and Hoek [12]; single colonies of *P. putida* and *B. subtilis* were respectively inoculated in TSB and Luria–Bertani broth (LB). Then, the inoculated media were shaken at 150 rpm in an incubator at 25 °C and the cells were harvested at mid-exponential phase by centrifugation 8 min at 3,800 g. *H. pacifica* was grown at 30°C in artificial seawater, which comprised sea salts (38.5 g/L, Sigma) supplemented with bacteriological peptone (5 g/L, Sigma), and yeast extract (1 g/L, Sigma) [13]. Cells were harvested at the mid-exponential growth by centrifugation 8 min at 3,689 g.

After bacterial harvesting, cells were washed twice using phosphate buffered saline (PBS) solution followed by a wash step using the corresponding water chemistry

(SWNaCl, SWI or SWO). The washing procedure consists in resuspending the pelletized cells in the washing solution using a vortex and then centrifugation. Following the last washing step cells were resuspended in the corresponding water matrix to reach a concentration of 10^9 cfu/L following the procedure described by Kang et al, 2004[14], and used in the adhesion assay.

4.2.3   *Preparation and characterization of cation exchanged zeolite crystals*

Zeolite crystals were purchased from NanoScape Company (Munich, Germany). These zeolites have a nominal size of 150 nm, a characteristic pore size of 4Å and an empirical formula of NaAlSiO4. These zeolites have extra-framework Na^+ cations in their internal channels, neutralizing the net charge of the aluminosilicate structure. In order to load the zeolites with antibacterial ions the originally present Na^+ must be exchanged with the antibacterial cation. Three cation exchanged zeolites were prepared ; silver ions loaded zeolite, Ag-LTA, copper ions loaded zeolite Cu-LTA and zinc ions loaded zeolite , Zn-LTA.

Initially, the commercial zeolite was washed with distillated water at least 5 times to remove the excess of NaOH from the manufacturing process. Each step included vortexing the zeolite with distillated water followed by centrifugation (10 min at 4000rpm) and disposal of the supernatant. Then, the washed zeolite was immersed in 1M solution of either $AgNO_3$, $Cu(NO_3)_2$ or $Zn(NO_3)_2$ and shaked overnight in a wrist action shaker (Burrel Scientific, Pittsburgh) protected from light. Subsequently, the antibacterial ion loaded zeolites were washed three times with distillated water and the resulting zeolite pellets were freeze-dried for 48 hrs and stored in a dessicator. Subsequently, the antibacterial content in the zeolites was determined from an elemental analysis performed

in ICP-OES. For this purpose Na-LTA, Ag-LTa, Zn-LTA and Cu-LTA samples were acid digested with HNO_3 following standard method 3030E, section 2 [15].

4.2.4 *Nanocomposites casting*

Mowiol® PVA 4-98 and 6-98, whose properties are shown in TABLE 2.2, were utilized to cast the PVA nanocomposites and films. PVA powders were purchased from Sigma-Aldrich Company (Sigma–Aldrich, St. Louis, Missouri, USA). Succinic acid and maleic acid (> 99%, Sigma–Aldrich, St. Louis, Missouri, USA) were used as cross-linking agents.

PVA powder was dissolved under mechanically stirring in de-ionized water (DI) at 90 °C. Unless otherwise specified, the PVA concentration was 0.10 wt%. Next, PVA solutions were cooled to room temperature and the cross-linking agent was added, along with 2 M HCl, as catalyst to adjust the pH to 2.3 under continuous stirring to produce the PVA casting solution. Cross-linking agent concentration was selected to produce a theoretical cross-linking degree of 10%, which was defined by

$$\chi_{CL}[\%] = \frac{W_{CL} \times MW_{PVAunit} \times 2}{W_{PVA} \times MW_{CL}} \times 100 \qquad (1)$$

where W_{CL}, W_{PVA}, $MW_{PVAunit}$, and MW_{CL} represented the weight of cross-linking agent, the weight of PVA, the molecular weight of one PVA unit (—CHOHCH$_2$—), and the molecular weight of the cross-linking agent, respectively.

Then, Na-LTA or the antibacterial ion exchanged zeolites , Ag-LTA, Cu-LTA, Zn-LTA were added to the casting solution at a loading rate of 0% (PVA film), 1% and 10% to the PVA weight. In addition to nanocomposites containing a single type of

antibacterial zeolites, nanocomposites with equal ammounts of Ag-LTA, Cu-LTA and Zn-LTA were prepared, these films are referred as AgCuZn-LTA nanocomposites along this chapter. The zeolites were dispensed from a 800 mg/L zeolite suspension in distillated water that had been sonicated for 1 min before the addition. The resulting casting solution was then kept under continuous stirring in a wrist shaker (model 75, Burrell Scientific, Pittsburgh) for at least 30 min.

4.2.5 *Nanocomposites contact angle and free energy of adhesion determination*

The free energy of cohesion and adhesion as defined previously in chapter 2 section 2.2.4 were estimated for the LTA-PVA nanocomposites from contact angle measurements of glycerol, diiodomethane and water. In order to determine the contact angle data, the nanocomposites were cast on glass slides. subsequently a sessile drop method was adopted and an automated contact angle goniometer (DSA10 KRÜSS GmbH, Hamburg, Germany) was utilized to perform the measurements . A minimun of 12 equilibrium contact angles were determined for each liquid and film and the highest and lowest values discarded. The average of the remaining left and right contact angles was taken as the equilibrium contact angle.

4.2.6 *Nanocomposites surface morphology and roughness determination*

The surface morphology of nanocomposite specimens prepared from Mowiol@6-98 PVA cross-linked with succinic acid at a 10% cross-linking degree and containing 10% (w/w to the PVA) Ag-LTA, Cu-LTA, Zn-LTA and Na-LTA and the corresponding film without zeolites was characterized by scanning electron microscopy (SEM, JEOL JSM-6700F FE-SEM). Nanocomposite samples were casted on glass slides gold coated with a sputterer to reduce samples charging. The SEM settings utilized were 5kVvoltage,

a working distance between 6.5 and 7.8 mm and a SEI detector to determine the topological information.

Additional inspection of the nanocomposite surfaces was done by atomic force microscopy (Bruker Dimension 5000 Scanning Probe Microscope) and surface roughness was calculated using WSxM 4.0 Beta6.2 software (Nanotec Electronic S. L.). At least three different areas of the nanocomposites were scanned by tapping mode in air, using an scanning area ranging from 1 to 9um^2 and their average surface roughness was reported.

4.2.7   *High throughput screening adhesion and inactivation assay*

LTA-PVA nanocomposites and bacterial adhesion and inactivation was performed utilizing a modified version of the adhesion assay previously discussed by Peng *et. al.* [16]. In the adhesion assay described in chapter 2, the number of bacterial attachments was evaluated as a whole without distinguishing between live and dead bacterial fractions. Conversely, in this chapter the number of viable and non viable bacteria is also determined. The assay consists in four steps: (1) PVA coating film preparation, (2) biofilm formation, (3) biofilm staining, and (4) imaging and analysis.

First, 50 µL of the casting solutions described in section 4.2.4 was dispense per well in 384 well microplates (Cat # 781091, Greiner Bio One, Frickenhausen, Germany). Each microplate was designed with 8 different films. Then, the aqueous casting solution in the microplates was air-dried at room temperature for 24 h (in a closed sterile chamber) to initiate the cross-linking reaction, followed by curing in a laboratory oven at

100 °C. Later, 50 µL of SWNaCl, SWI or SWO bacterial suspension (see section 4.2.2) or the respective bacterial free water solutions were added per well.

The microplates were incubated for 24 hours at 30 °C followed by the dyeing process to quantify the total cell adhesion and bacterial inactivation. For this the nucleic acid stains SYTO-9 and propidium iodide from (LIVE/DEAD® BacLightTM Bacterial Viability Kits, Invitrogen, Carlsbad, CA, USA) were dissolved in 30 mL sterile DI water to achieve a concentration of 2µM and 10µM respectively. When used in combination SYTO-9 and PI allow the distinction between bacterial cells with healthy and intact membranes from bacterial cells whose membrane permeability has been compromised. A multidrop was utilized to dispense 10 µL of the nucleic stain solution into eachwell, and the microplates were incubated for 15 min at room temperature protected from light.

Two sets of imaging were performed of the nanocomposites surfaces in order to determine the total and irreversible number of bacterial adhesion. The first set was performed immediately after the 15 min of staining and then the nanocomposites were re-imaged after a hydraulic wash. In this hydraulic wash each well was rinsed three times with 100 µL DI water using an ELX405 Microplate Washer (BIO-TEK Instruments, Inc., Winooski, VT, USA) and re stained using additional 10 µL of live/dead probes . The nanocomposite imaging was carry out by Image-Xpress Micro (Molecular Devices, Sunnyvale, CA, USA) and the images were processed in MetaXpress 1.74R software (Molecular Devices, Sunnyvale, CA, USA) using the "Multiple Wavelength Cell Scoring" module. The number of live cells in the field of view resulted from the SYTO-9 channel while the number of cells with compromised cell membranes was obtained from

the PI channel. The approximate minimum width was set to 1 μm, and the approximate maximum to 10 μm and the intensity above background was 1,000 gray levels.

4.3 Results and discussion

4.3.1 *Antibacterial ions loading into zeolites*

The elemental composition of the prepared cation-exchanged zeolites showed Si/Al molar ratios close to 1, while the average ratio Al to exchange- cation resulted on 1.2, 1.1, 0.5 and 1.9 for Na-LTA, Ag-LTA, Cu-LTA and Zn-LTA respectively. This indicates that most of extra frame sodium ions were exchange for silver ions and zinc ions (one silver ion for each sodium or one zinc ion for every two sodium). However, the result obtained for copper suggest some other mechanism since more than one Cu^{2+} per every two sodiums ions were associated to the zeolite, is possible that copper hydroxide precipitation had occurred at some extent, but this was not confirmed. Table 4.2 presents the elemental composition of the zeolites as used in the formation of the nanocomposites. Values were calculated from ICP-OES measurements.

Table 4.2   Elemental composition (by weight percent) of prepared zeolites.

	Si % (w/w)	Al % (w/w)	Na^+ % (w/w)	Ag^+% (w/w)	Cu^{2+} % (w/w)	Zn^{2+} % (w/w)
Na-LTA	20.3 ± 0.9	19.2 ± 3.0	14.1 ± 0.8	-	-	-
Ag-LTA	13.3 ± 0.3	11.6 ± 1.5	0.7 ± 0.1	44.1 ± 2.7	-	-
Cu-LTA	11.5 ± 3.1	10.8 ± 3.3	1.2 ± 0.5	-	50.0 ± 8.0	-
Zn-LTA	18.3 ± 0.7	17.0 ± 2.6	1.6 ± 0.1	-	-	21.2 ± 0.7

4.3.2   *Nanocomposites morphology characterization*

A subset of LTA-PVA nanocomposites were selected to illustrate the effect that zeolites addition have in their morphology. Analysis by SEM provides a visual characterization of the surface morphology and AFM offers a more quantitative analysis. PVA films prepared from 47kDa PVA and cross-linked with succinic acid (10% crosslinked degree) showed a very smooth surface (Figure 4.1) while the corresponding nanocomposites had rougher surfaces product of the zeolites inclusions (Figure 4.2).

The four imaged nanocomposites were prepared with 10% loading of zeolite to the PVA weight. All the nanocomposites exhibited submicron features covering all the viewed area and some scattered micron sized features . However, the nanocomposite prepared from Cu-LTA showed a larger quantity and slightly larger micron sized agglomerates. The nanocomposite prepared with Zn-LTA had the most smother surface by visual inspection.
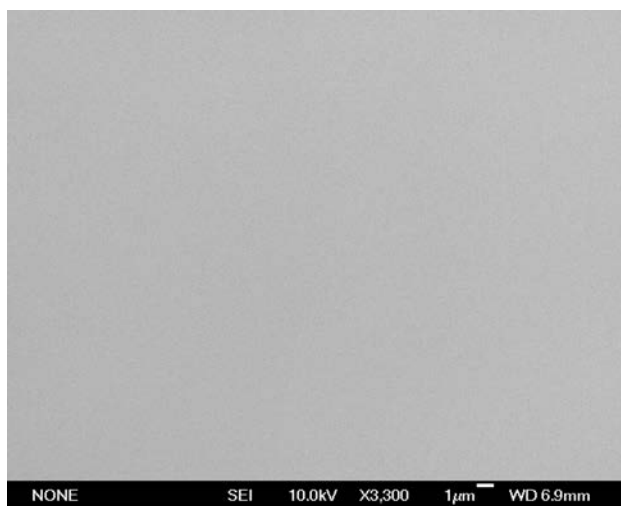

Figure 4.1   SEM images of PVA film prepared from 47KDa PVA (Mowiol 6-98) cross-linked with succinic acid at 10% cross-linking degree.

Na-LTA_PVA   Ag-LTA_PVA

Cu-LTA_PVA   Zn-LTA_PVA
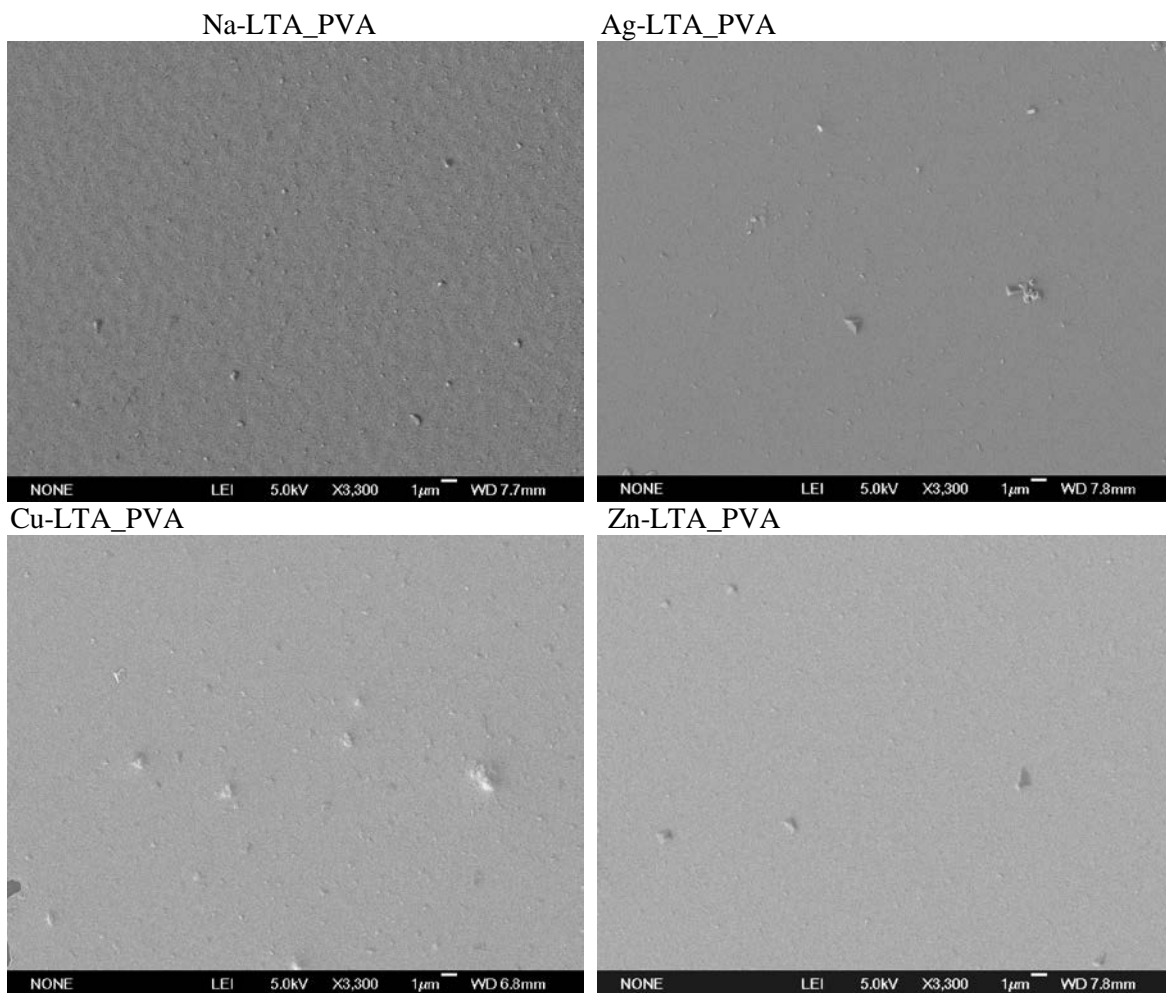

Figure 4.2   SEM images of LTA-PVA nanocomposites prepared from 47KDa PVA
              (Mowiol 6-98) cross-linked with succinic acid at a 10% cross-linking degree and
              the inclusion of 10% (w/w) to the PVA weight of Na-LTA (top left), Ag-LTA
              (top right), Cu-LTA (bottom left) and Zn-LTA (bottom right).

Roughness statistics derived from AFM measurements provide a quantitative

analysis of the surface morphology of the nanocomposites (Table 4.3). The roughness

analysis parameters selected to depict the surfaces morphology were average roughness

(Ra), root-mean-square roughness (Rq), and the surface area difference (SAD). The Ra,

as explained before by Hoek et al. can be understood as half the average peak-to-valley

depth; Rq describes the standard deviation of the entire distribution of morphological

116

feature height of the sample and the SAD is the increase in area due to roughness respect of a flat area of same planar dimensions[17].

Table 4.3   Roughness statistics for LTA-PVA nanocomposites and corresponding PVA films

Morphological parameter	rms roughness, Rq (nm)	average roughness, Ra (nm)	average height, (nm)	surface area difference, SAD(%)
6-98 maleic	0.5 ± 0.0	0.4 ± 0.0	2.1 ± 0.0	0.1 ± 0.0
6-98 succinic	0.6 ± 0.0	0.5 ± 0.0	2.7 ± 0.0	0.1 ± 0.0
6-98 succinic, Na-LTA 10%	1.5 ± 0.2	1.1 ± 0.1	6.1 ± 0.2	1.5 ± 0.6
6-98 succinic, Ag-LTA 1%	1.8 ± 0.3	0.8 ± 0.1	1.8 ± 0.3	0.3 ± 0.1
6-98 succinic, Ag-LTA 10%	3.3 ± 1.8	2.0 ± 1.0	15.0 ± 1.8	0.7 ± 0.5
6-98 succinic, Cu-LTA 1%	2.1 ± 1.2	2.1 ± 1.2	5.1 ± 1.2	0.2 ± 0.1
6-98 succinic, Cu-LTA 10%	10.5 ± 8.3	4.5 ± 3.3	67.6 ± 8.3	3.8 ± 2.8
6-98 succinic, Zn-LTA 10%	1.4 ± 0.2	1.4 ± 0.2	5.7 ± 0.2	0.7 ± 0.2
6-98 succinic, AgCuZn-LTA 10%	5.5 ± 4.8	4.3 ± 3.8	19.3 ± 4.8	0.6 ± 0.4

As expected the PVA films (6-98 maleic and 6-98 succinic) have low roughness values; the increase in surface area (SAD %) product of the roughness was only 0.1% respect of a perfectly flat surface, the was not a significant difference in roughness from the variation of cross-linking agent.   All the parameters confirmed the increase in roughness produced by the zeolite and it was observed that higher zeolite loading rates resulted in rougher nanocomposites. However, the nanocomposites roughness can still be considered in the nanoscale size. SAD (%) were low, below 1% with exception of Na-LTA nanocomposites and the nanocomposite containing 10% loading of Cu-LTA. The nanocomposite contaning the three antibacterial zeolites (6-98 succinic, For the same zeolite loading rate in the composites, Cu-LTA nanocomposite showed higher Ra, Rq and SAD values, what is consisting with the observations made in SEM images.

117

4.3.3   Nanocomposites surface tensions and interfacial free energies

LTA-PVA nanocomposite and solid surface tensions and interfacial free energies were derived from contact angles of diiodomethane, glycerol, and water (Table 4.4). The PVA films used for comparison 6-98 succinic and 6-98 maleic were both wettable, while the first was hydrophilic and the later slightly hydrophobic. All the LTA-PVA nanocomposites were wettable and showed a range of hydrophilicities. Ag-LTA and Cu-LTA nanocomposites at a 1% of zeolite loading showed the lowest free energies of cohesion, but when increasing the loadings to 10% both nanocomposites become more hydrophilic. Increasing hydrophilicity with increasing zeolite loadings is expectable since LTA zeolites are known hydrophilic, even considered superhydrophilic materials[18] with water contact angles of less than 5°. Increase of other nanocomposite's hydrophicity had been reporter previously, such as for polyamide-NaA thin films[19].

Bacterial cells are typically highly negatively charged, although their zeta potential is expected to decrease with increasing ionic strength, and exhibit highly monopolar surface properties[20]. *P. putida, B. subtilis and H. pacifica* water glycerol and diiodomethane, contact angle previously reported [12, 21] , were utilized to determine their respective surface tension components. All three strains had acid base electron donor components of two order of magnitude higher than the electron acceptor components, consistent with monopolar electron donor functionalities. Additionally, all 3 strains were hydrophilic, having *H. pacifica* the highest free energy of cohesion.

Table 4.4   Contact angle data, estimated surface tensions, wettability and free energy of cohesion for LTA-PVA nanocomposites and bacterial cells

Solid/Liquid Substrate	Raw/Measured Values			Intrinsic Substrate Properties					Wettability	Hydrophilicity		
	θ_{water} (deg)	$\theta_{glycerol}$ (deg)	$\theta_{diiodomethane}$ (deg)	γ^{LW} (mJ/m^2)	γ^{+} (mJ/m^2)	γ^{-} (mJ/m^2)	γ^{AB} (mJ/m^2)	γ^{TOT} (mJ/m^2)	$-\Delta G_{13}$ (mJ/m^2)	ΔG_{131}^{LW} (mJ/m^2)	ΔG_{131}^{AB} (mJ/m^2)	ΔG_{131}^{TOT} (mJ/m^2)
diiodomethane	n/a	n/a	n/a	50.8	0.0	0.0	0.0	50.8	n/a	n/a	n/a	n/a
glycerol	n/a	n/a	n/a	34.0	3.9	57.4	29.9	63.9	n/a	n/a	n/a	n/a
water	n/a	n/a	n/a	21.8	25.5	25.5	51.0	72.8	n/a	n/a	n/a	n/a
P. putida [a]	29.6 ± 3.1	35.9 ± 2.0	42.4 ± 3.9	38.4	0.0	61.9	1.9	40.3	136.1	-4.7	55.6	50.9
B. subtilis [a]	20.7 ± 4.2	22.5 ± 0.9	47.2 ± 1.3	35.8	0.2	64.0	6.7	42.5	140.9	-3.5	54.7	51.2
H. pacifica [b]	20.9 ± 0.7	42.1 ± 3.9	66.3 ± 8.6	25.0	0.1	80.3	6.5	31.5	140.8	-0.2	73.3	73.1
6-98 maleic	47.1 ± 4.9	45.4 ± 0.6	39.8 ± 1.1	39.7	0.9	28.7	10.0	49.7	122.4	-5.3	5.1	-0.3
6-98 succinic	42.0 ± 1.9	47.8 ± 2.8	39.7 ± 0.7	39.8	0.4	37.7	7.4	47.1	126.9	-5.4	19.3	14.0
6-98 succinic, Ag-LTA 1%	48.4 ± 2.7	46.8 ± 2.6	41.0 ± 0.7	39.1	0.8	28.0	9.7	48.8	121.1	-5.0	4.0	-1.0
6-98 succinic, Ag-LTA 10%	42.2 ± 1.8	51.9 ± 1.2	39.0 ± 1.3	40.1	0.1	41.2	3.5	43.7	126.8	-5.5	26.1	20.6
6-98 succinic, Cu-LTA 1%	59.1 ± 3.8	50.4 ± 2.1	39.0 ± 0.5	40.1	0.9	16.7	7.9	48.0	110.2	-5.5	-15.8	-21.3
6-98 succinic, Cu-LTA 10%	46.7 ± 2.4	52.4 ± 2.7	37.7 ± 0.6	40.8	0.1	35.0	4.0	44.8	122.8	-5.9	16.3	10.4
6-98 succinic, Zn-LTA 10%	39.5 ± 6.7	49.8 ± 2.6	37.4 ± 1.1	40.9	0.1	42.8	4.1	45.0	129.0	-6.0	28.2	22.3
6-98 succinic, Na-LTA 10%	51.6 ± 3.9	53.7 ± 1.8	39.3 ± 0.8	39.9	0.2	29.0	4.8	44.8	118.0	-5.5	6.3	0.8
6-98 succinic, AgCuZn-LTA 10%	39.6 ± 1.8	52.5 ± 2.7	40.0 ± 2.0	39.6	0.0	45.8	2.4	42.0	128.9	-5.3	33.4	28.1

Note a) Contact angle data for *P. putida* and *B. subtilis* in water, ethylene glycol and diiodomethane obtained Subramani[12]. b) Contact angle data for *H. pacifica* obtained from Huang[21b].

Based on the calculated surface tension for the bacterial strains and the LTA-PVA nanocomposites free energies of adhesion were drawn (Table 4.5). All combinations of bacteria and nanocomposite showed positive free energies of adhesion, even for the those nanocomposites classified as hydrophobic in Table 4.4. This indicates that the nanocomposites have a highest attraction for water than for the bacterial strains leading to a low propensity for bacterial adhesions.

Table 4.5   Free energy of adhesion between nanocomposites and bacteria

Solid/Liquid Substrate	Adhesional Propensity								
	P. putida			B. subtilis			H. pacifica		
	ΔG_{132}^{LW}	ΔG_{132}^{AB}	ΔG_{132}^{TOT}	ΔG_{132}^{LW}	ΔG_{132}^{AB}	ΔG_{132}^{TOT}	ΔG_{132}^{LW}	ΔG_{132}^{AB}	ΔG_{132}^{TOT}
	(mJ/m^2)	(mJ/m^2)	(mJ/m^2)	(mJ/m^2)	(mJ/m^2)	(mJ/m^2)	(mJ/m^2)	(mJ/m^2)	(mJ/m^2)
6-98 maleic	-5.0	26.2	21.2	-4.3	27.1	22.8	-1.1	35.1	34.0
6-98 succinic	-5.0	35.8	30.8	-4.3	36.3	32.0	-1.1	45.0	43.9
6-98 succinic, Ag-LTA 1%	-4.8	25.7	20.9	-4.2	26.7	22.5	-1.0	34.6	33.6
6-98 succinic, Ag-LTA 10%	-5.1	40.4	35.3	-4.4	40.9	36.5	-1.1	50.2	49.1
6-98 succinic, Cu-LTA 1%	-5.1	13.5	8.4	-4.4	15.1	10.7	-1.1	22.9	21.8
6-98 succinic, Cu-LTA 10%	-5.2	35.1	29.8	-4.5	35.8	31.3	-1.1	44.9	43.8
6-98 succinic, Zn-LTA 10%	-5.3	41.4	36.1	-4.5	41.7	37.2	-1.1	51.0	49.9
6-98 succinic, Na-LTA 10%	-5.0	29.3	24.2	-4.3	30.3	26.0	-1.1	39.2	38.1
6-98 succinic, AgCuZn-LTA 10%	-5.0	44.4	39.4	-4.3	44.6	40.4	-1.1	54.2	53.1

Nevertheless, the hydrophilicity and free energy of adhesion were estimated from contact angles in distillated water, i. e., did not consider the effect of the solution chemistries, such as the ionic strength, presence of divalent cations such as Ca^{2+} and the presence of organic material, which can induce changes in the hydrophilic and adhesion behaivor of the films.

4.3.4   *Bacterial adhesion on the nanocomposites*

The adhesion and inactivation experiments were designed to observe the adhesion behavior, of three model bacterial strain, to the nanocomposites containing different type of zeolites, added at different rates in three different simulated seawaters. The number of conditions in the experiments is quite large and thus the results have been combined in

heatmaps to analyze the general trends. However, individual plots for irreversible bacteria attachment of the 3 studied bacterial strains to each 44 analyzed nanocomposite are displayed in appendix A.

Figure 4.3 present the results of the observed total adhesion, i.e., before hydraulic wash of the films, and the irreversible adhesions, in other words, the number of bacterial attachment observed after the hydraulic wash. It can be noticed that independently of the experimental condition a large proportion of the total adhesions were successfully cleaned (note the difference in the scale bars).

Some general trends that emerge are as follow, total and irreversible adhesions were not strongly influenced by neither PVA molecular weight nor the cross-linking agent utilized. Overall, lower total bacterial adhesion occurred on SWNaCl, which is a simple NaCl electrolyte, when compared to the other two solution chemistries. In average, the marine bacteria *H. pacifica* produce a larger number of total bacterial adhesion than *P. putida* or *B. subtilis.*

The nanocomposites prepared from Na-LTA and Cu-LTA showed total and irreversible bacterial adhesion comparable or higher than the corresponding PVA films (same PVA chemistry but no zeolite added). On the other hand nanocomposites prepared from Ag-LTA (for 10% loading), Zn-LTA or the 3 antibacterial zeolites combined in the same nanocomposites had less propensity to adhesion.

In general terms, increase in the loading rates of zeolites produced less number of total and irreversible bacterial adhesion for nanocomposites containing Ag-LTA, while increased the number of adhesion in nanocomposites prepared with Cu-LTA. Increase in

the loading rate for Na-LTA, Zn-LTA and AgCuZn-LTA did not produce large difference in total or irreversible adhesions. It was discussed before that Cu-LTA nanocomposites have a larger surface roughness than the other composites, it seems that this feature significantly affect the propensity of cells attachments in the nanocomposites.
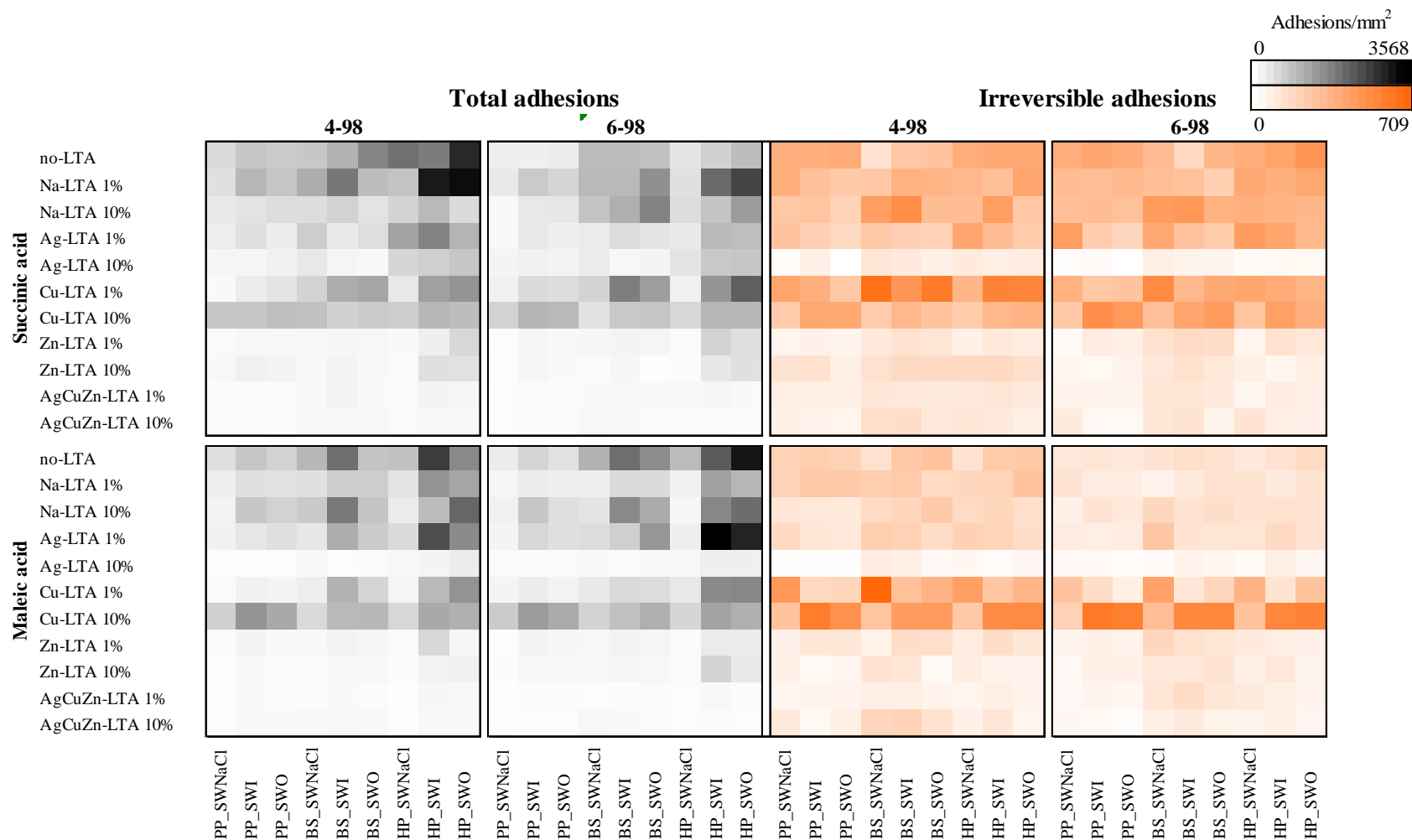
Figure 4.3   Heatmap representation of irreversible bacterial adhesion on LTA-PVA nanocomposites prepared from 27kDa (left) and 47kDa (right) molecular weight PVA; cross-linked with succinic acid (top) and maleic acid (bottom) in different simulated seawaters. Bacterial strains utilized *P. putida* (PP), *B. subtilis* (BS) and *H. pacifica* (HP).

4.3.5 *Attached bacterial cell viability*

The nanocomposites's antibacterial properties, were evaluated for each combination of bacteria_water chemistry_nanocomposite, by determining the proportion of dead to live cells within the adhered bacterial cells. These experimental results are extendedly displayed by bacteria type and nanocomposite in appendix A and summarized, as a heat map, in Figure 4.4.

Overall, higher inactivation rates were observed for irreversible adhesion than total adhesion. Nanocomposites loaded with 10% of Cu-LTA showed the highest inactivation rates for both total and irreversible attachment. These nanocomposites were also the ones that exhibit the higher total and irreversible bacterial attachment, showed the highest roughness and had lower hydrophilicities than Ag-LTA, Zn-LTA and AgCuZn-LTA nanocomposites of the same loading rate (although higher than Na-LTA ones).

The inactivation rates in PVA films and nanocomposites containing Na-LTA and low loadings of Ag-LTA or Cu-LTA were similar , while Zn-LTA and AgCuZn-LTA shown very low inactivation rates. Analysis of inactivation rates for irreversible adhesion shown no significant differences between bacteria types, and in average slightly higher proportions of the dead bacteria occurred for SWNaCl than in the other 2 more complex seawater compositions. Again, Cu-LTA containing nanocomposites produced very high inactivation rates for all water chemistry- bacteria combinations; Zn-LTA at 10% loading rates produced very high inactivation rates in SWNaCl but not much in the other water chemistries. AgCuZn-LTA produced similar number of inactivation rates across all the water chemistries and bacteria. The effectivity of an antibacterial ion depends on its

bioavailabity, which is dependent on the solution water chemistry. Having all the zeolites types combined in one nanocomposite is advantageous because is more likely that at least one ion type will be bioavailable at a given solution chemistry, additionally it offers a more broader spectrum of action to target different bacteria.
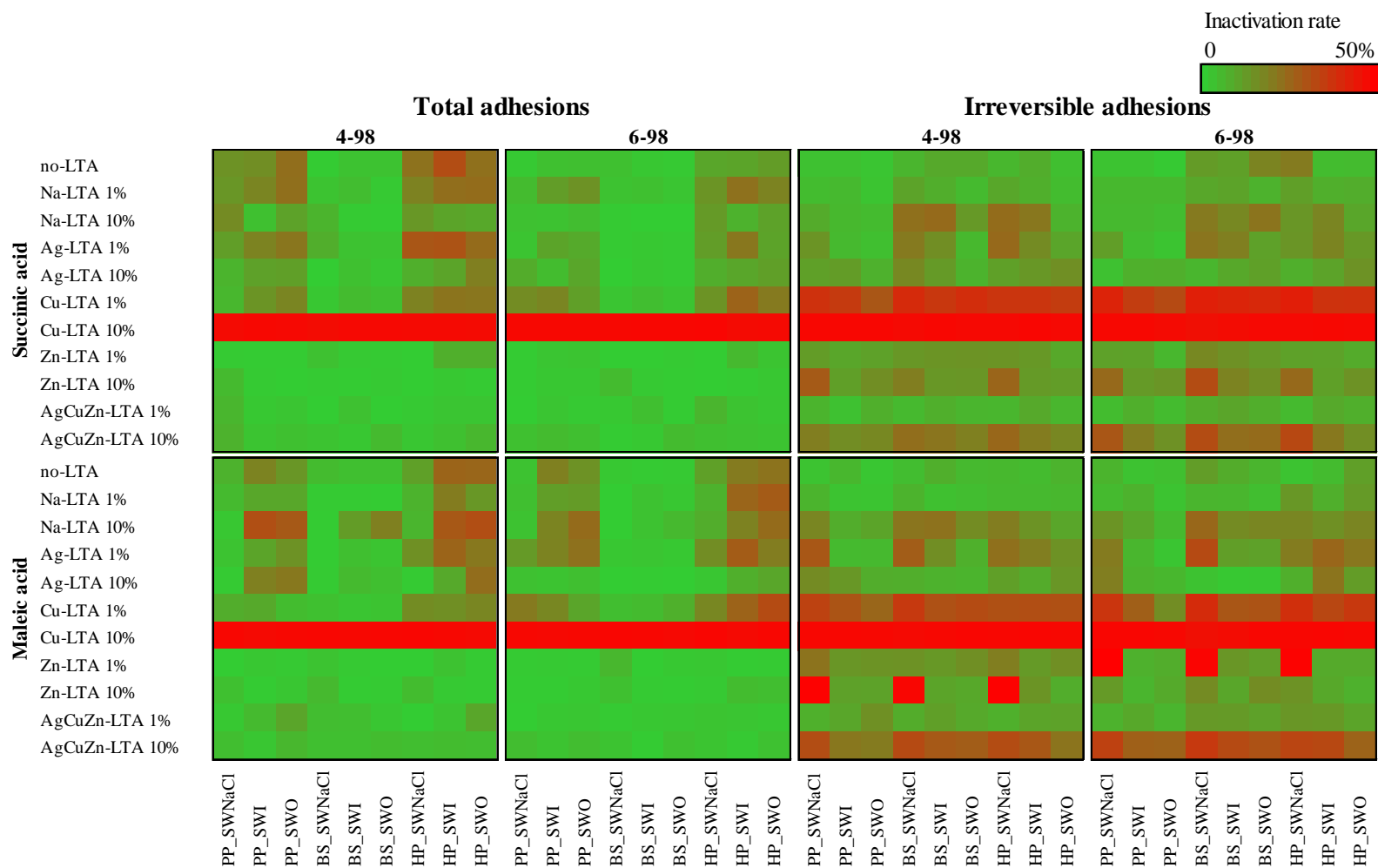
Figure 4.4   LTA-PVA nanocomposites estimated bacterial inactivation rate for total and irreversible bacterial adhesions. Nanocomposites prepared from 27kDa (left) and 47kDa (right) molecular weight PVA, cross-linked with succinic acid (top) and maleic acid (bottom) and a 10% loading (w/w to PVA weight) of LTA in different simulated seawaters. Bacterial strains utilized *P. putida* (PP), *B. subtilis* (BS) and *H. pacifica* (HP).

It was noted above that the percentage of dead bacteria was higher among irreversible than total bacterial adhesion, this might indicate that live cells were more effectively cleaned from the nanocomposites. The nucleic acid used to in this study indentifies live from dead bacteria based in the rupture of the membrane cell. This change in the cell surface morphology might lead to a higher hydraulic resistance thus decreasing the effectivity of the water cleaning. Additionally the surface properties of the dead bacteria is different from alive bacteria, for example zeta potential of dead bacteria, had been reported to be lower than alive healthy bacteria [22], mechanical damaged bacterial cells of *P. aeruginosa* showed zeta potential and water contact angles lower than healthy ones and their surface ratios of oxygen, nitrogen and phosphorus to carbon changed [23], suggesting changes in the functional groups. These changes will lead to variation of the adhesion propensity.

To illustrate, this point surface energies between nanocomposites and live and dead *H. pacifica* cells were calculated (Table 4.6). It was found that free energies between nanocomposites and dead cells were lower than for the alive cells, i.e., dead cells were less hydrophilic and more prone to attachment to the nanocomposites.

Table 4.6   Comparison between free energy of adhesion for selected
nanocomposites and alive or dead *H. pacifica* cells

Solid/Liquid Substrate	*H. pacifica (alive)*			*H. pacifica (dead)*		
	$\Delta G_{132}{}^{LW}$	$\Delta G_{132}{}^{AB}$	$\Delta G_{132}{}^{TOT}$	$\Delta G_{132}{}^{LW}$	$\Delta G_{132}{}^{AB}$	$\Delta G_{132}{}^{TOT}$
	(mJ/m^2)	(mJ/m^2)	(mJ/m^2)	(mJ/m^2)	(mJ/m^2)	(mJ/m^2)
H. pacifica [b]	-0.2	73.3	73.1	-1.8	67.8	65.9
6-98 maleic	-1.1	35.1	34.0	-3.1	30.9	27.8
6-98 succinic	-1.1	45.0	43.9	-3.1	41.0	37.9
6-98 succinic, Ag-LTA 1%	-1.0	34.6	33.6	-3.0	30.4	27.4
6-98 succinic, Ag-LTA 10%	-1.1	50.2	49.1	-3.2	46.0	42.8
6-98 succinic, Cu-LTA 1%	-1.1	22.9	21.8	-3.2	17.9	14.7
6-98 succinic, Cu-LTA 10%	-1.1	44.9	43.8	-3.3	40.5	37.2
6-98 succinic, Zn-LTA 10%	-1.1	51.0	49.9	-3.3	46.9	43.6
6-98 succinic, Na-LTA 10%	-1.1	39.2	38.1	-3.2	34.5	31.4
6-98 succinic, AgCuZn-LTA 10%	-1.1	54.2	53.1	-3.1	50.1	47.0

(Note: Bacteria contact angle data used in calculations was obtained from Huang [21b])

4.3.6   *Correlation of adhesion versus free energy of adhesion and nanocomposites roughness*

Irreversible adhesion and free energy of adhesion was correlated across all the nanocomposites with 10% LTA loadings (Figure 4.5). The linear correlation were very poor but general trends indicating decreasing adhesions with increasing free energy were observed. Free energies of adhesion were estimated based on water contact angles and not from contact angles of the simulated seawater solutions, this might explain partially the poor correlations observed.
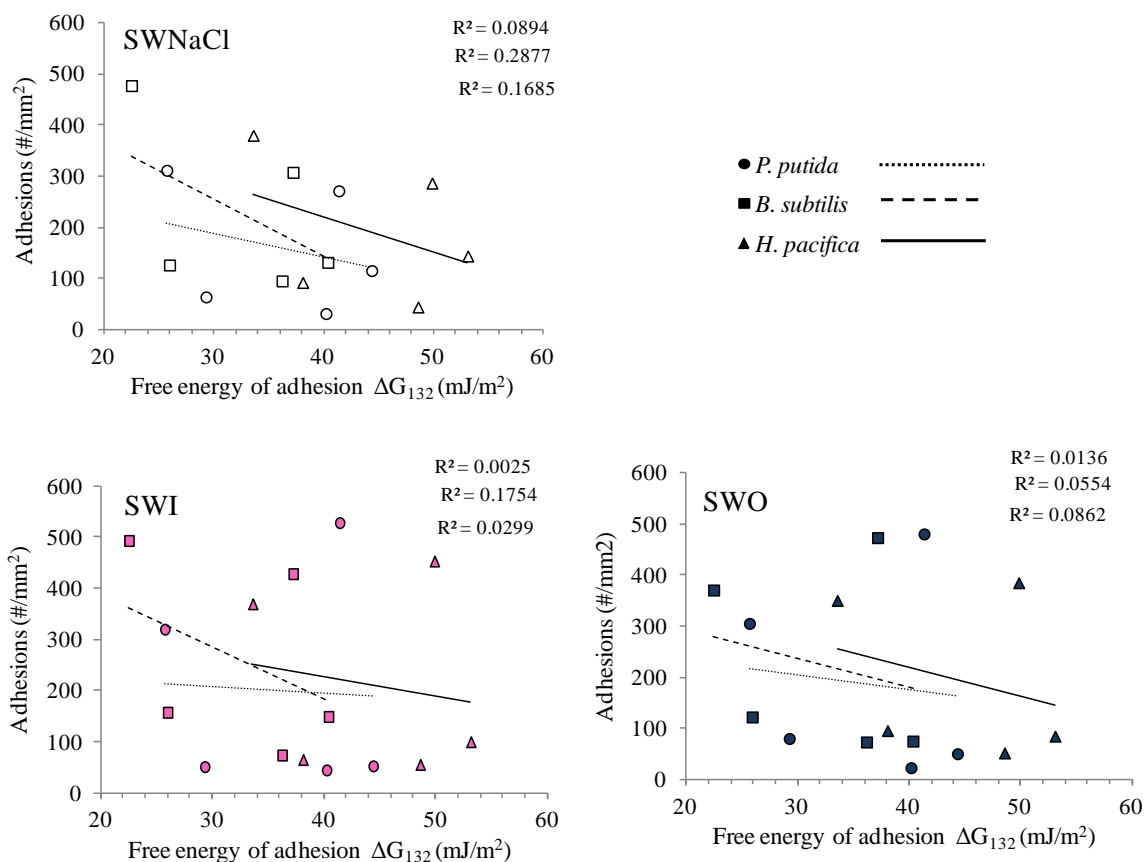
Figure 4.5   Correlation between irreversible number of adhesions and free energy of adhesion for nanocomposites with 10% zeolite loading in simulated seawater matrices. R^2 values organized from top to bottom for *P. putida*, *B. subtilis* and *H. pacifica.*

Irreversible adhesions correlated better with the nanocomposites roughness, expressed as SAD (Figure 4.6). Higher number of bacterial attachments occurred for lower roughness values. The irreversible adhesion had a low to moderate correlation with SAD in SWNaCl and a moderated to good correlation in the more complex water chemistries. Irreversible adhesion were also correlated with rms roughness, in this case the same trend as with SAD were observed, i.e., higher adhesion were observed for higher rms but the correlation coeficients were lower (appendix B)
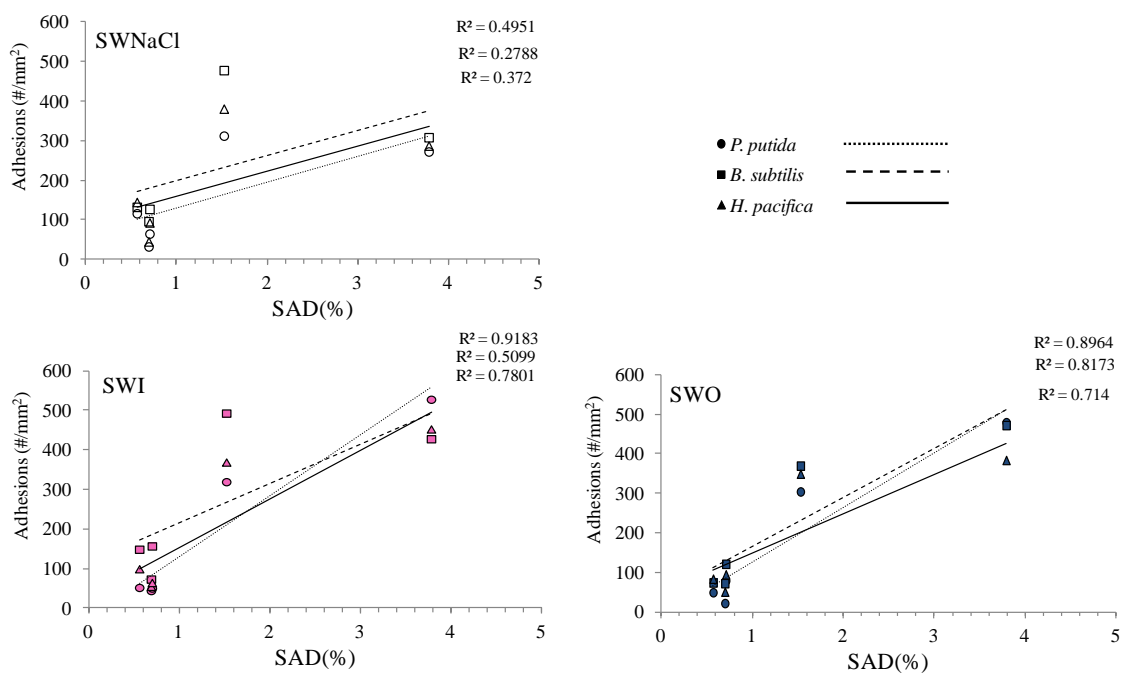
Figure 4.6   Correlation between irreversible number of adhesions and nanocomposite surface roughness SAD(%) for nanocomposites with 10% zeolite loading in simulated seawater matrices R^2 values organized from top to bottom for *P. putida*, *B. subtilis* and *H. pacifica.*

4.4   Conclusions

A combinatorial matrix of   LTA-poly(vinyl alcohol) nanocomposites were synthesized directly in 384-well microplates, and then bacterial adhesion, viability, and removal were quantitatively assessed using high throughput screening biofouling assays.

LTA-poly(vinyl alcohol) nanocomposites with a loading of 10% of LTA were hydrophilic based on distillated water contact angle. Two of the characterized nanocomposites with 1% zeolite loadings were slightly hydrophobic. However, all the films showed positive free energies of adhesion indicating low adhesion propensity.

Overall   PVA molecular weight or crosslinking agent were not a significant factor on total or irreversible adhesion. Of more relevance was the type of zeolite embedded in the film. The best performing film (lower number of irreversible adhesion) were the ones with 10% Ag-LTA closely followed by nanocomposites with Zn-LTA and the combined AgCuZn-LTA nanocomposites. Cu-LTA nanocomposite had total and irreversible adhesion comparable or even higher than the corresponding PVA film without zeolites. At the same time Cu-LTA showed the highest proportion of adhered dead cells, *i.e.,* a highest number of bacteria whose membrane were not intact, likely conditioning the film surface and making it less hydrophilic. Moreover Cu-LTA showed the highest roughness. All these factors made Cu-LTA more attractive for irreversible. bacterial attachment.

Irreversible adhesion did not correlated with free energy of adhesion for the nanocomposited loaded with 10% of antimicrobial zeolites. However, the surface roughness show a positive correlation with increasing irreversible adhesion.

Appendix 4A

NUMBER OF ADHESIONS (#/mm^2)
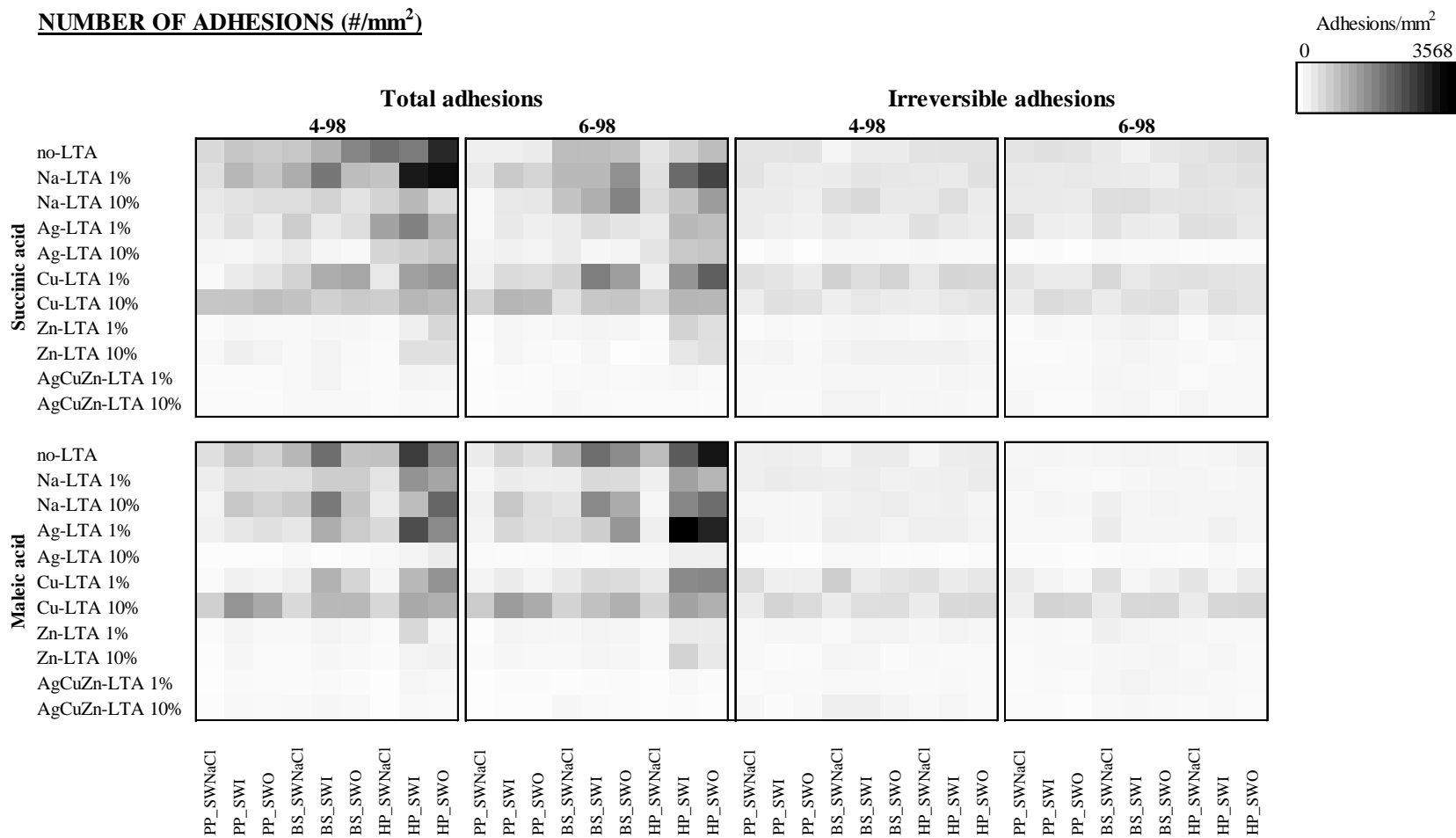
Figure 4A.1   Heatmap representation of irreversible bacterial adhesion on LTA-PVA nanocomposites prepared from   27kDa (left) and 47kDa (right) molecular weight PVA; cross-linked with succinic acid (top) and maleic acid (bottom) in different simulated seawaters. Bacterial strains utilized *P. putida* (PP), *B. subtilis* (BS) and *H. pacifica* (HP).
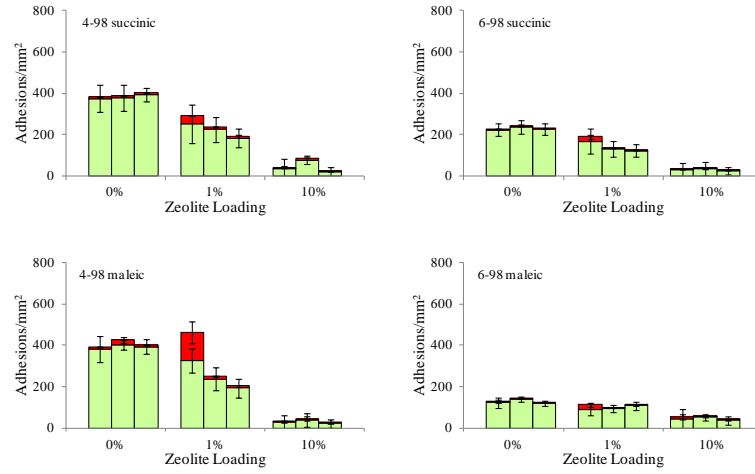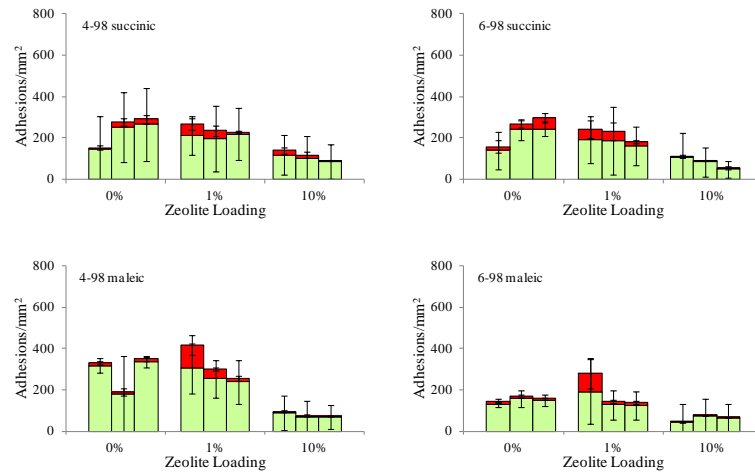
P. putida:
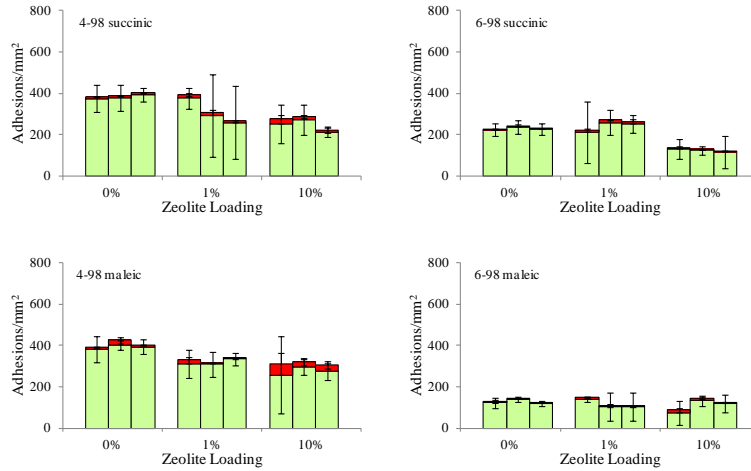
B. subtilis
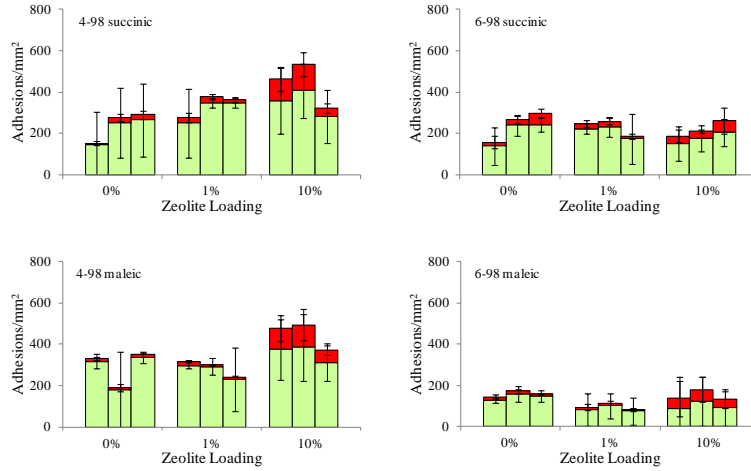
H. pacifica
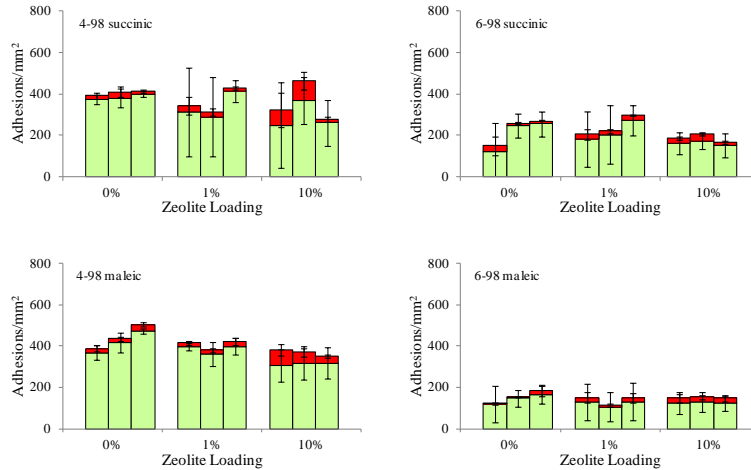
Figure 4A.2   Irreversible adhesions and inactivation of Na-LTA--PVA in SWNaCl, SWI and SWO (left, middle and right column in each cluster). Dead cells (red), alive cells (green) Nanocomposites prepared from   27kDa (4-98) and 47kDa (6-98) molecular weight PVA, cross-linked with succinic acid or maleic acid
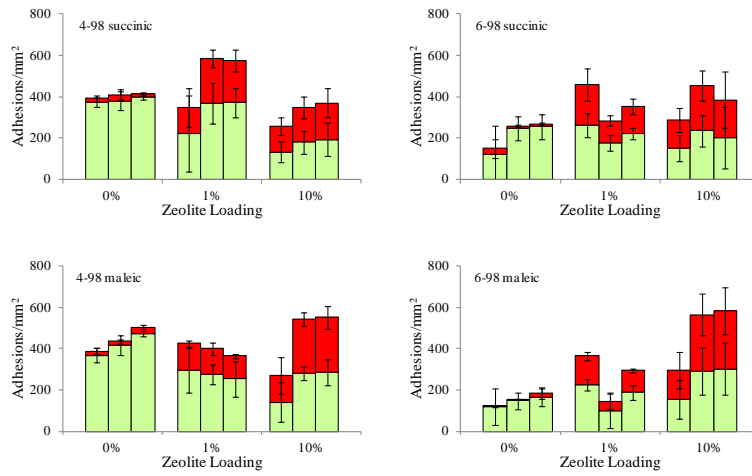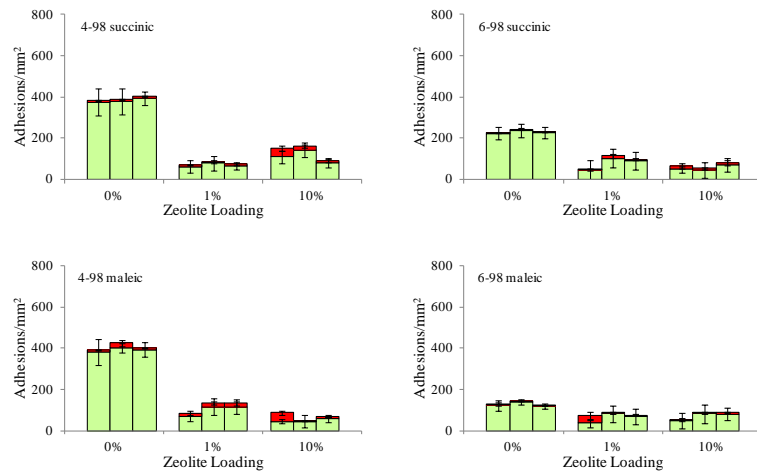
P. putida:

B. subtilis

H. pacifica
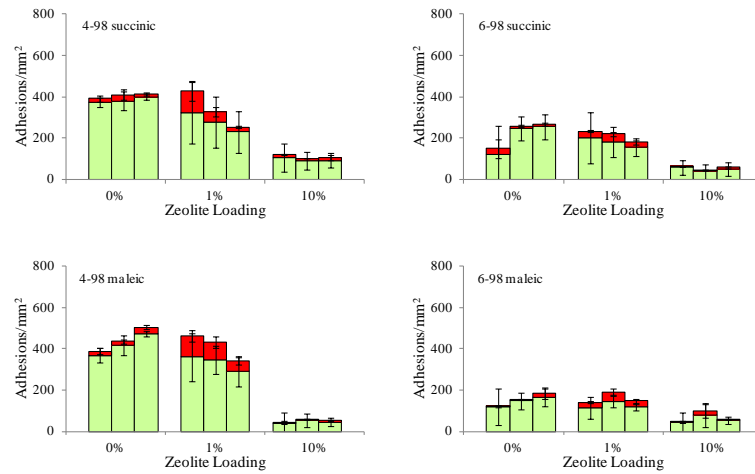
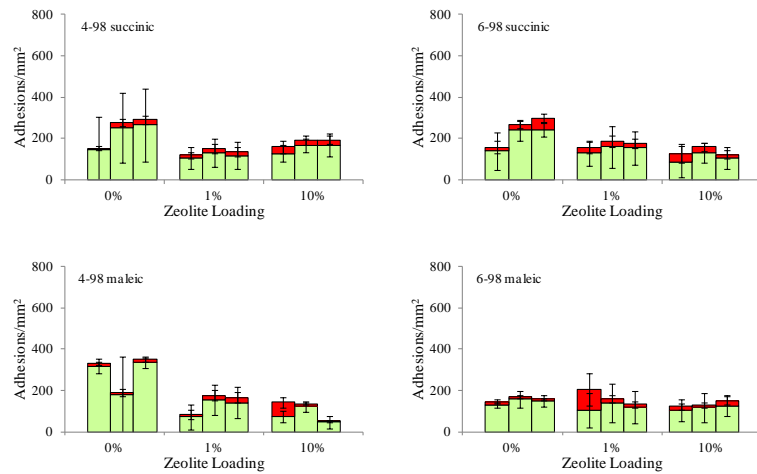
Figure 4A.3   Irreversible adhesions and inactivation of Ag-LTA--PVA in SWNaCl, SWI and SWO (left, middle and right column in each cluster).Nanocomposites prepared from 27kDa (4-98) and 47kDa (6-98) molecular weight PVA, cross-linked with succinic acid or maleic acid.
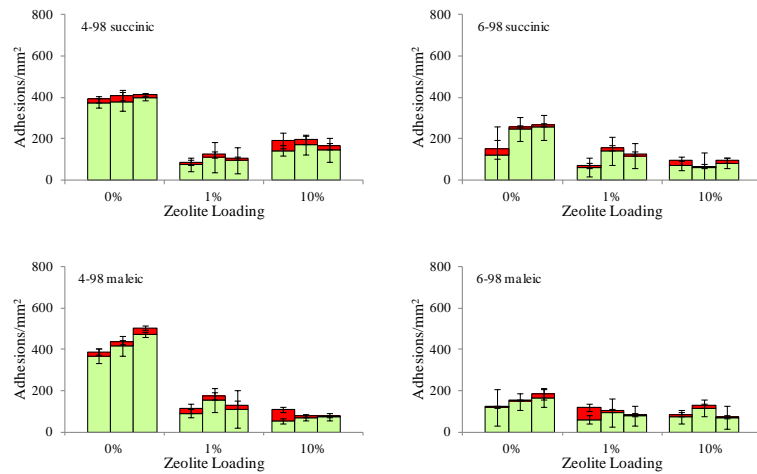
P. putida
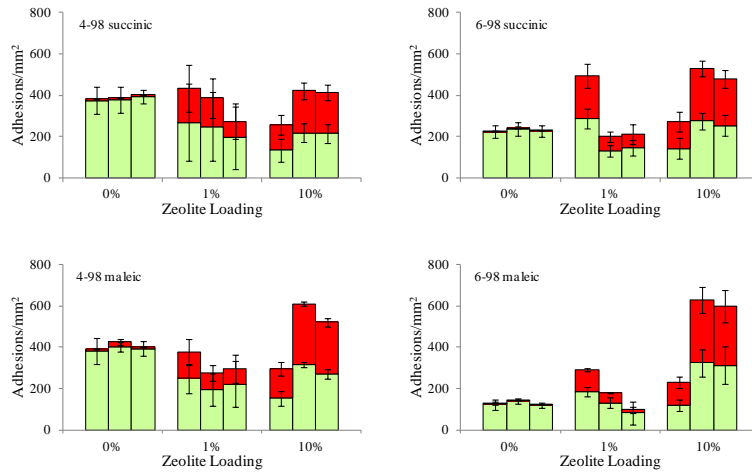
B. subtilis
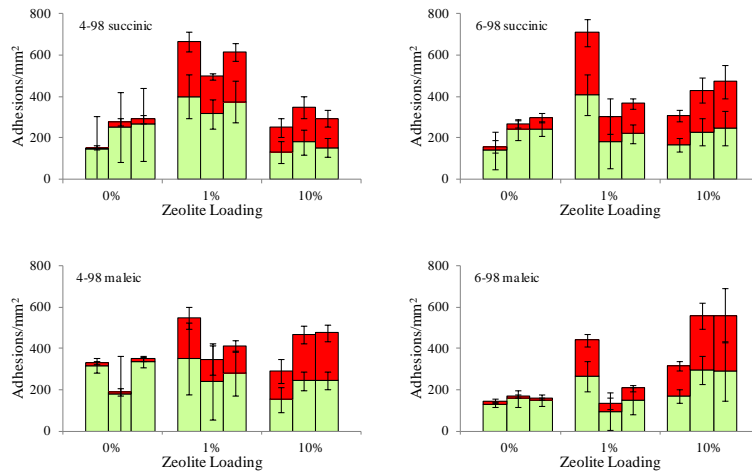
H. pacifica

Figure 4A.4   Irreversible adhesions and inactivation of Cu-LTA--PVA in SWNaCl, SWI and SWO (left, middle and right column in each cluster).Nanocomposites prepared from 27kDa (4-98) and 47kDa (6-98) molecular weight PVA, cross-linked with succinic acid or maleic acid.

P. putida

B. subtilis

H. pacifica

Figure 4A.5   Irreversible adhesions and inactivation of Zn-LTA--PVA in SWNaCl, SWI and SWO (left, middle and right column in each cluster).Nanocomposites prepared from 27kDa (4-98) and 47kDa (6-98) molecular weight PVA, cross-linked with succinic acid or maleic acid.
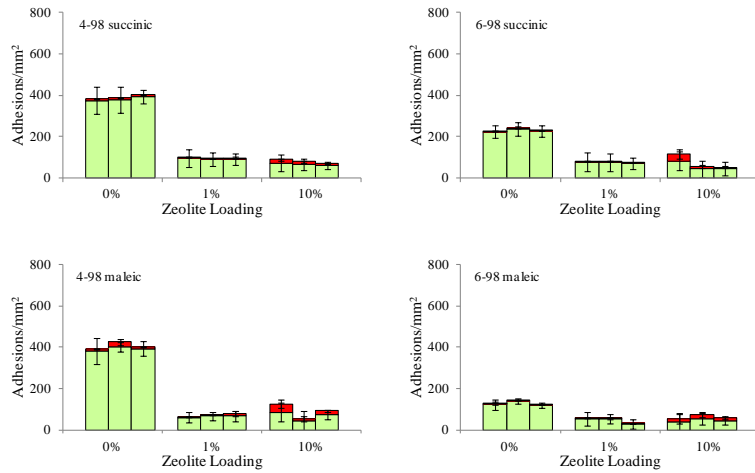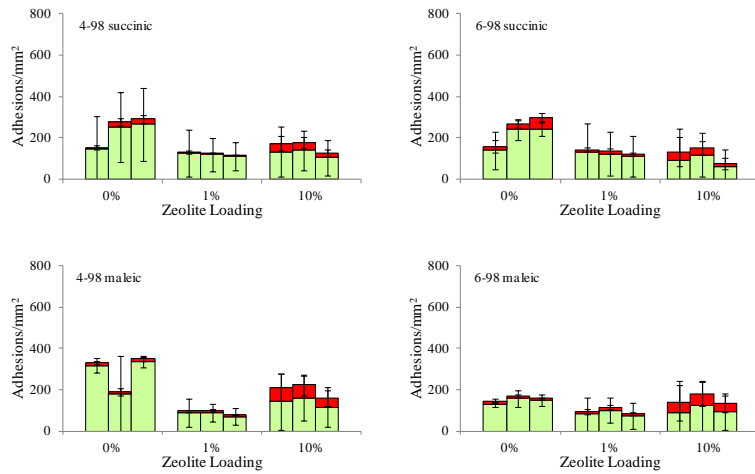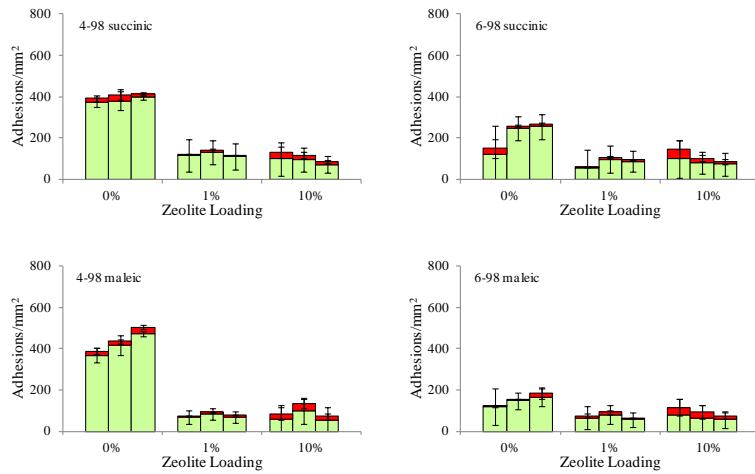
P. putida

B. subtilis

H. pacifica

Figure 4A.6   Irreversible adhesions and inactivation of AgCuZn-LTA--PVA in SWNaCl, SWI and SWO (left, middle and right column in each cluster).Nanocomposites prepared from 27kDa (4-98) and 47kDa (6-98) molecular weight PVA, cross-linked with succinic acid or maleic acid.
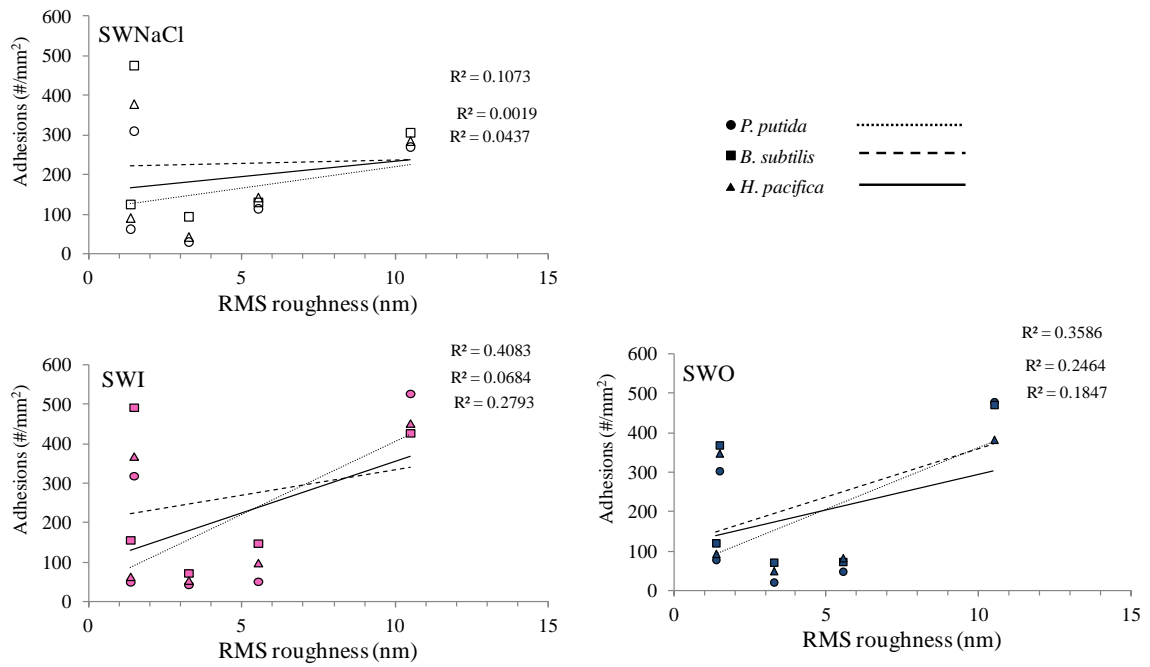
137

Figure 4B.1   Correlation between irreversible number of adhesions and nanocomposite RMS surface roughness for nanocomposites with 10% zeolite loading in simulated seawater matrices R^2 values organized from top to bottom for *P. putida*, *B. subtilis* and *H. pacifica.*

References

1. (a) Al-Ahmad, M.; Aleem, F. A. A.; Mutiri, A.; Ubaisy, A., Biofuoling in RO membrane systems Part 1: Fundamentals and control. *Desalination* **2000,** *132* (1-3), 173-179; (b) Baker, J. S.; Dudley, L. Y., Biofouling in membrane systems - A review. *Desalination* **1998,** *118* (1-3), 81-89.

2. Ridgeway, H. F., *Biological Fouling of Separation Membranes Used in Water Treatment Applications*. AWWA Research Foundation: 2003.

3. Characklis, W. G.; Marshall, K. C., *Biofilms*; Wiley: New York, 1990.

4. Nguyen, T.; Roddick, F.; Fan, L., Biofouling of Water Treatment Membranes: A Review of the Underlying Causes, Monitoring Techniques and Control Measures. *Membranes* **2012,** *2* (4), 804-840.

5. Tashiro, T., Antibacterial and bacterium adsorbing macromolecules. *Macromol Mater Eng* **2001,** *286* (2), 63-87.

6. Borkow, G.; Gabbay, J., Copper as a biocidal tool. *Curr Med Chem* **2005,** *12* (18), 2163-2175.

7. (a) Zodrow, K.; Brunet, L.; Mahendra, S.; Li, D.; Zhang, A.; Li, Q. L.; Alvarez, P. J. J., Polysulfone ultrafiltration membranes impregnated with silver nanoparticles show improved biofouling resistance and virus removal. *Water Res* **2009,** *43* (3), 715-723; (b) Lind, M. L.; Ghosh, A. K.; Jawor, A.; Huang, X. F.; Hou, W.; Yang, Y.; Hoek, E. M. V., Influence of Zeolite Crystal Size on Zeolite-Polyamide Thin Film Nanocomposite Membranes. *Langmuir* **2009,** *25* (17), 10139-10145; (c) Kang, S. W.; Kim, J. H.; Char, K.; Won, J.; Kang, Y. S., Nanocomposite silver polymer electrolytes as facilitated olefin transport membranes. *J Membrane Sci* **2006,** *285* (1-2), 102-107.

8. (a) Liu, L.; Xiao, L.; Yang, F., Terylene membrane modification with Polyrotaxanes, TiO_2 and Polyvinyl alcohol for better antifouling and adsorption property. *J Membrane Sci* **2009,** *333* (1-2), 110-117; (b) Kim, S. H.; Kwak, S.-Y.; Sohn, B.-H.; Park, T. H., Design of TiO2 nanoparticle self-assembled aromatic polyamide thin-film-composite (TFC) membrane as an approach to solve biofouling problem. *J Membrane Sci* **2003,** *211* (1), 157-165.

9.   Hoek, E. M. V.; Ghosh, A. K.; Huang, X. F.; Liong, M.; Zink, J. I., Physical-chemical properties, separation performance, and fouling resistance of mixed-matrix ultrafiltration membranes. *Desalination* **2011,** *283*, 89-99.

10.   Dobson, S. J.; Franzmann, P. D., Unification of the genera Deleya (Baumann et al 1983), Halomonas (Vreeland et al 1980), and Halovibrio (Fendrich 1988) and the species Paracoccus halodenitrificans (Robinson and Gibbons 1952) into a single genus, Halomonas, and placement of the genus Zymobacter in the family Halomonadaceae. *Int J Syst Bacteriol* **1996,** *46* (2), 550-558.

11.   Bakker, D. P.; Busscher, H. J.; van Zanten, J.; de Vries, J.; Klijnstra, J. W.; van der Mei, H. C., Multiple linear regression analysis of bacterial deposition to polyurethane coating after conditioning film formation in the marine environment. *Microbiol-Sgm* **2004,** *150*, 1779-1784.

12.   Subramani, A.; Hoek, E. M. V., Direct observation of initial microbial deposition onto reverse osmosis and nanofiltration membranes. *J Membrane Sci* **2008,** *319* (1-2), 111-125.

13.   Chen, G. X.; Walker, S. L., Role of solution chemistry and ion valence on the adhesion kinetics of groundwater and marine bacteria. *Langmuir* **2007,** *23* (13), 7162-7169.

14.   Kang, S. T.; Subramani, A.; Hoek, E. M. V.; Deshusses, M. A.; Matsumoto, M. R., Direct observation of biofouling in cross-flow microfiltration: mechanisms of deposition and release. *J Membrane Sci* **2004,** *244* (1-2), 151-165.

15.   Clesceri, L. S.; Greenberg, A. E.; Eaton, A. D.; Franson, M. A. H.; American Public Health Association; American Water Works Association; Water Environment Federation, *Standard Methods for the Examination of Water and Wastewater*. 20th ed.; American Public Health Association: Washington, DC 1998; p 1220.

16.   Peng, F. B.; Hoek, E. M. V.; Damoiseaux, R., High-Content Screening for Biofilm Assays. *J Biomol Screen* **2010,** *15* (7), 748-754.

17.   Hoek, E. M. V.; Bhattacharjee, S.; Elimelech, M., Effect of membrane surface roughness on colloid-membrane DLVO interactions. *Langmuir* **2003,** *19* (11), 4836-4847.

18. McDonnell, A. M. P.; Beving, D.; Wang, A. J.; Chen, W.; Yan, Y. S., Hydrophilic and antimicrobial zeolite coatings for gravity-independent water separation. *Adv Funct Mater* **2005,** *15* (2), 336-340.

19. Jeong, B. H.; Hoek, E. M. V.; Yan, Y. S.; Subramani, A.; Huang, X. F.; Hurwitz, G.; Ghosh, A. K.; Jawor, A., Interfacial polymerization of thin film nanocomposites: A new concept for reverse osmosis membranes. *J Membrane Sci* **2007,** *294* (1-2), 1-7.

20. Chen, G.; Strevett, K. A., Microbial surface thermodynamics and interactions in aqueous media. *J Colloid Interf Sci* **2003,** *261* (2), 283-290.

21. (a) Subramani, A.; Hoek, E. M. V., Biofilm formation, cleaning, re-formation on polyamide composite membranes. *Desalination* **2010,** *257* (1-3), 73-79; (b) Huang, X. Mechanisms of bacterial adhesion to seawater reverse osmosis membranes. Thesis (Ph. D.), UCLA, Los Angeles, 2010.

22. (a) Klodzinska, E.; Szumski, M.; Dziubakiewicz, E.; Hrynkiewicz, K.; Skwarek, E.; Janusz, W.; Buszewski, B., Effect of zeta potential value on bacterial behavior during electrophoretic separation. *Electrophoresis* **2010,** *31* (9), 1590-1596; (b) Soni, K. A.; Balasubramanian, A. K.; Beskok, A.; Pillai, S. D., Zeta potential of selected bacteria in drinking water when dead, starved, or exposed to minimal and rich culture media. *Curr Microbiol* **2008,** *56* (1), 93-97.

23. Bruinsma, G. M.; Rustema-Abbing, M.; van der Mei, H. C.; Busscher, H. J., Effects of cell surface damage on surface properties and adhesion of *Pseudomonas aeruginosa*. *J Microbiol Meth* **2001,** *45* (2), 95-101.